Neurologische Universitätsklinik Tübingen

Abteilung Neurologie mit Schwerpunkt

neurovaskuläre Erkrankungen

Muscarinic acetylcholine receptor-mediated central cholinergic neurotransmission in TMS-EEG responses

at the
Faculty of Medicine
Eberhard Karls Universität
Tübingen

presented by

Song, Yufei

2026

Dean:	Professorin Dr. S. Y. Brucker
1st reviewer:	Professor Dr. U. Ziemann
2nd reviewer:	Professor Dr. H. Preißl
3rd reviewer:	Professor Dr. L. J. Volz

Date of oral examination: 10.02.2026

Abbreviations

ACh	Acetylcholine
AD	Alzheimer's disease
AEPs	Auditory-evoked EEG potentials
AG	Angular gyrus
BF	Basal forebrain
BIP	Biperiden
CCC	Concordance correlation coefficient
ChIs	Cholinergic interneurons
CNS	Central nervous system
DBS	Deep brain stimulation
dlPFC	Dorsal lateral prefrontal cortex
E-field	Electrical field
E/I	Excitation and inhibition
ERPs	Event-related EEG potentials
ES	Electrical stimulation
fMRI	Functional magnetic resonance imaging
GABA	γ-aminobutyric acid
GMFA	Global mean field amplitude
ICA	Independent component analysis
ITPC	Inter-trial phase coherence
LFPs	Local field potentials
LMFA	Local mean field amplitude
M1	Primary motor cortex
mAChR	Muscarinic acetylcholine receptor
nAChR	Nicotinic acetylcholine receptor
NMDA	N-methyl-D-aspartate
PCI	Perturbation complexity index
PD	Parkinson's disease
PLA	Placebo
RMT	Resting motor threshold
ROI	Region of interest
SCO	Scopolamine
SEPs	Sensory-evoked EEG potentials
SIO	Sensory-induced EEG oscillations
SMA	Supplementary motor area

SNR	Signal-to-noise ratio
SSEPs	Somatosensory-evoked EEG potentials
STN	Subthalamus nucleus
TEPs	TMS-evoked EEG potentials
TFR	Time-frequency representation
TIOs	TMS-induced EEG oscillations
TMS–EEG	Transcranial Magnetic Stimulation–Electroencephalography
TMS	Transcranial Magnetic Stimulation
TRSP	TMS-related spectral perturbation

Table of Contents

1 Introduction

1.1 TMS–EEG

When people hear ’non-invasive brain stimulation,’ they might picture dramatic scenes from fiction where patients, strapped down, endure electric shocks for mental disorder treatment. Although inaccurately portrayed, electroconvulsive stimulation or electroshock does cause significant discomfort, as stimulating neurons for action potential generation requires sufficiently high currents to penetrate the skull, often inevitably stimulating scalp nerves and muscles (Peterchev et al., 2010; Taylor, 2007). Therefore, modern electroconvulsive therapy is generally under anesthesia to ensure a safe and painless experience for patients. The development of Transcranial Magnetic Stimulation (TMS) since 1985 has opened a new chapter in non-invasive brain stimulation (Barker et al., 1985). TMS works by generating a brief and strong current pulse within a coil, which produces a rapidly changing magnetic field that penetrates the skull without distortion (Hernandez-Pavon et al., 2023) (Figure 1). This magnetic field induces a time-varying electric field (E-field) in the brain and, consequently, an electric current that can excite the neurons and produce local and distant activation through cortical-cortical and cortical-subcortical connections. TMS is considered as a safe and well-tolerated procedure that does not require anesthesia (Rossi et al., 2009). Over the years, it has become a well-established method for non-invasively stimulating the human brain.

Brain reactivity to TMS can be measured using concurrent neuroimaging techniques such as electroencephalography (EEG), functional magnetic resonance imaging (fMRI), positron emission tomography, and near-infrared spectroscopy (reviewed in (Siebner et al., 2009) and (Bergmann et al., 2016)). Among these, TMS–EEG has gained popularity due to its high temporal resolution, measured in milliseconds, making it ideal for capturing fast, dynamic brain responses to TMS (Ilmoniemi et al., 1997). TMS–EEG has been applied in both health and disease, providing insights into cortical excitability (how responsive the brain region is) and connectivity (how the activation spreads through structural and functional connections) (Tremblay et al., 2019). In the following two sections, I will introduce single-pulse TMS–EEG from its electrophysiological perspective (1.1.1) and outline its commonly used outcome indices (1.1.2).

1.1.1 Electrophysiological Aspects of TMS–EEG

How does the brain react to a TMS pulse? TMS initiates a cascade of electrical and biochemical processes that begin with the depolarization of axons in a mixed population of excitatory and inhibitory neurons in the targeted cortex (Siebner et al., 2022). Whether action potentials can be further generated depends on multiple factors, such as the magnitude and direction of the induced E-field, axon geometry and electrophysiological properties of neurons (Aberra et al., 2020; Maccabee et al., 1998). When action potentials are triggered, they travel along the axon in two directions: orthodromically (away from the soma) and antidromically (toward the soma). At the synapses, neurotransmitters are released from the presynaptic neurons to activate channels at the postsynaptic, and the influx and outflux of ions in the dendrites of postsynaptic neurons generate postsynaptic potentials (either excitatory or inhibitory) (Hernandez-Pavon et al., 2023; Siebner et al., 2022). The spatial and temporal integration of these postsynaptic potentials can further trigger and propagate postsynaptic action potentials once the membrane threshold is exceeded. Depending on how the stimulated area is structurally and functionally connected to the rest of the brain, this transsynaptic excitation or inhibition can occur locally or widely, facilitating neural information transfer within neural circuits and networks (Figure 1).

Not all neural events triggered by TMS can be detected by scalp EEG. Given the physiological principles of EEG, mainly the synchronous postsynaptic potentials generated by a large number of neurons can give rise to measurable EEG signals (Buzsáki et al., 2012; Cohen, 2014; Jackson & Bolger, 2014). Accordingly, 1) TMS–EEG signals mainly reflect the temporal and spatial summation of excitatory and inhibitory postsynaptic potentials produced by the TMS effect, with little contribution from action potentials (Hernandez-Pavon et al., 2023; Rogasch & Fitzgerald, 2013). This is because action potentials have a short duration and are rarely synchronized, resulting in weak E-fields that can hardly be detected by scalp EEG (Buzsáki et al., 2012). 2) TMS–EEG signals do not reflect individual molecular or synaptic events, but rather represent a population of neurons aligned in parallel with synchronized activity (Cohen, 2014). The parallel geometric orientation and synchronization of a large population of neurons (estimated between 10,000 and 50,000) are essential for producing strong E-fields to be detectable (Murakami & Okada, 2006). 3) TMS–EEG signals are mainly dominated by

neurons in the superficial cortical layers. The strength of E-fields produced by neurons decreases exponentially with distance (Buzsáki et al., 2012; Cohen, 2014). Therefore, even when deep brain structures such as the thalamus, hippocampus, and basal ganglia produce strong E-fields, they only have a minimal impact on the voltage recorded from scalp EEG. Additionally, neurons in these deep structures are not often arranged in parallel. The E-fields generated by neuronal individuals may effectively cancel each other, even when there is a synchronous population-level activity. 4) The positive and negative deflections of TMS–EEG signals alone, measured at a particular location, do not directly imply whether the involved generator is excitatory or inhibitory (Jackson & Bolger, 2014).

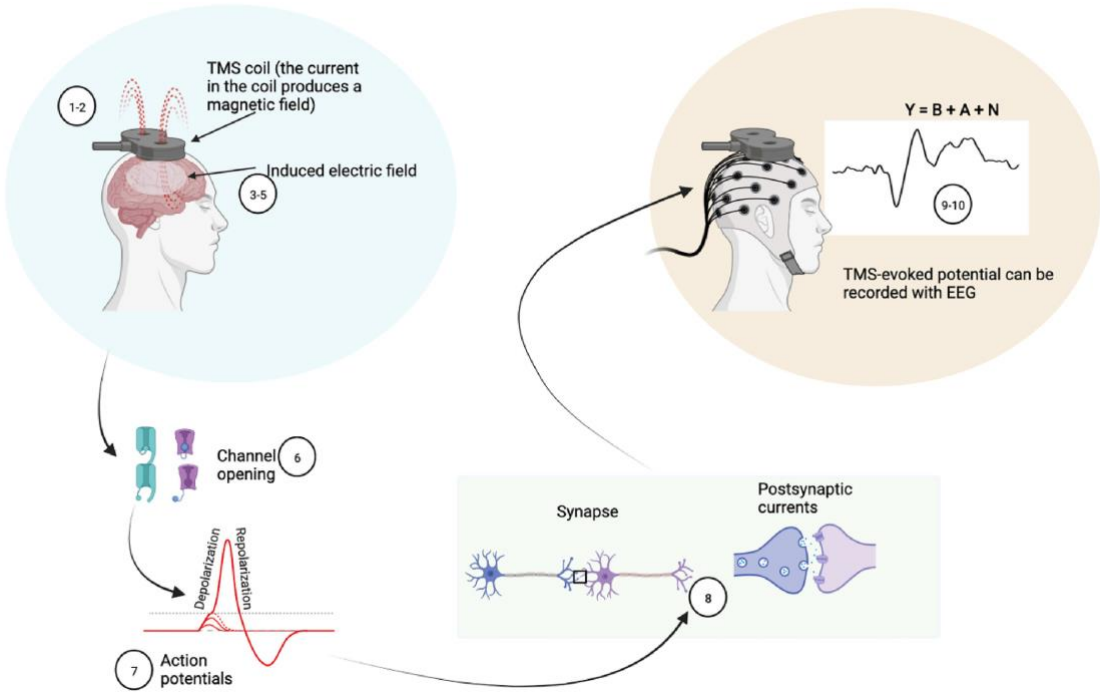

Figure 1. TMS–EEG technique. (1–5) A current pulse within a coil, producing a rapidly changing magnetic field. This magnetic field induces a time-varying E-field in the brain, which consequently produces an electric current in the brain tissue. (6–8) The electric current depolarizes the axon and generates action potentials. At the synapse, neurotransmitters are released, which generates postsynaptic excitatory (and inhibitory) potentials/currents. (9–10) TMS-induced activation can be recorded with EEG. *Figure is reproduced from Hernandez-Pavon et al., 2023, under the CC BY-NC-ND license.*

1.1.2 TMS–EEG Outcome Indices

TMS–EEG signals can be analyzed in the time domain and/or frequency domain (Farzan & Bortoletto, 2022; Pellicciari et al., 2017). In the time domain, TMS-evoked EEG

potentials (TEPs) are typically computed. TEPs are a form of event-related potentials (ERPs) that are time-locked and phase-locked EEG responses, averaged across trials (Cohen, 2014). TEP waveforms feature a series of positive (P) and negative (N) peaks, lasting up to 300 ms post-stimulus, with distinct topographies that illustrate voltage distribution across the scalp (reviewed in (Farzan & Bortoletto, 2022)). TEP characteristics are influenced by both extrinsic factors, such as TMS intensity and coil orientation, and intrinsic properties of the stimulation site at the time of stimulation. TEPs elicited from single-pulse TMS applied to the primary motor cortex (M1) are the most extensively studied. Commonly reported components include N15, P30, N45, P60, N100, and P180 (Ahn & Fröhlich, 2021; Biabani et al., 2019; Komssi et al., 2002; Paus et al., 2001; Premoli et al., 2014). These components are conventionally named according to the polarity (N or P) and the latency (in milliseconds) of TEP waveform peaks, measured from the electrode near the stimulation site or from Cz. The global mean field amplitude (GMFA) and local mean field amplitude (LMFA) are derived from TEPs (Esser et al., 2006; Lehmann & Skrandies, 1980). The GMFA shows the overall activation across the scalp, while the LMFA indicates activation within a specific region of interest (ROI).

Time-frequency decomposition techniques such as the Morlet wavelet transform, Hilbert transform, and short-term Fourier analysis can be used to analyze rhythmic activity in response to TMS (Pellicciari et al., 2017). These methods first compute trial-wise time-frequency representations (TFRs), which are then averaged across trials (Cohen, 2014; Hernandez-Pavon et al., 2023; Herrmann et al., 2014; Pellicciari et al., 2017). The trial-averaged TFR, known as TMS-related spectral perturbation (TRSP), represents the total oscillatory power that includes both phase-locked (evoked) and non-phase-locked (induced) (Cohen, 2014). While the power of TMS-induced EEG oscillations (TIOs) can be conceptually isolated by removing phase-locked oscillatory power from the total, there are currently no ideal methods to achieve this. One attempting method involves subtracting the evoked potential from single trial TMS–EEG signals before time-frequency decomposition (Cohen, 2014; Premoli et al., 2017). Another involves performing decomposition on both single trial signals and evoked potential separately, then subtracting the power of the evoked potential (Gordon et al., 2023; Herrmann et al., 2014; Pellicciari et al., 2017). A typical TFR often shows oscillatory power increases (synchronization) and/or decreases (desynchronization) as a function of time and

frequency. For example, TMS–EEG studies targeting the M1 reveal the oscillatory pattern with a triphasic dynamic: an early (< 200 ms) synchronization in the alpha and beta band, followed by a desynchronization (Belardinelli et al., 2021; Premoli et al., 2017), and a subsequent beta rebound after 400 ms (Gordon et al., 2018). In addition to power, one can extract phase information. For example, inter-trial phase coherence (ITPC) assesses the consistency of phase angles across multiple trials (Cohen, 2014), measuring the strength of phase-locking and neuronal synchronization induced by TMS.

There are also more complex TMS–EEG metrics, such as the perturbation complexity index (PCI). PCI measures the integration and segregation of cortical activation in response to TMS, which has proven effective in assessing levels of consciousness (Sarasso et al., 2014). In general, many EEG-based connectivity methods can be utilized to probe the network activation following TMS targeting specific nodes (Bortoletto et al., 2015; Kida et al., 2016).

Over the years, single-pulse TMS–EEG has proven valuable for assessing cortical reactivity to TMS when targeting different brain regions (Ilmoniemi et al., 1997; Lioumis et al., 2009) and indexing changes in brain activity caused by experimental manipulations (Casula et al., 2016; Moffa et al., 2022). It also holds great potential as a diagnostic, prognostic, and therapeutic tool in clinical settings. Altered TMS–EEG measures have been observed in neurological disorders like Alzheimer's disease (AD) (Casula et al., 2023; Ferreri et al., 2016) and stroke (Pellicciari et al., 2018; Tscherpel et al., 2020), as well as in psychiatric conditions such as schizophrenia (Ferrarelli et al., 2012) (reviewed in (Tremblay et al., 2019)).

1.2 Artifacts in TMS–EEG Recordings

The approach of single-pulse TMS–EEG is straightforward: a single TMS pulse stimulates a specific brain region, and concurrent EEG captures the resulting cortical responses. However, applying TMS pulses during EEG recordings introduces various artifacts that can challenge the assessment and interpretation of TMS–EEG results in many ways (Bergmann et al., 2024). Isolating true TMS–EEG responses from unwanted artifacts remains a complex issue, as highlighted in recent reviews (Farzan & Bortoletto, 2022; Hernandez-Pavon et al., 2023; Rogasch et al., 2022). TMS–related EEG artifacts can be classified into two categories (Hernandez-Pavon et al., 2023): non-physiological

and physiological. Non-physiological artifacts include TMS pulse, recharge, and decay artifacts. In contrast, physiological artifacts can be caused by blinks and eye movements, cranial muscle twitches, and auditory and somatosensory inputs due to peripheral co-stimulation. While non-physiological artifacts can often be minimized through instrument optimization and careful experimental preparation, physiological artifacts, particularly EEG responses to TMS-associated sensory co-stimulation, pose a more complex challenge (Bergmann et al., 2024; Hernandez-Pavon et al., 2023). In the following sections, I will outline the sources of these sensory co-stimulation, discuss why they are particularly problematic (1.2.1), and review approaches available to mitigate their impact (1.2.2).

1.2.1 Sensory Confounds during TMS–EEG

The auditory inputs associated with TMS come from the 'click' sound whenever a TMS pulse is discharged, which can activate the auditory system through air and bone conduction (Siebner et al., 2022). For TMS-associated somatosensory inputs, multiple possible sources have been suggested (Mancuso et al., 2023; Siebner et al., 2022): craniofacial muscle twitch caused by TMS may activate receptors of muscle, tendons, and skin, resulting in reafferent somatosensory stimulation; cutaneous somatosensory nerve endings and somatosensory nerve trunks (e.g., facial, trigeminal and occipital nerves) may be directly excited by TMS; skin and dura mechanoreceptors may be excited by coil vibration and TMS induced E-field. Consequently, the auditory and somatosensory systems can be activated during EEG recordings, producing sensory-related EEG responses.

These sensory-related EEG responses can resemble genuine TMS–EEG responses that result from direct cortical activation by TMS. Sensory-related EEG responses are time-locked to sensory stimuli and exhibit specific temporal, spatial, and spectral features. For instance, auditory-evoked EEG potentials (AEPs) typically feature a sequence of peaks, with an N100-P200 complex being spatially symmetric and prominent over the frontocentral channels (e.g., Cz, FCz, and Fz) (Rocchi et al., 2021). Somatosensory-evoked EEG potentials (SSEPs), on the other hand, can vary depending on the type of stimulus used. They also include an N100-P200 component, which can be spatially symmetric (Novembre et al., 2019), or asymmetric with stronger voltage observed over

the contralateral hemisphere (Bennett & Jannetta, 1980; Hashimoto, 1988). This has led to the hypothesis that the N100-P200 complex of these sensory-evoked EEG potentials (SEPs) represents a salience-related response associated with arousal and attention during sensory processing, regardless of the modality of sensory stimulus (Mouraux & Iannetti, 2009; Novembre et al., 2019). Since a similar N100-P200 TEP component is often observed in TMS–EEG studies (Ahn & Fröhlich, 2021; Biabani et al., 2019; Komssi et al., 2002; Paus et al., 2001; Premoli et al., 2014), it raises the question of whether this component represents direct cortical activation by TMS, sensory processing, or a combination of both. This ambiguity also applies to analyses in the time-frequency domain. Both somatosensory and auditory stimuli cause changes in oscillatory power in alpha and beta frequency bands (Novembre et al., 2019). However, such oscillatory features were similarly observed in TMS–EEG signals following stimulation of different brain areas (Biondi et al., 2022; Casula et al., 2016; Premoli et al., 2017).

The issue that 'off-target' sensory EEG responses can mislead TMS–EEG interpretations has been emphasized in recent publications (Biabani et al., 2019; Conde et al., 2019). Biabani et al. demonstrated significant similarities between EEG responses following M1 stimulation and those following TMS over the ipsilateral shoulder, particularly in latencies >60 ms poststimulus (Biabani et al., 2019). The debate over the extent to which sensory-related EEG responses contaminate TMS–EEG results was further intensified by a study that assessed the correlations between the EEG response to TMS over the prefrontal and parietal sites and those to multisensory stimulation designed to replicate TMS-associated sensory inputs in a sham condition (Conde et al., 2019). Despite the use of sophisticated procedures (noise masking and the placement of a foam layer underneath the coil) to attenuate TMS-associated sensory co-stimulation, Conde and colleagues showed that EEG responses to active TMS highly correlated with those to the sham stimulation, including both early (20 to 80 ms) and late latencies. While it is debatable to what extent this close resemblance arises from inadequate cortical activation by TMS and/or incomplete auditory masking (Belardinelli et al., 2019; Siebner et al., 2019), these studies have emphasized the issue of sensory confounds in TMS–EEG.

1.2.2 Addressing Sensory Confounds

Several methods have been proposed to eliminate or minimize sensory co-stimulation during TMS–EEG recordings. One sophisticated method is a combination of active auditory noise masking, foam padding between the coil and the head, and passive sound dampening using earmuffs (Ross et al., 2022; ter Braack et al., 2015; Tervo et al., 2022). Different types of masking noise have been explored, including white noise and noise specifically adapted to the spectral characteristics of the TMS 'click' sound and adjusted in real-time, tailored according to participants' perceptions (Massimini et al., 2005; Russo et al., 2022; ter Braack et al., 2015). While these approaches have proven useful in reducing the perception of TMS 'click' and suppressing AEPs, it is unlikely to achieve complete elimination of sensory confounds as long as the TMS coil remains positioned on the scalp (Bergmann et al., 2024; ter Braack et al., 2015). Besides, the effectiveness of noise masking may decrease when the TMS 'click' sound exceeds the tolerable volume of the masking noise, mainly when the TMS intensity is high or when stimulation sites are close to the ear. Notably, the use of foam padding itself inevitably increases the required TMS intensity. As for somatosensory inputs, one may reduce scalp muscle contractions during TMS by optimizing stimulation parameters. Casarotto and colleagues recently introduced a graphical user interface to monitor TMS–EEG signals in real-time (Casarotto et al., 2022). They showed that small adjustments in coil position and/or rotation can minimize scalp muscle contraction and improve TMS–EEG data quality. However, its effectiveness tends to decrease if the stimulation site is more lateral, anterior, or posterior, where avoiding cranial muscle contractions becomes remarkably challenging.

When sensory co-stimulation cannot be entirely eliminated, a control condition–in the form of sham stimulation–can be incorporated to rule out alternative explanations of the TMS–EEG results (Farzan & Bortoletto, 2022). The idea is to compare EEG responses to sham stimulation that replicates TMS-related sensory inputs with those in response to active TMS. This allows any differences in EEG to be attributed to direct cortical activation elicited by TMS. However, designing an effective sham stimulation is complex and challenging. A few studies have implemented different approaches to reproduce TMS-associated sensory inputs. One way is to place the TMS coil at a short distance or tilt it away from the head (Du et al., 2017; ter Braack et al., 2015). While this preserves

the ’click’ sound and avoids inducing a current in the brain, it fails to replicate bone conduction and entirely lacks somatosensory stimulation. Another method used by Herring et al. (Herring et al., 2015) and Biabani et al. (Biabani et al., 2019) involves magnetic stimulation over the shoulder blade, which induces both somatosensory and auditory stimulations. However, because sensory inputs from the shoulder differ from those of the scalp, shoulder stimulation alone may not serve as a fully comparable sham condition. To more closely mimic TMS-associated sensory inputs, several studies have used electrical stimulation (ES) applied through electrodes placed near the TMS site on the scalp to simulate somatosensory inputs (Chowdhury et al., 2022; Conde et al., 2019; Gordon et al., 2018; Raffin et al., 2020; Rocchi et al., 2021). This was often coupled with the TMS ’click’ sound for auditory inputs.

Despite these efforts to create a multisensory sham, participants often reported a distinct difference in their perceptions of active TMS versus sham stimulation, likely due to the different biophysical mechanisms involved in TMS and cutaneous ES (Conde et al., 2019). This distinction suggests that the EEG responses to active TMS and sham stimulation may not be sufficiently matched. In an attempt to better match sensory responses from the sham with those from active TMS, our group recently developed and validated a sensory control procedure (Gordon et al., 2021, 2022). Like previous approaches, this method used scalp ES to simulate somatosensory inputs and TMS ’click’ sound for auditory inputs. However, a key difference in our approach was the application of high-intensity ES in both sham and active TMS conditions. This aimed to saturate the EEG responses to sensory stimulation, thereby minimizing the impact of any additional somatosensory inputs caused by TMS in the active condition. As a result, sensory components between the two conditions become more closely matched. Our previous work targeting the left M1 demonstrated that sensory-related EEG responses were similar (as indicated by N100-P200 amplitude) in both active and sham conditions, with comparable perceptions reported by participants (Gordon et al., 2021). Additionally, comparisons between EEG responses in active and sham conditions revealed significant differences, which were mainly driven by early (< 80 ms) and late (around 500 ms) activities near the TMS site. Notably, similar results were found even in participants who could not reliably distinguish between active and sham conditions, suggesting that the ability to differentiate the stimulation may not significantly influence the TEP findings.

As such, the 'cleaned' TMS–EEG responses, obtained by subtracting sham EEG responses from the active, are proposed to represent direct cortical activation by TMS, assuming that this activation is largely independent of sensory-related activity. This assumption was further strengthened by a follow-up experiment showing that the 'cleaned' TEPs remained largely unchanged despite varying sensory input intensity used in the sensory control procedure (Gordon et al., 2022).

1.3 Neurotransmission involved in TMS–EEG

Having discussed the challenges posed by sensory confounds in TMS–EEG signals and possible ways to mitigate their impact, I now turn to the neurophysiological mechanisms underlying single-pulse TMS–EEG responses. Understanding the neural basis involved is important for rigorously applying the TMS–EEG technique and effectively interpreting results. As outlined in section 1.1.1, the neural information flow induced by TMS involves multiple electrical and biochemical processes. Combining TMS–EEG with pharmacological interventions is a useful approach for investigating the roles of specific receptor-mediated neurotransmission in TMS–EEG measures in humans (Belardinelli et al., 2021; Darmani et al., 2016, 2019; Gordon et al., 2023; Hui et al., 2020; Premoli et al., 2014, 2017; Rogasch et al., 2020; Salavati et al., 2018). By comparing TMS–EEG responses before and after administering drugs that selectively enhance or inhibit certain neurotransmission pathways, one can assess the contribution of these processes to the generation of TMS–EEG signals. This section will review what is currently known–and what remains unclear–about how receptor-mediated neurotransmission shapes single-pulse TMS–EEG outcomes. Notably, the pharmaco-TMS–EEG approach is not constrained to single-pulse TMS–EEG; it can be extended to paired-pulse stimulation paradigms (e.g., the long-interval CI) (Salavati et al., 2018). However, given the complexity of controlling sensory confounds in these paired-pulse TMS–EEG paradigms (Ilmoniemi et al., 2024; Siebner et al., 2022), this thesis will only focus on single-pulse TMS–EEG.

1.3.1 GABA- and Glutamatergic Neurotransmission

Glutamate and γ-aminobutyric acid (GABA) are important neurotransmitters in the central nervous system (CNS) (Purves et al., 2018). Upon binding to and activating their respective receptors, glutamate can produce excitatory, while GABA mainly produces

inhibitory postsynaptic potentials, increasing or decreasing the probability of firing the postsynaptic neurons. Diazepam is a GABA receptor-positive allosteric modulator, enhancing the affinity of channel opening by GABA when binding to the ionotropic $GABA_A$ receptor (Purves et al., 2018). Previous pharmacological TMS–EEG studies have demonstrated that diazepam caused an increase in the amplitude of the N45 TEP component and a decrease in the amplitude of the P60, N100, and P150 upon the M1 stimulation (Gordon et al., 2023; Premoli et al., 2014). Furthermore, diazepam also caused an increased power of TIOs in the alpha frequency band (8–12 Hz) and a decreased power in the beta frequency band (13–30 Hz) (Gordon et al., 2023; Premoli et al., 2017). By contrast, the selective α-$GABA_A$ receptor antagonist S44819 was found to decrease the amplitude of N45 when stimulating the M1 (Darmani et al., 2016). The N-methyl-Daspartate (NMDA) receptor is an ionotropic glutamate receptor that can be blocked by dextromethorphan (Siu & Drachtman, 2007). Similar to the effect of diazepam, dextromethorphan was found to increase N45 amplitude upon stimulating the M1(Belardinelli et al., 2021). These findings corroborate the long-held notion that the transsynaptic process is activated following single-pulse TMS, and TEPs likely reflect the synaptic excitation and inhibition (E/I) balance of this process (Belardinelli et al., 2021).

1.3.2 Cholinergic Neurotransmission

Apart from GABA and glutamate, the transfer of neural information in the neural circuits is under the regulation of a group of neurotransmitters known as neuromodulators (Kandel et al., 2000; Nadim & Bucher, 2014; Purves et al., 2018; Tsuboi et al., 2024). Neuromodulators typically act through metabotropic receptors, which affect intrinsic neuronal properties such as membrane excitability by opening or closing ion channels, and influence synaptic efficacy such as by altering neurotransmitter release probability. These modifications can reconfigure the wires of neural circuits in order to adapt to the ever-changing environment (Nadim & Bucher, 2014). To date, the role of neuromodulator-mediated neurotransmission in TMS–EEG remains largely unexplored. This section will focus on acetylcholine (ACh) mediated transmission in the CNS, serving as a representative example for understanding how neuromodulators shape TMS–EEG. More importantly, if successful, identifying the TMS–EEG signatures of central cholinergic neurotransmission holds potential clinical value. Central cholinergic

signaling is important for regulating cognitive and motor functions (Bentley et al., 2011; Maurice et al., 2015). Disruptions in cholinergic neurotransmission are implicated in neurological and psychiatric disorders such as AD, Parkinson's disease (PD), schizophrenia, and depression (Bohnen et al., 2018; Záborszky et al., 2018). These neuropathological conditions have been investigated with TMS–EEG. For example, compared to controls, patients with AD demonstrated an increased amplitude of the P30 TEP component following TMS over the M1 (Ferreri et al., 2016). A follow-up 6-year prospective study that investigated the progression from mild cognitive impairment to AD using TMS–EEG over M1 showed that a GMFA-derived parameter, known as dipolar activity, was able to differentiate patients who converted from mild cognitive impairment to AD (Ferreri et al., 2021). Similarly, when stimulating the precuneus, patients with AD showed a higher TEP amplitude ~30–90 ms post-stimulus at the precuneus and frontal regions than healthy control (Casula et al., 2023). Moreover, the amplitude of precuneus TEPs correlates with the level of cognitive impairment, as measured by mini-mental state examination. Therefore, the cholinergic TMS–EEG signatures will help interpret these TMS–EEG alterations and possibly act as a non-invasive indicator of the cholinergic system's (dys)function, guiding and monitoring treatment.

ACh acts through two classes of receptors, metabotropic muscarinic receptors (mAChRs) and ionotropic nicotinic receptors (nAChRs), upon being released from cholinergic neurons in the CNS (Kandel et al., 2000). ACh is primarily synthesized in projecting cholinergic neurons in the basal forebrain (BF), brain stem, as well as local cholinergic interneurons (ChIs) in the striatum (Ballinger et al., 2016; Picciotto et al., 2012; Thiele, 2013). mAChRs are classified into five subtypes, M1-M5, which are grouped into two families: M1-type mAChRs (M1, M3, and M5) are coupled with G_q proteins, and M2-type mAChRs (M2 and M4) are coupled with $G_{i/o}$. Although mAChRs are widely distributed in the CNS, their subtype expression varies across brain regions. For instance, M1-M4 mAChRs are mostly expressed in the cortex, striatum, and hippocampus, while M5 is predominantly distributed in the substantia nigra and ventral tegmental area. mAChRs are located both pre- and post-synaptically (Colangelo et al., 2019; Thiele, 2013). mAChR activation induces diverse effects on cellular properties and synaptic transmission depending on the recruited receptor subtype and neuron type. For example, presynaptic receptors are typically M2-type, which act as inhibitory autoreceptors on

cholinergic terminals and heteroreceptors at GABAergic and glutamatergic terminals, reducing transmitter release. Postsynaptic receptors, which are common in both interneurons and pyramidal neurons (layer II/III and layer V), can either decrease or increase neuronal activity. nAChRs, on the other hand, are nonselective, excitatory cation channels. Like mAChRs, nAChRs have multiple subtypes and are expressed both pre- and post-synaptically by various cell types (Colangelo et al., 2019). Consequently, nAChR activation also has variable effects.

1.4 Aims

The aims of this thesis were twofold. First, it sought to evaluate whether a sensory control procedure, adapted from previous work, could effectively mitigate sensory confounds in TMS–EEG signals. Second, it intended to explore the role of central cholinergic neurotransmission in shaping TMS–EEG responses. To achieve these, we conducted a randomized, placebo-controlled crossover study involving twenty-four healthy participants. Each participant received a single oral dose of the non-selective mAChR antagonist scopolamine, the selective mAChR antagonist biperiden, or placebo across three separate sessions. During each session, TEPs and TIOs in response to stimulation of three brain regions were measured before and after drug administration using a sensory control procedure designed to mitigate sensory confounds. Although both mAChR and nAChR antagonists can inhibit cholinergic transmission, nAChR antagonists are excluded from this study due to their potential to cause temporary muscle paralysis by blocking nicotinic transmission at the neuromuscular junction (Kunnath et al., 2023). We used mAChR antagonists scopolamine and biperiden: scopolamine blocks mAChRs non-selectively, while biperiden specifically targets the M1 receptor (Bakker et al., 2021; Klinkenberg & Blokland, 2010). The inclusion of both drugs in the study allows a further investigation into the role of mAChR subtypes in TMS–EEG responses. Three brain regions selected for this study are the left medial prefrontal cortex (mPFC), angular gyrus (AG), and supplementary motor area (SMA). The mPFC and AG are chosen due to their involvement in cognition brain networks, where central cholinergic signaling plays an important role (Bentley et al., 2011; Klinkenberg et al., 2011). The SMA, a cortical region involved in motor control and learning, is under the regulation of neuromodulator systems, including the cholinergic (Maurice et al., 2015). Our main hypotheses were: 1) ’cleaned’ TMS–EEG responses obtained using the sensory control procedure would

reliably reflect the direct cortical activation by TMS. 2) 'cleaned' TMS–EEG responses would be altered by scopolamine and biperiden, but not placebo. We further hypothesized that scopolamine and biperiden had differential effects on these TMS–EEG responses because of their receptor selectivity.

2 Results

This section contains two original research works, each corresponding to one aim of this thesis. All results presented have been published in peer-reviewed journals.

2.1 Evoked EEG Responses to TMS Targeting Regions Outside the Primary Motor Cortex and Their Test–Retest Reliability (Song et al., 2024)

Brain Topography (2024) 37:19–36
https://doi.org/10.1007/s10548-023-01018-y

ORIGINAL PAPER

Evoked EEG Responses to TMS Targeting Regions Outside the Primary Motor Cortex and Their Test–Retest Reliability

Yufei Song[1,2] · Pedro C. Gordon[1,2] · Johanna Metsomaa[1,2,3] · Maryam Rostami[4] · Paolo Belardinelli[1,2,5] · Ulf Ziemann[1,2]

Received: 16 June 2023 / Accepted: 25 October 2023 / Published online: 23 November 2023

Abstract

Transcranial magnetic stimulation (TMS)–evoked electroencephalography (EEG) potentials (TEPs) provide unique insights into cortical excitability and connectivity. However, confounding EEG signals from auditory and somatosensory co-stimulation complicate TEP interpretation. Our optimized sham procedure established with TMS of primary motor cortex (Gordon in JAMA 245:118708, 2021) differentiates direct cortical EEG responses to TMS from those caused by peripheral sensory inputs. Using this approach, this study aimed to investigate TEPs and their test–retest reliability when targeting regions outside the primary motor cortex, specifically the left angular gyrus, supplementary motor area, and medial prefrontal cortex. We conducted three identical TMS–EEG sessions one week apart involving 24 healthy participants. In each session, we targeted the three areas separately using a figure-of-eight TMS coil for active TMS, while a second coil away from the head produced auditory input for sham TMS. Masking noise and electric scalp stimulation were applied in both conditions to achieve matched EEG responses to peripheral sensory inputs. High test–retest reliability was observed in both conditions. However, reliability declined for the 'cleaned' TEPs, resulting from the subtraction of evoked EEG response to the sham TMS from those to the active, particularly for latencies > 100 ms following the TMS pulse. Significant EEG differences were found between active and sham TMS at latencies < 90 ms for all targeted areas, exhibiting distinct spatiotemporal characteristics specific to each target. In conclusion, our optimized sham procedure effectively reveals EEG responses to direct cortical activation by TMS in brain areas outside primary motor cortex. Moreover, we demonstrate the impact of peripheral sensory inputs on test–retest reliability of TMS-EEG responses.

Keywords Transcranial magnetic stimulation · Electroencephalography · TMS-EEG · Optimized sham procedure · Evoked potentials · Test–retest reliability

Introduction

Transcranial magnetic stimulation (TMS) is a non-invasive technique that can activate neuronal circuits in the cortex via an induced electric field (Barker et al. 1985). Simultaneous electroencephalography (EEG) can be combined with TMS to probe cortical responsivity to stimuli with millisecond-level temporal resolution (Ilmoniemi et al. 1997). TMS-evoked potentials (TEPs) are one of the resulting outcomes, and they are time-locked deflections that demonstrate high consistency and responsiveness to variations in the stimulation parameters, e.g., TMS intensity and cortical locations (Bortoletto et al. 2015; Tremblay et al. 2019). TEPs are hypothesized to reflect the effects of TMS on the local neural circuits and networks, which suggests their application as a measure of cortical excitability and connectivity. However,

Handling Editor: Carlo Miniussi.

✉ Ulf Ziemann
ulf.ziemann@uni-tuebingen.de

[1] Department of Neurology and Stroke, University of Tübingen, Hoppe-Seyler-Straße 3, 72076 Tübingen, Germany

[2] Hertie Institute for Clinical Brain Research, University of Tübingen, Tübingen, Germany

[3] Department of Neuroscience and Biomedical Engineering, Aalto University School of Science, Espoo, Finland

[4] Faculty of Electrical and Computer Engineering, University of Tehran, Tehran, Iran

[5] Center for Mind/Brain Sciences, CIMeC, University of Trento, Trento, Italy

a recent discussion has arisen about the extent to which TEPs truly reflect the direct cortical activation induced by TMS (Belardinelli et al. 2019; Conde et al. 2019; Siebner et al. 2019). This is because the spatiotemporal patterns of TEPs resemble those of peripheral evoked potentials (PEPs), which are evoked by, e.g., electric stimulation (ES) applied to the scalp, or TMS applied to the shoulder (Conde et al. 2019; Herring et al. 2015). Findings from studies using PEP controlling approaches have reinforced the TEPs' capability to reflect direct cortical activation (Biabani et al. 2019; Gordon et al. 2021, 2023; Rocchi et al. 2021). However, supporting evidence for TMS of cortical regions outside the primary cortex (M1) is still limited.

Proper control of PEPs is essential for revealing direct cortical response to TMS and avoiding potential misinterpretation of TEPs. Nevertheless, achieving this can be challenging. PEPs are the cortical responses to multisensory inputs that are not directly related to the transcranial effects of TMS but still exhibit a time-locked relationship with it (Farzan and Bortoletto 2022; Hernandez-Pavon et al. 2023). The two main contributing EEG sources to PEPs are the auditory-evoked potentials (AEPs) and the somatosensory-evoked potentials (SEPs). The former is caused by the 'click' sound of the TMS pulse, which reaches the participant's inner ears through air and bone conduction. The latter is generated by multiple sources, including coil vibration and cranial muscle twitches. The activation of cranial sensory and motor axons, nerve bundles, and peripheral sensory receptors is believed to play a role (Siebner et al. 2022). To date, the approaches available to control these confounding factors have remained limited. For instance, masking noise (Massimini et al. 2005; Russo et al. 2022) has been commonly used during TMS–EEG data recording, aiming to minimize the AEPs by suppressing the auditory perception. However, complete effectiveness cannot be guaranteed when high TMS intensities are required as the louder 'click' sound from the TMS pulse may overwhelm the masking noise (Conde et al. 2019). Moreover, even when an optimal masking procedure is implemented (masking noise through earphones plus over-ear defender), TMS–EEG measurements are still at risk of presenting PEPs due to the effects of somatosensory inputs (Conde et al. 2019; Ross et al. 2022). Proposed approaches to deal with the confounding of SEPs include using foam padding to reduce coil vibration, limiting cortical targets to regions close to the midline where cranial muscle artifact is minimal, and online fine-tuning stimulation parameters to minimize artifacts (Casarotto et al. 2022). These strategies certainly offer some benefits, but each has its caveats, and none is reliable enough to address the contamination by PEPs sufficiently.

An alternative approach is to apply a sham condition that recreates the same multisensory inputs expected from TMS without transcranially activating the cortex. In this instance, the contribution of sensory inputs to the TMS–EEG responses can be determined by comparing the results between active and sham conditions. Sham TMS conditions often include a second TMS coil placed away from the scalp to produce a 'click' sound and scalp ES to simulate TMS-associated somatosensory inputs (Conde et al. 2019; Fernandez et al. 2021; Raffin et al. 2020; Rocchi et al. 2021). In principle, PEPs generated in the sham TMS condition can be subtracted from, or statistically compared to, the EEG responses elicited by the active TMS condition, thus revealing the EEG responses to direct cortical activation by TMS. However, since the somatosensory inputs related to TMS are qualitatively different from cutaneous ES, one drawback of this design is the potential mismatch of PEPs elicited by sham and active TMS conditions. To mitigate this issue, our group introduced an optimized sham stimulation procedure: By delivering high-intensity ES during both active and sham TMS pulses, we aimed to saturate the EEG response to sensory inputs. Consequently, the additional sensory input from TMS in the active condition is negligible, resulting in matched PEPs from the sham and the active TMS conditions. We successfully tested this approach using TMS targeting the left M1. After removing PEPs from the evoked EEG responses in the active TMS condition, we identified typical deflections lateralized to the TMS site within the first hundred milliseconds after the TMS pulse (Gordon et al. 2021).

Here, we sought to utilize this approach further to investigate the TMS evoked EEG responses of regions outside M1. To this end, three cortical areas, the left angular gyrus (AG), supplementary motor area (SMA) and medial prefrontal cortex (mPFC) were targeted. These areas are known to be involved in various cognitive and motor functions and have gained growing interest in TMS studies as possible targets for therapeutic interventions (Gordon et al. 2022; Lefaucheur et al. 2020; Seghier 2023). In the present study, participants underwent three identical sessions at least one week apart. Within each session, the three cortical areas were targeted separately, and an optimized sham procedure adapted from our previous study was applied (Gordon et al. 2021). As outcomes, we investigated the test-retest reliability of TMS–EEG responses between repeated sessions. Then, the EEG responses elicited by the active TMS were compared with those from the sham TMS condition for all TMS targets. We hypothesized that, using this approach, differences in EEG responses between the active and sham TMS conditions could be identified, which would reflect the target area specific characteristics of direct cortical activation caused by TMS.

Methods

Participant and General Procedure

Twenty-four healthy participants were recruited (mean age ± SD, 25.7 ± 4.8 years; 14 females) for the study. Inclusion criteria were no history of neurological or psychiatric disorders and no intake of medication acting on the central nervous system. The experimental procedures were approved by the ethics committee of the medical faculty of Tübingen University (protocol number 638/2020BO1). All participants provided written informed consent at enrollment in accordance with the declaration of Helsinki.

Prior to the main measurements, magnetic resonance imaging (MRI) with a T1-weighted sequence was obtained for each participant. The individualized MRI was used for TMS neuronavigation, EEG electrode location pin-pointing, and EEG source reconstruction. The main experiment consisted of three sessions (at least one week apart). During each session, participants' resting motor threshold (RMT) was determined, and then they underwent three TMS–EEG blocks. In each block, either mPFC, AG, or SMA was targeted, and the order of the blocks was randomized for each participant and session. Both sham and active TMS were conducted for every block (see details in section "Optimized sham TMS procedure"). Participants were instructed to sit on a chair in a relaxed and still position with their eyes open throughout the measurements. To ensure head stability and comfort, a vacuum pillow was fitted around the neck. At the beginning of each TMS–EEG block during the first session, participants were asked to rate their perception of auditory and somatosensory inputs from the active and sham conditions (Gordon et al. 2021). This was done using a visual analog scale (VAS) ranging from 0 to 10, with 0 representing no perception and 10 representing maximal perception. The VAS included items assessing the intensity of auditory sensation, the intensity of scalp sensation, the area size of scalp sensation, and the intensity of pain or discomfort.

TMS–EEG Setup

Two identical TMS stimulators (Magstim® 200^2, monophasic mode, UK) equipped with figure-of-eight coils (external diameter = 90 mm) were used in the study (one for active TMS condition, one for sham condition). A navigation system (TMS Navigator, Localite GmbH, Germany) was used for planning and monitoring coil positioning throughout the measurement. We aligned the individual MRI with the MNI coordinate system, and the cortical targets were defined with the following MNI coordinates: mPFC (− 4, 52, 36); left AG (− 42, − 69, 31); SMA (− 2, − 7, 55). The active TMS coil was positioned perpendicularly to the underlying gyrus, with the induced current running approximately from lateral to medial for targeting mPFC and SMA, and from posterior-medial to anterior-lateral for TMS at AG. We set the intensity for each target in active TMS conditions to 120% RMT. The RMT was measured in a standard manner (Groppa et al. 2012): bipolar surface Electromyographic (EMG) electrodes were attached to the abductor pollicis brevis (APB), and first dorsal interosseus (FDI) muscles of the right-hand, EMG signals were sampled at 5 kHz (device filter DC-1250 Hz). The hotspot for M1 was determined as the cortical representation of the hand eliciting the largest and consistent motor-evoked potential (MEP) with slightly suprathreshold TMS pulses. The RMT was defined as the lowest intensity that produced MEP over 50 μV in at least 5 out of 10 pulses.

We recorded EEG signals with a TMS-compatible system (NeurOne, Bittium, Kuopio, Finland). Ag/AgCl sintered ring electrodes were placed according to the International 10-5 system in an elastic cap (EasyCap BC-TMS-64, EasyCap, Germany). EEG positions relative to each participant's MRI were digitized and saved in the navigation system. EEG signals were sampled at 5 kHz (device filter DC-1250Hz), and electrode CPz served as the reference online while the ground was placed at PPO1h. EEG electrode impedances were maintained below 5 kΩ.

Optimized Sham TMS Procedure

The optimized sham stimulation procedure was adapted from our previous research (Gordon et al. 2021). To recreate TMS-associated somatosensory inputs for the sham TMS condition, we applied ES pulses with a stimulator (Digitimer DS7A, Digitimer Ltd.UK) through short-distance bipolar electrodes attached to the scalp. To reproduce the 'click' sound, a TMS coil was placed away from the participant's head, ensuring minimal magnetic-field impact on the cortex. The TMS intensity in sham was set to 1.6 times of active TMS to account for the increased distance (Gordon et al. 2021). Additionally, masking noise was played throughout the measurement to suppress the auditory perception (Massimini et al. 2005). The volume of masking noise was individually adjusted so that the 'click' sound became barely audible but not too loud to induce discomfort. For the active TMS condition, the TMS coil positions were defined as in section "TMS–EEG setup", and masking noise was also applied. Fig. 1 illustrates the example of targeting SMA.

To ensure comparable PEPs between the sham and active TMS conditions, we aimed to saturate the EEG response to sensory inputs. For this purpose, the scalp ES

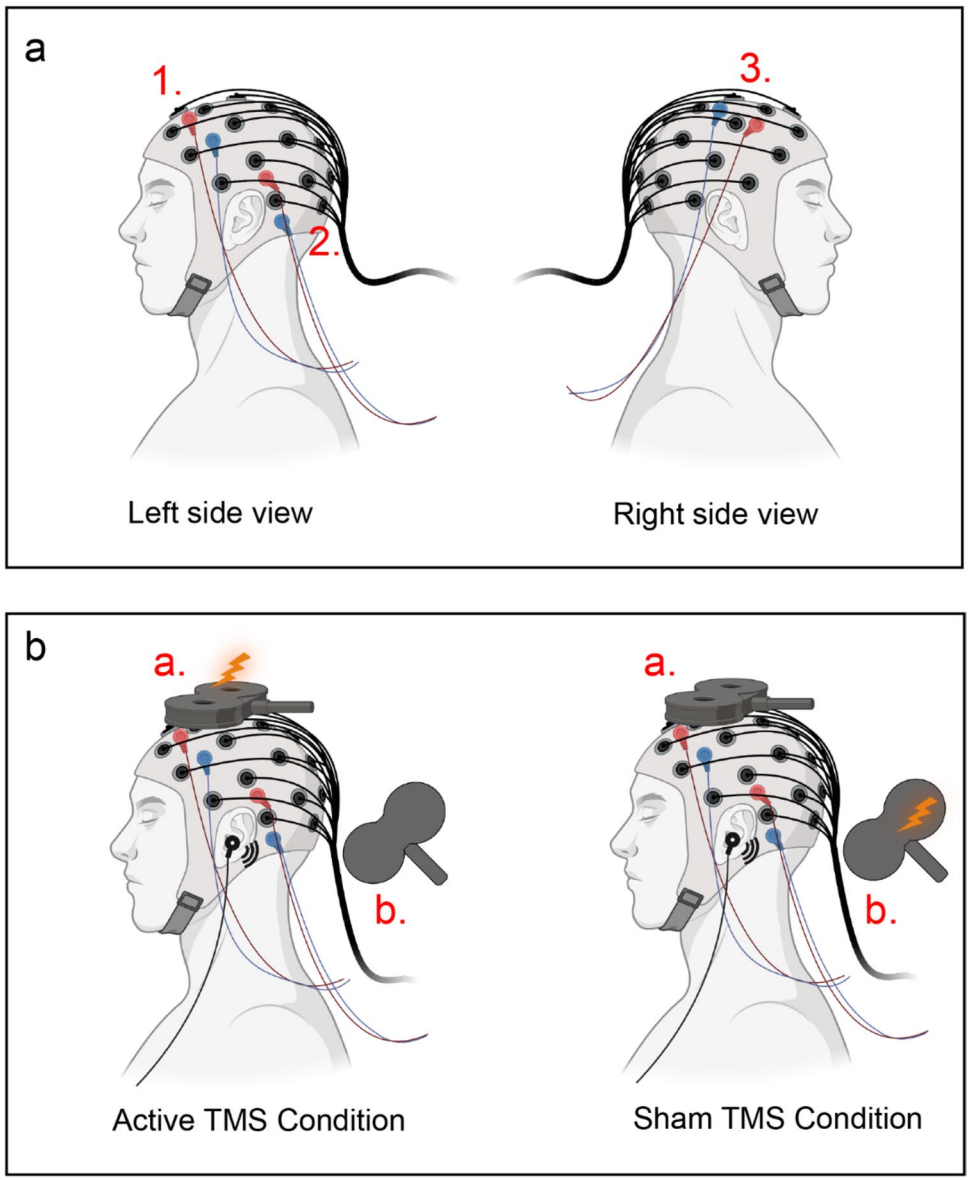

Fig. 1 Schematic illustration of the optimized sham procedure during SMA stimulation. **a** Electrodes montage for ES. Three pairs of short-distance bipolar electrodes were attached to the EEG cap. Pair 1 (frontal: AFF1H, AFF5H) and 2 (parietal: TPP7H, TPP9H) were placed in the left hemisphere, and pair 3 (central: FFC4H, FCC4H) was in the right hemisphere. The color code used is red for the anode and blue for the cathode. **b** Experimental setup for the sham and active TMS conditions. Two identical TMS coils (**a** and **b**) were used. Coil a was positioned over the participant's head to target SMA. Coil b was placed away from the head. Coil a was active in the active condition, while coil b was active in the sham condition. Concomitant ES (via three electrode pairs, intensity 24 mA, pulse width 200 µs), and masking noise were applied in both conditions (icons were created with BioRender.com). *ES* electric stimulation, *SMA* supplementary motor area, *TMS* transcranial magnetic stimulation (Color figure online)

pulses were applied to both conditions with a high intensity of 24 mA (width 200 µs, maximum voltage of 400 V) through three pairs of bipolar electrodes. These electrode pairs were positioned near the three TMS targets: the first pair was in the frontal area (AFF1h and AFF5h), the second pair was in the parietal area (TPP7h, TPP9h), and the last pair was in the central area (FFC4h, FCC4h) (Fig. 1a). All pairs were fired together, and the polarity of each pair was switched after each pulse. These ES parameters were chosen according to a pilot test during which the participant reported a strong, spread but tolerable perception. For each TMS–EEG block, we recorded 150 pulses for the active TMS conditions and 50 for sham conditions, with the sham stimulation trials randomly interleaved within the active TMS conditions. Consequently, a total of 150 pulses were recorded for the sham conditions across the three TMS–EEG blocks. The interstimulus interval (ISI) was 3s (± 1s jitter; 2–4s range).

TMS–EEG Data Preprocessing

Offline EEG analyses were performed in Matlab environment (version 2022a, MathWorks Inc.). EEGLAB (Delorme and Makeig 2004), FieldTrip (Oostenveld et al. 2011), and customized scripts were used.

Individual TMS–EEG data were preprocessed separately for each TMS target with the following steps. First, the continuous raw data were epoched around TMS pulses with a time window of − 1500 to 1500 ms, and baseline correction was done with respect to the time window of − 1000 to − 5 ms. We then concatenated the data from the sham (150 epochs) and active condition (150 epochs)

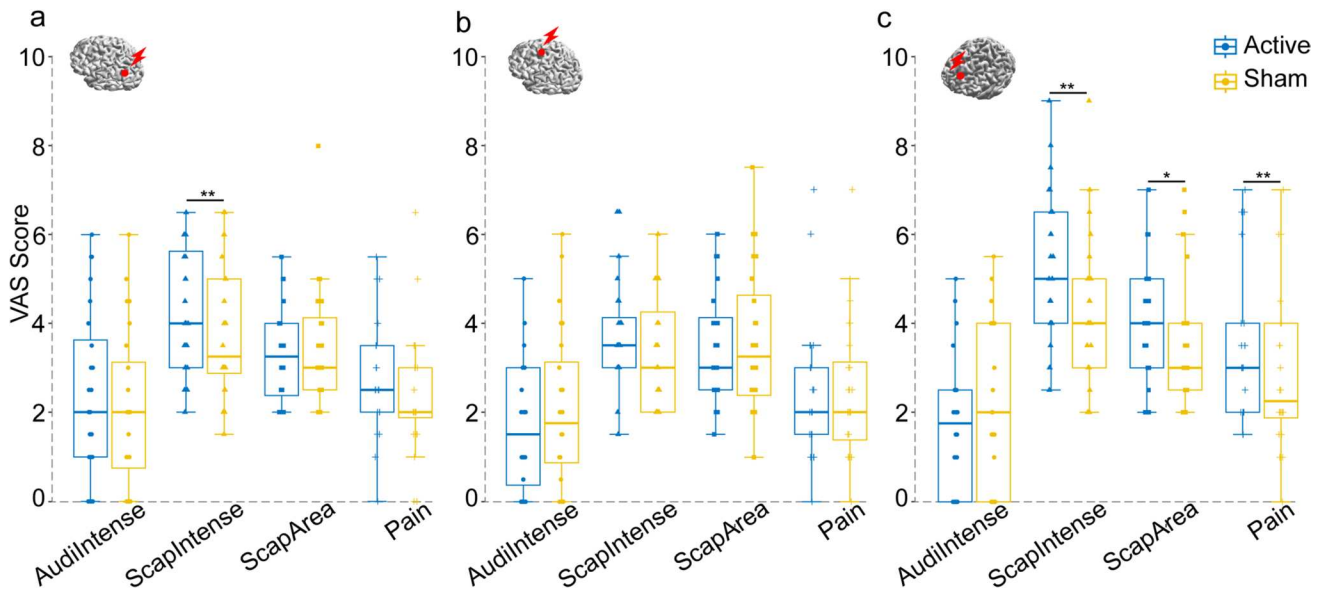

Fig. 2 Comparison of perceptions in active TMS vs. sham TMS conditions. Box plots show the VAS scores for the four perception items: auditory intensity (AudiIntense), scalp intensity (ScapIntense), scalp area size (ScapArea), and pain or discomfort (Pain) following AG (**a**), SMA (**b**), and mPFC (**c**) stimulations, *p < 0.05; ** p < 0.001. *AG* angular gyrus, *mPFC* medial prefrontal cortex, *SMA* supplementary motor area, *TMS* transcranial magnetic stimulation, *VAS* visual analogue scale

before proceeding with the rest of the steps. The rationale is to ensure an equal artifact rejection procedure for both conditions and avoid bias from inconsistent data processing. A robust detrending function (3rd-order polynomial fitting) was then performed to remove the ongoing trend. To estimate the trend line based on the pre-and post-evoked EEG signal only, the time interval of − 20 to 600 ms containing the evoked potentials were excluded from the polynomial fitting (de Cheveigné and Arzounian 2018; Hernandez-Pavon et al. 2022). Subsequently, we re-segmented the data into a shorter time window (− 1000 to 1000 ms) to cut out edge artifacts. The decay artifacts were then removed with a customized fit decay function (brief description in Supplementary Materials: section 1.1). Next, TMS and ES pulse artifacts (− 4 to 17 ms) were eliminated and cubic-interpolated before resampling to 1 kHz. Channels and trials heavily contaminated by noise or artifacts were manually excluded via visual inspection. The following preprocessing steps were based on a newly proposed framework (Metsomaa et al. in submission): The ocular artifact topographies were identified using FastICA and saved for removal in a later step (Hyvarinen 1999). Next, the SSP–SOUND joint algorithm was used to estimate the signal subspace containing the TMS-related artifacts and suppress them from EEG signals. To maintain consistent spatial properties, the saved ocular topographies were also modified with the same SSP–SOUND correction matrix as the data. Data were then re-referenced to the average, and ocular artifacts were corrected using the beamforming filter with the modified ocular topographies (Hernandez-Pavon et al. 2022). In the end, the removed channels were interpolated using spherical interpolation based on the surrounding channels. We then separated data into sham and active TMS conditions. The epochs within each condition were averaged, resulting in the evoked EEG potentials. To obtain the 'cleaned' TEPs, the evoked potential from the sham was subtracted from the active conditions (Active-Sham) (Gordon et al. 2021).

Analysis and Statistics

Visual Analogue Scales VAS

The VAS scores regarding the perception of auditory and somatosensory inputs in the active TMS and sham conditions were analyzed using R software. To assess the differences in perception between active TMS and sham conditions, we compared each sensation item using the Wilcoxon signed-rank test (for two dependent conditions) for each TMS target. The difference was considered significant at $p < 0.05$.

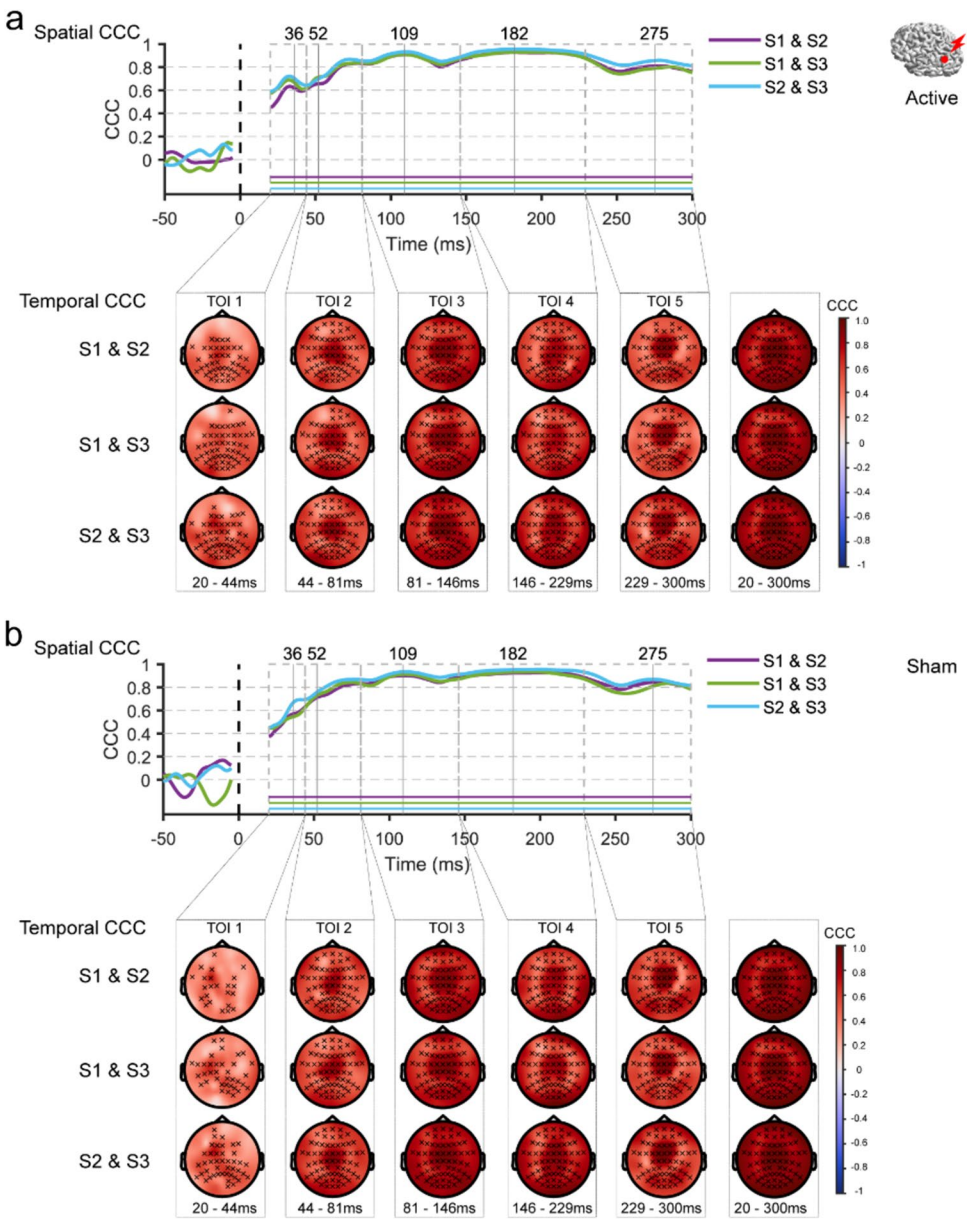

Fig. 3 Test–retest reliability of the evoked EEG potentials by active TMS (**a**) and sham TMS (**b**) of AG. The red dot on a template brain indicates the cortical target. The upper panel shows the spatial inter-session CCCs, with traces (purple, green, and blue) representing the group averages of CCCs for each pair of sessions. Horizontal lines indicate time points where CCCs significantly differ from zero. The lower panel displays topography of the temporal CCCs within each TOI, x indicating electrodes with CCCs significantly different from zero. *AG* angular gyrus, *CCC* concordance correlation coefficient, *S1*, *S2*, *S3* sessions 1–3, *TMS* transcranial magnetic stimulation, *TOI* time window of interest (Color figure online)

Global Mean Field Amplitude (GMFA)

GMFA is the standard deviation of voltage values across all electrodes at a given time point. As shown below, t is time, V_i is the voltage at channel i, V_{mean} is the mean of the voltage over all channels, and K is the number of channels.

$$GMFA = \sqrt{\frac{\sum_i^k \left(V_i(t) - V_{mean}(t)\right)^2}{K}} \quad (1)$$

Besides indicating global EEG activities, GMFA was also used to identify time windows of interest (TOIs). The determination of TOIs involved using a peak detection algorithm to divide the 20–300 ms post-stimulation window into shorter epochs based on the detected peaks (Rogasch et al. 2020). Specifically, the algorithm was applied to the mean GMFA of sham and active conditions, ensuring an independent data selection approach that is uncorrelated with the condition comparison (Cohen 2014). As early peaks were not identifiable in the mean GMFA, peaks (or troughs) were extracted from the mean evoked potentials of sham and active conditions, averaged across electrodes near the TMS target. This approach resulted in the identification of five TOIs for each target.

Test–Retest Reliability

The test-retest reliability of TMS–EEG measures was assessed via the intersession concordance correlation

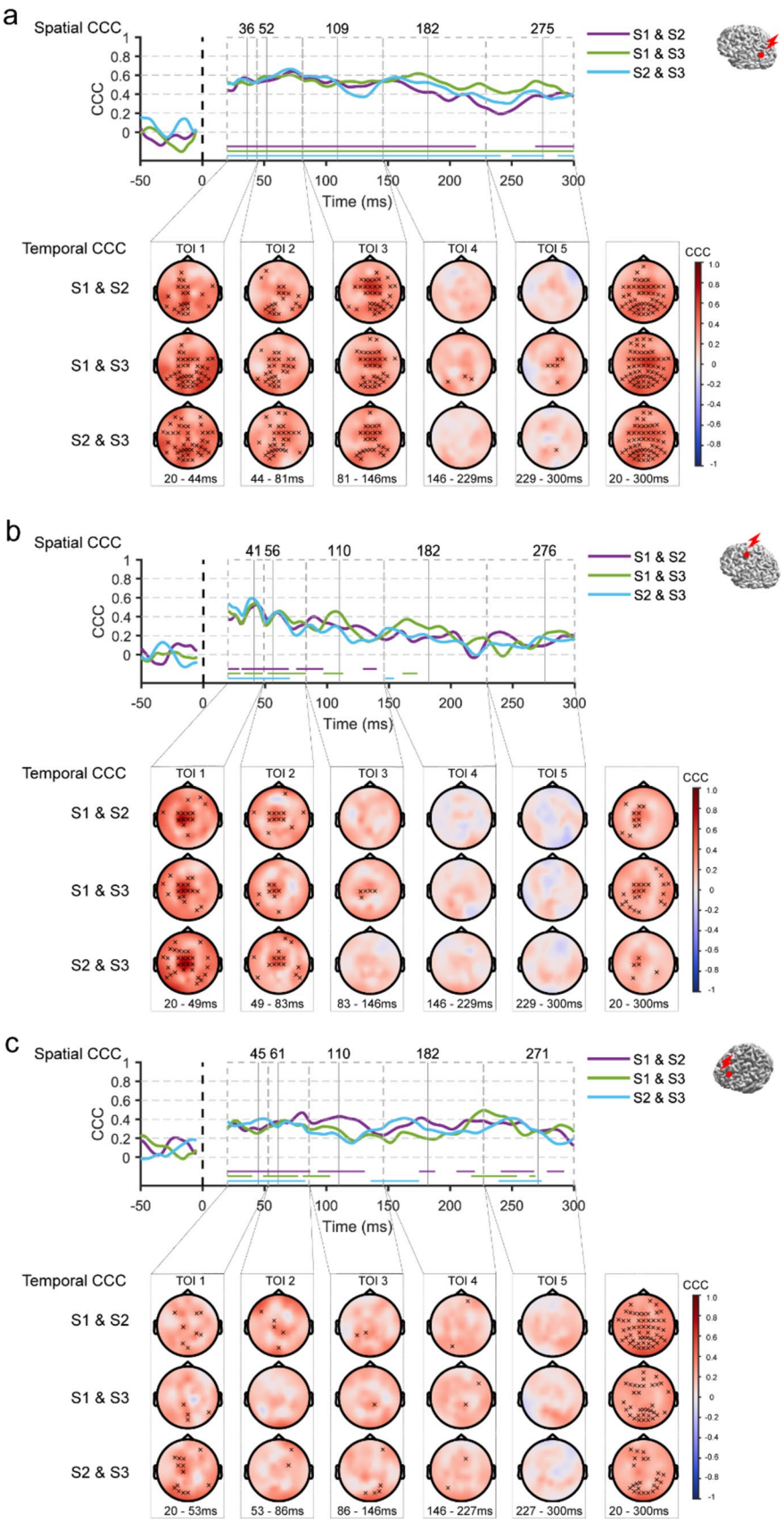

Fig. 4 Test–retest reliability of the'cleaned' TEPs (Active-Sham) following AG (**a**), SMA (**b**) and mPFC (**c**) stimulations. The red dot on a template brain indicates the cortical target. The upper panel shows the spatial inter-session CCCs, with traces (purple, green, and blue) representing the group averages of CCCs for each pair of sessions. Horizontal lines indicate time points where CCCs significantly differ from zero. The lower panel displays topography of the temporal CCCs within each TOI, x indicating electrodes with CCCs significantly different from zero. *AG* angular gyrus, *CCC* concordance correlation coefficient, *mPFC* medial prefrontal cortex, *S1*, *S2*, *S3* sessions 1–3, *SMA* supplementary motor area, *TMS* transcranial magnetic stimulation, *TOI* time window of interest (Color figure online)

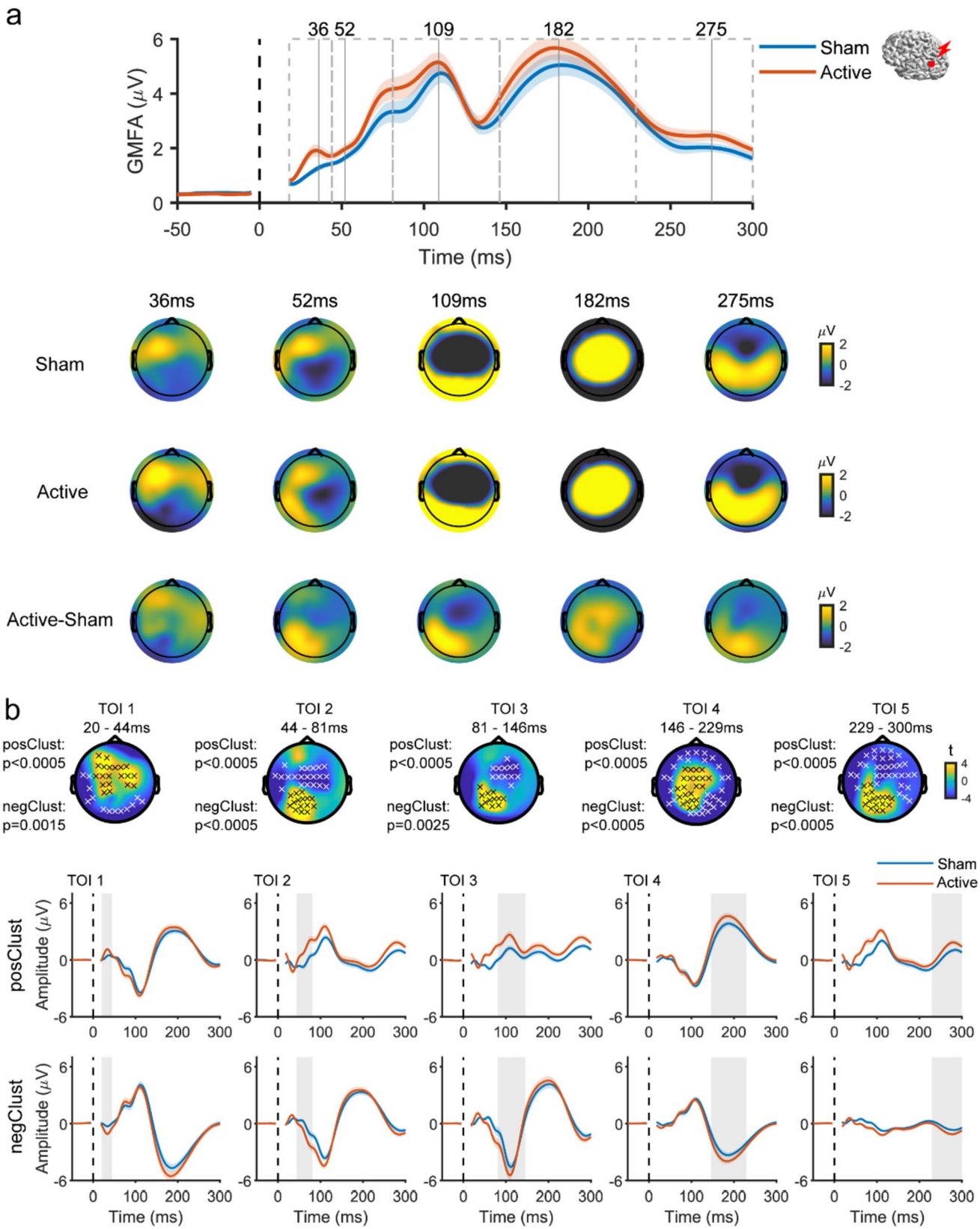
a
36 52
109
182
275
Sham
Active
GMFA (μV)
Time (ms)
36ms
52ms
109ms
182ms
275ms
Sham
Active
Active-Sham
μV
b
TOI 1
20 - 44ms
TOI 2
44 - 81ms
TOI 3
81 - 146ms
TOI 4
146 - 229ms
TOI 5
229 - 300ms
posClust:
p<0.0005
negClust:
p=0.0015
negClust:
p<0.0005
negClust:
p=0.0025
t
posClust
negClust
Amplitude (μV)
Time (ms)

◂**Fig. 5** Comparison of the evoked EEG potentials by active TMS vs. sham TMS of AG **a** Above, GMFA of the evoked EEG potentials. The solid lines (blue: sham, red: active) represent the group averages, and shaded areas indicate the standard error. Dashed boxes represent TOIs with vertical lines indicating the timing of peaks. Below, topographies show the spatial distribution of the evoked EEG potentials at peak latencies in three conditions: sham (top row), active (middle row), and 'cleaned' (active-sham; bottom row). **b** Results of cluster-based t-test. Topographies show t-statistic maps within each TOI. Above, electrodes that contribute to significant positive and negative clusters are highlighted with black x and white x, respectively. The corresponding p values are displayed to the left. Below, evoked EEG potentials were averaged across electrodes comprising the significant clusters (top: positive, bottom: negative). The solid lines (blue: sham, red: active) represent the group averages, and the shaded areas are the standard error. Shaded grey columns correspond to the TOIs. *AG* angular gyrus, *GMFA* global mean field amplitude, *TMS* transcranial magnetic stimulation, *TOI* time window of interest (Color figure online)

coefficient (CCC). CCC is a form of intraclass correlation coefficient to assess agreement between partitions. It has been used for evaluating the test-rest reliability of TEPs across repeated tests (Bertazzoli et al. 2021; Kerwin et al. 2018; Moffa et al. 2022; Schambra et al. 2015).

$$CCC = \frac{2\sigma_{12}}{\sigma_1^2 + \sigma_2^2 + \left(u_1 - u_2\right)^2} \quad (2)$$

where σ_{12} is the covariance between two partitions, σ_x is the variance, μ_x is the mean (Lawrence and Lin 1989). Inter-session CCCs for TMS–EEG responses were calculated pair-wisely between sessions (S1 v S2, S1 v S3, S2 v S3) in spatial (for each given time point across all electrodes) and temporal (for each given electrode across TOIs) domains. For temporal reliability, CCCs were calculated within each TOI and the whole time window. Since the estimated CCCs follow an asymptotic normal distribution, the inverse hyperbolic tangent transformation (Fisher z-transformation) was used to improve the approximation to a normal distribution (Lawrence and Lin 1989). At the group level, CCCs were averaged across participants. We expected the CCC values to fluctuate around zero if the EEG responses could not be replicated between sessions. Therefore, one-sample permutation t-tests were applied with the null hypothesis that CCCs from each time point (spatial correlation) or each electrode (temporal correlation) were no different from zero. Multiple comparisons were controlled by the t_{max} method (Blair and Karniski 1993). Averaged CCCs were transformed back to the original scale with inverse Fisher z-transformation for visualization. In addition, we employed a scale proposed by (Shrout 1998) to interpret CCC values as in previous research (Bertazzoli et al. 2021; Moffa et al. 2022): 0.00–0.10 virtually no reliability, 0.11–0.40 slight, 0.41–0.60 fair, 0.61–0.80 moderate, and 0.81–1.0 substantial reliability. Additionally, the CCCs were also examined at the individual level to explore whether the TMS-EEG responses were stable across sessions within and between individuals (Ozdemir et al. 2021). The methods and results can be found in Supplementary Materials: Sects. 1.2 and "Participant and general procedure".

Comparing the Evoked EEG Responses to the Active and Sham TMS

We next investigated the difference in the EEG spatiotemporal profile between the active and sham conditions for each TMS target. The cluster-based permutation t-test was applied to compare evoked EEG potentials from both conditions across time points and electrodes (Maris and Oostenveld 2007). Since the size of later clusters could bias the detection of smaller earlier clusters, statistical analysis was performed within each TOI instead of the whole time window. The statistical significance was assessed by testing the null hypothesis that evoked EEG responses were exchangeable between active and sham conditions (cluster threshold: $p < 0.05$ dependent t-test, alpha < 0.05 two-tailed; randomization = 2000), and the critical alpha level was corrected with Bonferroni by the number of TOIs.

To better visualize cortical activation, we projected the scalp EEG signals from the active and sham conditions to source space using l2-minimum-norm estimation (MNE). For the forward solution, each participant's T1 image was processed through a pipeline involving the Fieldtrip, FreeSurfer software (Fischl 2012), HCP-workbench, and SPM toolboxes jointly with custom-made scripts. The source model was built on a triangulated cortical mesh with 15,684 vertices. The resulting cortical meshes were surface-registered to a common spherical template, which enables direct comparison of source locations with the same index across participants. A 3-D compartment volume conductor model was created individually with the Boundary Element Method (Stenroos and Nummenmaa 2016). Three meshes were constructed to define the following compartments: inner skull, outer skull, and scalp. The conductivity inside each boundary surface was set to 0.33 S/m, 0.0041 S/m, and 0.33 S/m, respectively. EEG electrode positions were aligned with the generated scalp surface. For the inverse estimation, the cortical distributed sources were assumed to have fixed orientations (perpendicular to the gray-white matter surface). The source covariance matrix was assumed such that nearby sources were more correlated than distant sources (according to Gaussian as a function of distance), and Tikhonov regularization was used for numerical stabilization of the matrix inverse (more details in Supplementary Materials: sect. 1.3). The reconstructed current source density for evoked EEG responses was z-score normalized with respect to a pre-stimuli time window (− 600 to − 100 ms). At group level, normalized current density was averaged across participants,

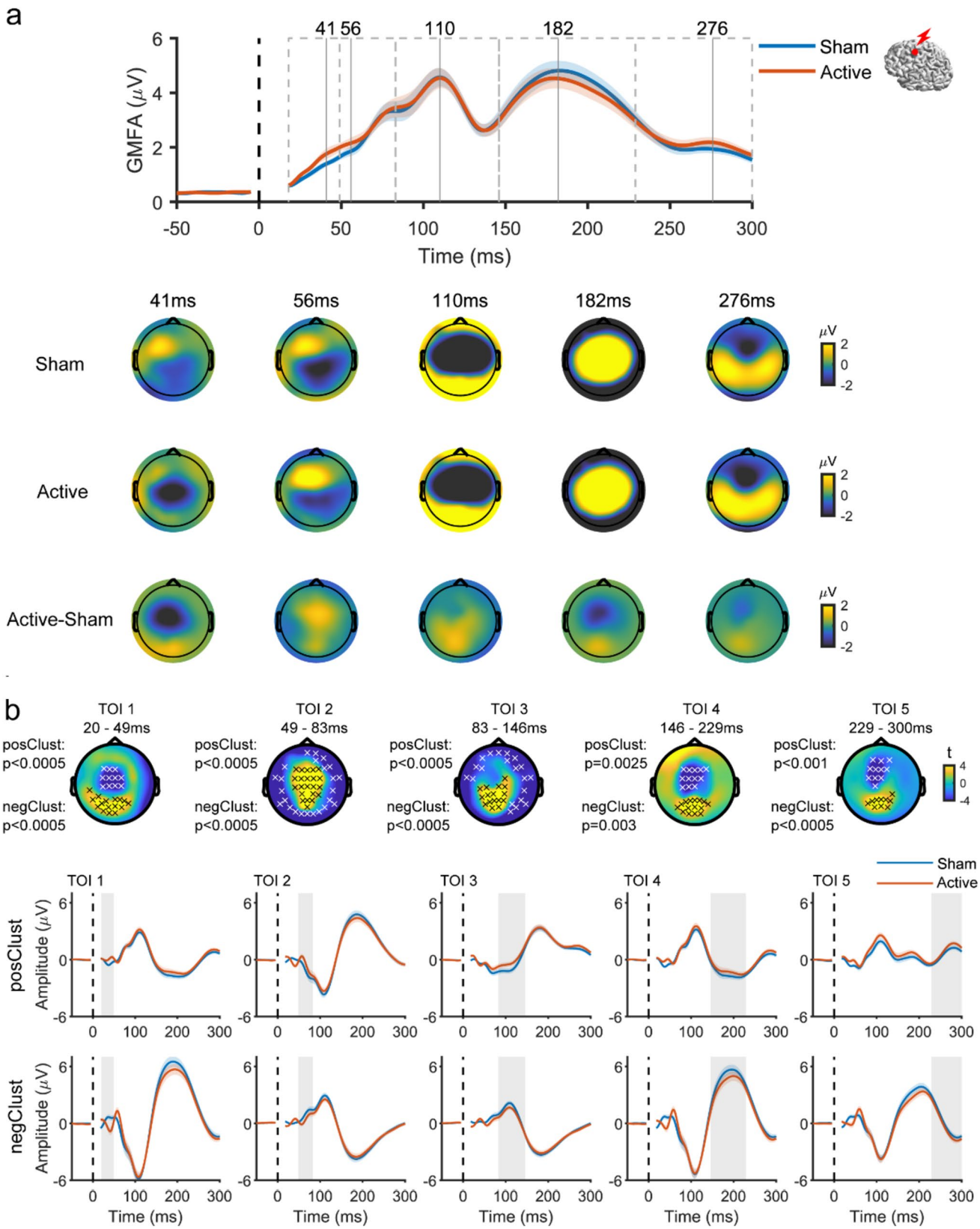
a
41 56
110
182
276
Sham
Active
GMFA (μV)
Time (ms)
41ms
56ms
110ms
182ms
276ms
Sham
Active
Active-Sham
μV
b
TOI 1
20 - 49ms
TOI 2
49 - 83ms
TOI 3
83 - 146ms
TOI 4
146 - 229ms
TOI 5
229 - 300ms
posClust:
p<0.0005
negClust:
p<0.0005
posClust:
p<0.0005
negClust:
p<0.0005
posClust:
p<0.0005
negClust:
p<0.0005
posClust:
p=0.0025
negClust:
p=0.003
posClust:
p<0.001
negClust:
p<0.0005
t
Sham
Active
posClust
negClust
Amplitude (μV)
Time (ms)

◂**Fig. 6** Comparison of the evoked EEG potentials by active TMS vs. sham TMS of SMA **a** Above, GMFA of the evoked EEG potentials. The solid lines (blue: sham, red: active) represent the group averages, and shaded areas indicate the standard error. Dashed boxes represent TOIs with vertical lines indicating the timing of peaks. Below, topographies show the spatial distribution of the evoked EEG potentials at peak latencies in three conditions: sham (top row), active (middle row), and 'cleaned' (active-sham; bottom row). **b** Results of cluster-based t-test. Topographies show t-statistic maps within each TOI. Electrodes that contribute to significant positive and negative clusters are highlighted with black x and white x, respectively. The corresponding p values are displayed to the left. Below, evoked EEG potentials were averaged across electrodes comprising the significant clusters (top: positive, bottom: negative). The solid lines (blue: sham, red: active) represent the group averages, and the shaded areas are the standard error. Shaded grey columns correspond to the TOIs. *GMFA* global mean field amplitude, *SMA* supplementary motor area, *TMS* transcranial magnetic stimulation, *TOI* time window of interest (Color figure online)

and the spatiotemporal patterns were displayed on the common cortical template.

Results

VAS: Active TMS Condition vs. Sham TMS Condition

The differences in VAS scores between active and sham TMS conditions are shown in Fig. 2. For AG stimulation, a significant difference was present only in the intensity of scalp between the active TMS and the sham condition (auditory intensity: $p = 0.393$; scalp intensity: $p = 0.005$; scalp area size: $p = 0.659$; pain: $p = 0.096$;). However, there were no significant differences in perception between the two conditions when SMA was stimulated (auditory intensity: $p = 0.111$; scalp intensity: $p = 0.086$; scalp area size: $p = 0.778$; pain: $p = 0.904$;). For mPFC stimulation, the perception of the scalp intensity, the scalp area size, and the discomfort significantly differed between the two conditions, but not for the auditory intensity (auditory intensity: $p = 0.075$; scalp intensity: $p = 0.001$; scalp area size: $p = 0.026$; pain: $p = 0.008$).

Test–Retest Reliability of TMS–EEG Responses

We first assessed how reliable TMS–EEG responses were between repeated sessions. To this end, inter-session CCCs for EEG responses from the sham and the active TMS were calculated in spatial and temporal domains. For all TMS targets, the values of spatial CCCs from the active and sham conditions reached a high level (CCC > 0.8) from approximately 90 ms onwards. Likewise, significantly high temporal CCCs were observed at most electrodes after the earliest TOI. Figure 3 illustrates the spatiotemporal reliability pattern of the EEG responses elicited by active TMS when targeting AG. Similar patterns were observed for the sham and active TMS conditions at mPFC and SMA (Figs. S1, S2 in Supplementary Materials).

Given the similar results observed between the active and sham TMS conditions, it is likely that PEPs explain the high spatiotemporal CCCs between sessions in the active TMS condition. To investigate whether EEG responses remained highly reliable after the removal of PEPs, we further assessed the CCCs for the 'cleaned' TEPs (Active-Sham) in spatial and temporal domains between sessions. TMS of AG resulted in significant spatial CCCs over the first 200 ms (Fig. 4a). Specifically, a fair to moderate CCC ($0.4 < CCCs < 0.67$) was observed until approximately 190 ms, with a slight decrease after 100 ms. Many electrodes displayed significant temporal CCCs up to 150 ms after the TMS pulse. For SMA, spatial CCCs remained consistently significant until around 80 ms after the TMS pulse ($0.2 < CCCs < 0.6$), but the values dropped considerably thereafter. Temporal CCCs were highly significant within the first 80 ms in electrodes in the central area, corresponding to the targeted area (Fig. 4b). For mPFC, spatial CCCs were significant until approximately 80 ms after the TMS pulse ($0.2 < CCCs < 0.47$). However, low temporal CCCs were observed across the scalp, with few electrodes reaching significance between sessions (Fig. 4c). These results showed that inter-session CCC values for late EEG responses decreased after the removal of PEPs. Notably, significant spatial CCCs for early 'cleaned' TEPs were found for each target, while the strength of temporal CCCs varied.

Evoked EEG Responses to Active TMS vs. Sham TMS

We next assessed differences in the evoked EEG responses between the active and sham TMS conditions. The high test-retest reliability (as shown in Fig. 3 and Figs. S1, S2) indicated stable and consistent evoked EEG responses from both active and sham TMS conditions between sessions, so we combined the stimulation trials across the three sessions for each condition, aiming to maximize the signal-to noise ratio (SNR) of the evoked responses to both active and sham conditions. For each TMS site, the evoked potentials by the active and sham TMS conditions were compared using the cluster-based permutation t-test.

Despite the similarity of responses from both conditions, cluster analysis revealed significant differences in evoked EEG responses between the active and sham TMS conditions when applying TMS to the AG. Specifically, TMS of AG led to a higher positive amplitude deflection in frontal electrodes within the initial 40 ms, followed by a higher amplitude positive deflection at the left parietal area (the targeted region) up to and beyond 300 ms. In addition,

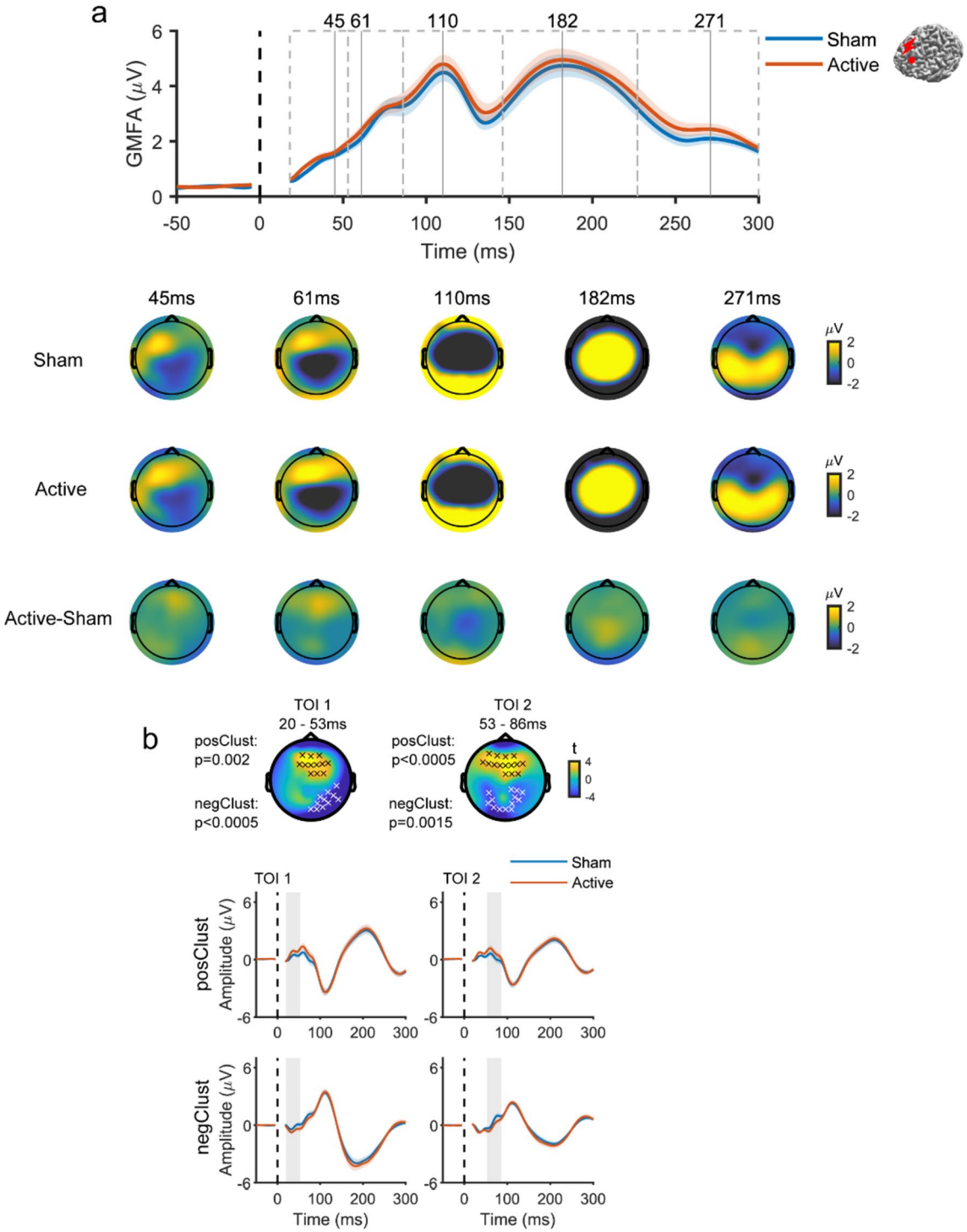

Fig. 7 Comparison of the evoked EEG potentials by active TMS vs. sham TMS of mPFC **a** Above, GMFA of the evoked EEG potentials. The solid lines (blue: sham, red: active) represent the group averages, and shaded areas indicate the standard error. Dashed boxes represent TOIs with vertical lines indicating the timing of peaks. Below, topographies show the spatial distribution of the evoked EEG potentials at peak latencies in three conditions: sham (top row), active (middle row), and 'cleaned' (active-sham; bottom row). **b**. Results of cluster-based t-test. Topographies show t-statistic maps within each TOI. Electrodes that contribute to significant positive and negative clusters are highlighted with black x and white x, respectively. The corresponding p values are displayed to the left. Below, evoked EEG potentials were averaged across electrodes comprising the significant clusters (top: positive, bottom: negative). The solid lines (blue: sham, red: active) represent the group averages, and the shaded areas are the standard error. Shaded grey columns correspond to the TOIs. *GMFA* global mean field amplitude, *mPFC* medial prefrontal gyrus, *TMS* transcranial magnetic stimulation, *TOI* time window of interest (Color figure online)

increased response amplitude was detected in the central area at around 200 ms (Fig. 5). TMS of SMA resulted in a negative deflection in the central area (the targeted region) within the first 50 ms, significantly differing from sham. The deflection transitioned into positive with significantly larger amplitude until 80 ms, then again became negative from 150 ms until and beyond 300 ms (Fig. 6). TMS to the mPFC resulted in a significantly higher amplitude positive deflection around the prefrontal area (the targeted region) within the first 80 ms when compared to the response from sham TMS (Fig. 7). These results showed that spatially distinguishable differences between the EEG responses in the active and sham TMS conditions could be detected for each TMS target.

To better visualize cortical activation following TMS at different targets, we applied source estimations to the evoked EEG responses from both sham and active TMS conditions. Sham responses were subtracted from the active TMS response. Three cortical regions of interest (ROIs) were chosen, corresponding to mPFC, SMA and AG (Fig. 8). The time series of local source activation was obtained by averaging the dipole activities within each ROI. Rapidly changing deflections were observed shortly after the TMS pulse for each target and subsided to baseline at around 300 ms. The spatial distribution illustrates the propagation of the TMS-evoked EEG response as time evolved. Instead of remaining localized to the targeted area, we noticed that the activation due to TMS propagated to distal regions. The evolved propagation became more apparent when inspecting the animations (see Animations 1-3 in Supplementary Materials for mPFC, SMA and AG, respectively). Reciprocal propagation of activation between prefrontal and parietal regions was observed when mPFC and AG were stimulated. In contrast, when stimulating SMA, the activation was more confined to the central and left sensorimotor cortex.

Discussion

We assessed the EEG responses resulting from TMS of three brain regions, the mPFC, AG, and SMA, focusing on their differences from EEG responses to multisensory inputs and their test-retest reliability. It is essential to distinguish the EEG responses arising from direct cortical activation and those resulting from multisensory co-stimulation. Failure to do so could leads to erroneously interpreting PEPs as 'true' TEPs (Biabani et al. 2019; Conde et al. 2019). To this aim, we used a recently developed optimized sham procedure that can consistently remove the entirety of the overlapping PEPs (Gordon et al. 2021). Our study yielded several findings. First, significant differences in the EEG responses between the active and the sham TMS conditions were revealed for all TMS targets, mainly in the first 90 ms after the TMS pulse. Moreover, specific spatial and temporal characteristics of these EEG responses varied depending on each target. Lastly, the test-retest reliability of late EEG responses considerably decreased after removing PEPs, in particular at latencies $> 80 - 100$ ms after the TMS pulse, and the reliability of early responses < 80 ms was variable across the targeted areas.

Separation of TEPs from PEPs

We found significant differences in EEG responses between the active and sham TMS conditions within the first 90 ms for all targets. Notably, these differences were centered around the respective targeted regions. Source estimation further demonstrated that the activation of cortical regions near the targeted area most likely accounted for the site-specific difference. Unlike the early responses (< 90 ms), which are known to be relatively unaffected by PEPs (Belardinelli et al. 2019; Conde et al. 2019; Gordon et al. 2021; Rogasch et al. 2020), the late TEPs can be heavily contaminated by components such as N100 and P200 (Biabani et al. 2019; Conde et al. 2019). N100 and P200 are commonly identified PEP components and various brain areas are thought to be involved, including primary and secondary somatosensory cortices, superior temporal cortex, insula, posterior and anterior cingulate cortices, and frontal cortex (Mouraux and Iannetti 2009). Thus, N100 and P200 typically exhibit large amplitudes with a broad frontocentral scalp distribution, whereas the 'true' TEPs have comparatively smaller amplitudes and greater topographical specificities, which can be overshadowed by the presence of PEPs. Nevertheless, when stimulating SMA, we identified a positive component of 'cleaned' TEPs at around 100 ms and a negative one at 200 ms in the central area (i.e., with opposite polarity to N100-P200). Moreover, the source estimation suggests these components are more evident in the central and left sensorimotor cortex (as shown Fig. 8b: middle row), which differs from the widespread PEPs with amplitudes usually greater in the hemisphere contralateral to stimulation (Hashimoto 1988). When stimulating AG, a negative component of 'cleaned' TEPs at around 100 ms and a positive at 200 ms in the central area were detected, which can also be inspected at the source level (Fig. 8b: top row). However, these responses more likely correspond to residual PEPs, in which the sensory inputs from the sham did not match those from the active TMS. The significant difference in VAS scores (the intensity of scalp sensation) between the sham and the active TMS condition may support this explanation (Fig. 2a). Interestingly, for mPFC stimulation, despite evident differences in perceptions between conditions (Fig. 2c), no significant components were detected in the late latencies of 'cleaned'

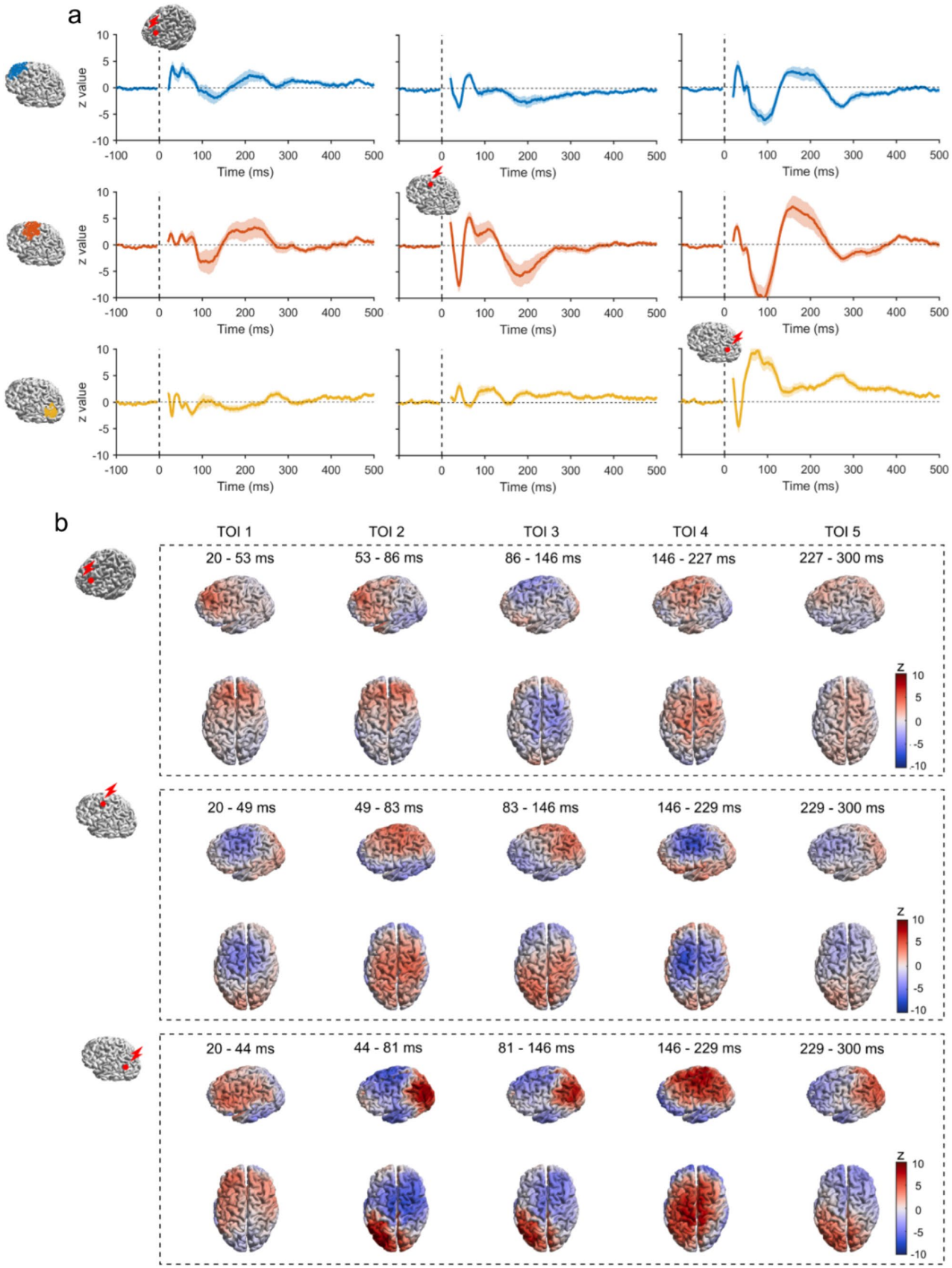
a
z value
Time (ms)
b
TOI 1
TOI 2
TOI 3
TOI 4
TOI 5
20 - 53 ms
53 - 86 ms
86 - 146 ms
146 - 227 ms
227 - 300 ms
20 - 49 ms
49 - 83 ms
83 - 146 ms
146 - 229 ms
229 - 300 ms
20 - 44 ms
44 - 81 ms
81 - 146 ms
146 - 229 ms
229 - 300 ms
z

◂**Fig. 8** Source activation pattern. **a** Temporal dynamics of source activation following mPFC (left column), SMA (middle column), or AG (right column) stimulations. The red dot on a template brain indicates the cortical target. The time series of normalized current density were averaged within the ROIs: mPFC (blue; top row), SMA (red; middle row), and AG (yellow; bottom row). The solid trace is the group average, and the shaded areas are the standard error. Plots on the diagonal are the effects of TMS on local cortical regions. Plots off the diagonal are the effects of TMS on distal cortical regions. **b** Spatial propagation of source activation following mPFC (top row), SMA (middle row), or AG (bottom row) stimulations. The normalized current density was averaged within the TOIs, and the spatial distribution of the group average is visualized from the left side and top views. *AG* angular gyrus, *mPFC* medial prefrontal gyrus, *ROI* region of interest, *SMA* supplementary motor area, *TMS* transcranial magnetic stimulation, *TOI* time window of interest (Color figure online)

TEPs (Fig. 7), indicating that PEPs from both conditions were considerably equivalent.

Besides the confinement of 'cleaned' TEPs to each targeted area (Farzan and Bortoletto 2022), our findings from stimulating three distinct areas provide further evidence of successful measures of 'true' TEPs. First, although the same sham TMS procedure was applied to all three active TMS conditions, comparing responses from each active TMS target to the sham responses revealed significant differences with specific spatiotemporal patterns that varied depending on each target. This is highly likely the result of direct cortical activation of each targeted area rather than unspecific cortical responses to sensory inputs. Moreover, these site-specific EEG responses suggest that different neuronal populations were recruited, adding to the evidence that TEPs reflect the effects of TMS on local cortical circuitry (Li et al. 2017; Romero et al. 2019; Rosanova et al. 2009). Lastly, responses at the source level provided a more accurate visualization of the propagation of the TMS effects. Depending on the target, the propagation of activation was either between the frontal and parietal cortex (TMS of mPFC and AG) or more confined to the central and left somatosensory cortex (TMS of SMA) (Fig. 8, and Animations 1-3 in Supplementary Materials). The specific propagation patterns suggest that different brain regions, structurally and functionally connected to the targeted areas, were engaged during the time of stimulation. Our findings provide additional evidence that the TEPs have the potential to index network-level dynamics (Bortoletto et al. 2015; Ozdemir et al. 2020).

Reliability of TEPs Following PEPs Removal

Recently, several studies assessed the test-retest reliability of TEPs resulting from the left dorsolateral prefrontal cortex stimulation using the inter-session CCC, a metric that is better suited to determine the agreement of measures between repeated tests (Bertazzoli et al. 2021; Kerwin et al. 2018; Moffa et al. 2022). These studies consistently reported that late TEP components had better reliability between sessions than the early ones, with CCC values reaching the moderate and substantial range. Though auditory masking and foam padding were implemented in these studies, they have been considered inadequate in dealing with PEP contamination (Conde et al. 2019; Ross et al. 2022). Hence, the high reliability after 100 ms is likely attributed to residual PEPs such as the N100-P200 components. Due to their greater amplitude and broader spatial distribution, N100-P200 tends to be more stable and reliable. Accordingly, in our study, the inter-session CCCs for evoked EEG responses in the active TMS conditions reached a substantial level from around 90 ms onwards, i.e., during the presence of PEPs. However, after removing PEPs, the CCC values decreased markedly for the 'cleaned' TEPs for SMA and mPFC. In contrast, the comparatively higher CCC values beyond 100 ms following TMS of AG are likely the results of residual PEPs.

Regarding early responses, we found that 'cleaned' TEPs generally showed significant spatial reliability within the first 90 ms. When stimulating AG and SMA, electrodes near TMS targets tended to show better temporal reliability. This is consistent with the spatiotemporal profile of 'true' TEPs, and it further suggests that these early responses are physiologically meaningful rather than the result of PEPs or unrelated cortical activity. However, lower temporal reliability with few electrodes reaching significance was observed following TMS of mPFC. Likewise, two recent studies reported either slight to fair (P20, P50) (Bertazzoli et al. 2021) or little test-retest reliability (N40, P20) (Moffa et al. 2022) of TEPs resulting from stimulating dorsolateral prefrontal cortex as measured by inter-session CCCs. The inter-individual variability, as suggested by the low between-participants CCC values (Fig. S3 and Table S1), could partially explain the poor test-retest reliability of TEPs in response to mPFC stimulation. The higher TMS intensity (120% RMT) used in our study might be another reason. It was intended to increase cortical response based on the observation of relatively smaller TEPs when stimulating the prefrontal and parietal cortex with an intensity of 100% RMT (Rogasch et al. 2020). Nevertheless, this may have contributed to low SNR of TEPs due to amplified noise at the same time, such as muscle artifacts in the frontal regions. In this regard, TMS-induced E-field estimates may help determine TMS intensity, but the desired E-field (strength, orientation) for neuronal activation in mPFC is still unknown (Hernandez-Pavon et al. 2023; Janssen et al. 2014). In addition, the online evaluation of TMS-EEG responses has also been recommended for searching optimal TMS parameters (intensity, coil orientation and location) (Casarotto et al. 2022). Yet, it may not be advantageous for targeting frontotemporal regions where the blinks and cranial muscle twitches could overwhelm the real-time readout. Future studies should explore strategies that can optimize

the SNR to enhance the reliability of TEPs in frontal regions (Parmigiani et al. 2022).

Limitations

One methodological concern about the optimized sham design is the potential modulation effect of concomitant ES on the 'true' TEPs. The strong sensory inputs induced by the high-intensity ES might directly change the cortical excitability or indirectly alter brain states through attention and saliency-related processes. Furthermore, this hypothesis would imply that the PEPs and the 'true' TEPs may not be independent and linearly separable phenomena. Thus, simply subtracting evoked EEG responses by sham from active TMS conditions or statistical comparisons between them may be physiologically inappropriate. Nonetheless, it is a common concern in the TMS–EEG field that the 'true' TEPs might be altered by unwanted sources. For instance, the inevitable multisensory co-stimulations (e.g., facial and trigeminal nerve activation) might intrinsically modify cortical excitability and brain states at the time of stimulation (Hernandez-Pavon et al. 2023; Mizukami et al. 2019; Pellegrino et al. 2022) and lead to changes of the brain's responsiveness to TMS. However, our recent study targeting left M1 using such an optimized sham design showed that, at least at the macroscopic level of EEG, there is no evidence supporting the presence of any interaction between true TEPs and PEPs (Gordon et al. 2023). In light of this, it appears justified to employ the linear assumption as used in some TMS–EEG data cleaning methods (e.g., ICA (Biabani et al. 2019) and SSP–SIR (Mutanen et al. 2016)) and in the subtraction of sham from active TMS.

Another limitation is the residual impact of PEPs on late EEG responses following the TMS of AG, which implies that the PEPs elicited by the sham and active TMS were not equally matched. The mismatch may be due to the engaged cranial nerves and fibers for generating SEPs needing even higher ES to saturate. Because a fixed ES intensity was used for all conditions, it may underestimate the intensity to reach saturation when stimulating AG. To address this, an online titration method could be used, which involves recording simultaneous EEG with gradually increasing ES intensities until a steady PEP is reached (Gordon et al. 2021). This may help to tailor ES parameters for saturation purposes. In addition, the residual auditory perception of TMS pulses was reported in all conditions despite the use of masking noise (Fig. 2). Over-ear protection might help, but the complete suppression of the TMS 'click' sound may not be achievable when applying high-intensity stimulation, which could be necessary for certain cortical targets and individuals with high RMT (Conde et al. 2019; Ross et al. 2022). Nevertheless, our experimental design led to a matched auditory perception in sham and active conditions at the group level, and the auditory effects might be mathematically removed with the comparison between conditions. In summary, though the optimized sham procedure helps disentangle the sensory effects on TEPs, future studies should assess multisensory contributions as a function of the target region and calibrate the sham TMS design accordingly.

Lastly, implementing concomitant ES introduces new sources of noise and exacerbates decay artifacts. Combining the stimulation trials across three sessions allowed us to increase the number of trials per condition and enhance the SNR of the evoked EEG responses, which enabled more robust statistical comparisons between the active and sham TMS conditions. However, a potential limitation of pooling data from multiple sessions is the assumption of stable and reproducible EEG responses over time, which need to be carefully considered and assessed as indicated by the high test-retest reliability in our study (Fig. 3 and Figs. S1, S2). A more sensible way is to obtain a higher SNR during single-session TMS–EEG recording, possibly by reducing the intensity of ES or recording a higher number of trials, but this might cause lengthy experiments with limited benefits.

Conclusions

In the present study, we assessed the EEG responses resulting from TMS of three brain regions, the AG, SMA and mPFC, using an optimized sham design. We conclude that EEG responses to the direct cortical activation by TMS can be revealed within the first 90 ms for all TMS targets. Moreover, the spatial and temporal characteristics of the revealed EEG responses are specific to each target and most likely reflect the effects of TMS on local cortical circuits and networks. Lastly, the test-retest reliability of late TMS–EEG responses may be considerably affected by the presence of PEPs, and the reliability of early responses varies depending on the TMS target.

Supplementary Information The online version contains supplementary material available at https://doi.org/10.1007/s10548-023-01018-y.

Acknowledgements We would like to thank Elina Fanglin Song, Francesco Motolese, and Rafael Marques for their assistance in collecting data. We would like to thank David Emanuel Vetter for the scripts to generate and visualize concordance correlation coefficient matrices. We would like to acknowledge the contributions of all the participants.

Author Contributions YS, PCG, and UZ designed the study. YS and PCG set up the experiment. YS carried out the data acquisition. JM contributed to the TMS–EEG data preprocessing pipeline and MNE source estimation algorithm. MR designed the decay artifact removal algorithm. PB created the head models. YS analyzed the experimental data and drafted the manuscript. PCG and UZ critically reviewed the manuscript. All authors contributed to the writing of the manuscript and approved its final version.

Funding Open Access funding enabled and organized by Projekt DEAL. Y.S. reports funding from the China Scholarship Council (CSC). P.C.G. reports funding from the German Research Foundation (Deutsche Forschungsgemeinschaft—DFG—project number 466 458 984). The work was funded by the European Research Council (ERC Synergy) under the European Union's Horizon 2020 research and innovation program (ConnectToBrain, grant number 810377).

Data Availability The preprocessed tms-eeg data, individual head models, lead field matrices and VAS scores that support the findings of the manuscript are deposited in the repository Zenodo: https://zenodo.org/records/10004794, and the access could be granted under conditions, i.e., EULA (End User License Agreement) signed by the user. The code used is available in GitHub: https://github.com/Song-Yufei/tms-eeg-using-optimized-sham-outside-M1.

Declarations

Competing interests None of the authors has competing interests to declare that are relevant to the content of this article.

Ethical Approval The study was approved by the ethics committee of the medical faculty of Tübingen University (protocol number 638/2020BO1).

Informed Consent Informed consent was obtained from all individual participants included in the study.

References

Barker AT, Jalinous R, Freeston IL (1985) Non-invasive magnetic stimulation of human motor cortex. Lancet 325(8437):1106–1107

Belardinelli P, Biabani M, Blumberger DM, Bortoletto M, Casarotto S, David O, Desideri D, Etkin A, Ferrarelli F, Fitzgerald PB et al (2019) Reproducibility in TMS–EEG studies: a call for data sharing, standard procedures and effective experimental control. Brain Stimul Basic Transl Clin Res Neuromodulation 12(3):787–790

Bertazzoli G, Esposito R, Mutanen TP, Ferrari C, Ilmoniemi RJ, Bortoletto M (2021) The impact of artifact removal approaches on TMS-EEG signal 1. BioRxiv. https://doi.org/10.1101/2021.01.15.426817

Biabani M, Fornito A, Mutanen TP, Morrow J, Rogasch NC (2019) Characterizing and minimizing the contribution of sensory inputs to TMS-evoked potentials. Brain Stimul 12(6):1537–1552. https://doi.org/10.1016/j.brs.2019.07.009

Blair RC, Karniski W (1993) An alternative method for significance testing of waveform difference potentials. Psychophysiology 30(5):518–524

Bortoletto M, Veniero D, Thut G, Miniussi C (2015) The contribution of TMS-EEG coregistration in the exploration of the human cortical connectome. Neurosci Biobehav Rev 49:114–124. https://doi.org/10.1016/j.neubiorev.2014.12.014

Casarotto S, Fecchio M, Rosanova M, Varone G, D'Ambrosio S, Sarasso S, Pigorini A, Russo S, Comanducci A, Ilmoniemi RJ et al (2022) The rt-TEP tool: real-time visualization of TMS-Evoked Potentials to maximize cortical activation and minimize artifacts. J Neurosci Methods 370:109486

Cohen MX (2014) Analyzing neural time series data: theory and practice. MIT press, Cambridge

Conde V, Tomasevic L, Akopian I, Stanek K, Saturnino GB, Thielscher A, Bergmann TO, Siebner HR (2019) The non-transcranial TMS-evoked potential is an inherent source of ambiguity in TMS-EEG studies. NeuroImage 185:300–312. https://doi.org/10.1016/j.neuroimage.2018.10.052

de Cheveigné A, Arzounian D (2018) Robust detrending, rereferencing, outlier detection, and inpainting for multichannel data. Neuroimage 172:903–912. https://doi.org/10.1016/j.neuroimage.2018.01.035

Delorme A, Makeig S (2004) EEGLAB: an open source toolbox for analysis of single-trial EEG dynamics including independent component analysis. J Neurosci Methods 134(1):9–21

Farzan F, Bortoletto M (2022) Identification and verification of a'true'TMS evoked potential in TMS-EEG. J Neurosci Methods 378:109651

Fernandez L, Biabani M, Do M, Opie GM, Hill AT, Barham MP, Teo W-P, Byrne LK, Rogasch NC, Enticott PG (2021) Assessing cerebellar-cortical connectivity using concurrent TMS-EEG: a feasibility study. J Neurophysiol 125(5):1768–1787

Fischl B (2012) FreeSurfer. Neuroimage 62(2):774–781

Gordon PC, Belardinelli P, Stenroos M, Ziemann U, Zrenner C (2022) Prefrontal theta phase-dependent rTMS-induced plasticity of cortical and behavioral responses in human cortex. Brain Stimul 15(2):391–402

Gordon PC, Jovellar DB, Song Y, Zrenner C, Belardinelli P, Siebner HR, Ziemann U (2021) Recording brain responses to TMS of primary motor cortex by EEG–utility of an optimized sham procedure. Neuroimage 245:118708

Gordon PC, Song Y, Jovellar B, Belardinelli P, Ziemann U (2023) No evidence for interaction between TMS-EEG responses and sensory inputs. Brain Stimul 16(1):25–27. https://doi.org/10.1016/j.brs.2022.12.010

Groppa S, Oliviero A, Eisen A, Quartarone A, Cohen LG, Mall V, Kaelin-Lang A, Mima T, Rossi S, Thickbroom GW et al (2012) A practical guide to diagnostic transcranial magnetic stimulation: report of an IFCN committee. Clin Neurophysiol 123(5):858–882

Hashimoto I (1988) Trigeminal evoked potentials following brief air puff: enhanced signal-to-noise ratio. Ann Neurol 23(4):332–338

Hernandez-Pavon JC, Kugiumtzis D, Zrenner C, Kimiskidis VK, Metsomaa J (2022) Removing artifacts from TMS-evoked EEG: a methods review and a unifying theoretical framework. J Neurosci Methods 376:109591

Hernandez-Pavon JC, Veniero D, Bergmann TO, Belardinelli P, Bortoletto M, Casarotto S, Casula EP, Farzan F, Fecchio M, Julkunen P et al (2023) TMS combined with EEG: Recommendations and open issues for data collection and analysis. Brain Stimul. https://doi.org/10.1016/j.brs.2023.02.009

Herring JD, Thut G, Jensen O, Bergmann TO (2015) Attention modulates TMS-locked alpha oscillations in the visual cortex. J Neurosci 35(43):14435–14447. https://doi.org/10.1523/JNEUROSCI.1833-15.2015

Hyvarinen A (1999) Fast and robust fixed-point algorithms for independent component analysis. IEEE Trans Neural Networks 10(3):626–634

Ilmoniemi RJ, Virtanen J, Ruohonen J, Karhu J, Aronen HJ, Näätänen R, Katila T (1997) Neuronal responses to magnetic

stimulation reveal cortical reactivity and connectivity. NeuroReport 8(16):3537–3540
Janssen AM, Oostendorp TF, Stegeman DF (2014) The effect of local anatomy on the electric field induced by TMS: evaluation at 14 different target sites. Med Biol Eng Compu 52(10):873–883. https://doi.org/10.1007/s11517-014-1190-6
Kerwin LJ, Keller CJ, Wu W, Narayan M, Etkin A (2018) Test-retest reliability of transcranial magnetic stimulation EEG evoked potentials. Brain Stimul 11(3):536–544. https://doi.org/10.1016/j.brs.2017.12.010
Lawrence I, Lin K (1989) A concordance correlation coefficient to evaluate reproducibility. Biometrics 45:255–268
Lefaucheur J-P, Aleman A, Baeken C, Benninger DH, Brunelin J, Di Lazzaro V, Filipović SR, Grefkes C, Hasan A, Hummel FC et al (2020) Evidence-based guidelines on the therapeutic use of repetitive transcranial magnetic stimulation (rTMS): an update (2014–2018). Clin Neurophysiol 131(2):474–528
Li B, Virtanen JP, Oeltermann A, Schwarz C, Giese MA, Ziemann U, Benali A (2017) Lifting the veil on the dynamics of neuronal activities evoked by transcranial magnetic stimulation. Elife 6:1–22. https://doi.org/10.7554/eLife.e30552
Maris E, Oostenveld R (2007) Nonparametric statistical testing of EEG-and MEG-data. J Neurosci Methods 164(1):177–190
Massimini M, Ferrarelli F, Huber R, Esser SK, Singh H, Tononi G (2005) Breakdown of cortical effective connectivity during sleep. Science 309(5744):2228–2232
Mizukami H, Kakigi R, Nakata H (2019) Effects of stimulus intensity and auditory white noise on human somatosensory cognitive processing: a study using event-related potentials. Exp Brain Res 237:521–530
Moffa AH, Nikolin S, Martin D, Loo C, Boonstra TW (2022) Reliability of transcranial magnetic stimulation evoked potentials to detect the effects of theta-burst stimulation of the prefrontal cortex. Neuroimage Reports 2(3):100115
Mouraux A, Iannetti GD (2009) Nociceptive laser-evoked brain potentials do not reflect nociceptive-specific neural activity. J Neurophysiol 101(6):3258–3269
Mutanen TP, Kukkonen M, Nieminen JO, Stenroos M, Sarvas J, Ilmoniemi RJ (2016) Recovering TMS-evoked EEG responses masked by muscle artifacts. Neuroimage 139:157–166. https://doi.org/10.1016/j.neuroimage.2016.05.028
Oostenveld R, Fries P, Maris E, Schoffelen J-M (2011) FieldTrip: open source software for advanced analysis of MEG, EEG, and invasive electrophysiological data. Comput Intell Neurosci 2011:1–9
Ozdemir RA, Tadayon E, Boucher P, Momi D, Karakhanyan KA, Fox MD, Halko MA, Pascual-Leone A, Shafi MM, Santarnecchi E (2020) Individualized perturbation of the human connectome reveals reproducible biomarkers of network dynamics relevant to cognition. Proc Natl Acad Sci 117(14):201911240. https://doi.org/10.1073/pnas.1911240117
Ozdemir RA, Tadayon E, Boucher P, Sun H, Momi D, Ganglberger W, Westover MB, Pascual-Leone A, Santarnecchi E, Shafi MM (2021) Cortical responses to noninvasive perturbations enable individual brain fingerprinting. Brain Stimul 14(2):391–403. https://doi.org/10.1016/j.brs.2021.02.005
Parmigiani S, Ross JM, Cline C, Minasi C, Gogulski J, Keller CJ (2022) Reliability and validity of TMS-EEG biomarkers. Biol Psychiatr Cogn Neurosci Neuroimaging. https://doi.org/10.1016/j.bpsc.2022.12.005
Pellegrino G, Schuler A-L, Arcara G, Di Pino G, Piccione F, Kobayashi E (2022) Resting state network connectivity is attenuated by fMRI acoustic noise. Neuroimage 247:118791
Raffin E, Harquel S, Passera B, Chauvin A, Bougerol T, David O (2020) Probing regional cortical excitability via input–output properties using transcranial magnetic stimulation and electroencephalography coupling. Hum Brain Mapp 41(10):2741–2761
Rocchi L, Di Santo A, Brown K, Ibáñez J, Casula E, Rawji V, Di Lazzaro V, Koch G, Rothwell J (2021) Disentangling EEG responses to TMS due to cortical and peripheral activations. Brain Stimul 14(1):4–18. https://doi.org/10.1016/j.brs.2020.10.011
Rogasch NC, Zipser C, Darmani G, Mutanen TP, Biabani M, Zrenner C, Desideri D, Belardinelli P, Müller-Dahlhaus F, Ziemann U (2020) The effects of NMDA receptor blockade on TMS-evoked EEG potentials from prefrontal and parietal cortex. Sci Rep 10(1):3168. https://doi.org/10.1038/s41598-020-59911-6
Romero MC, Davare M, Armendariz M, Janssen P (2019) Neural effects of transcranial magnetic stimulation at the single-cell level. Nat Commun 10(1):2642
Rosanova M, Casali A, Bellina V, Resta F, Mariotti M, Massimini M (2009) Natural frequencies of human corticothalamic circuits. J Neurosci 29(24):7679–7685
Ross JM, Sarkar M, Keller CJ (2022) Experimental suppression of transcranial magnetic stimulation-electroencephalography sensory potentials. Hum Brain Mapp 43(17):5141–5153
Russo S, Sarasso S, Puglisi GE, Dal Palù D, Pigorini A, Casarotto S, D'Ambrosio S, Astolfi A, Massimini M, Rosanova M et al (2022) TAAC-TMS adaptable auditory control: a universal tool to mask TMS clicks. J Neurosci Methods 370:109491
Schambra HM, Ogden RT, Martinez-Hernandez IE, Lin X, Chang YB, Rahman A, Edwards DJ, Krakauer JW (2015) The reliability of repeated TMS measures in older adults and in patients with subacute and chronic stroke. Front Cell Neurosci 9:335
Seghier ML (2023) Multiple functions of the angular gyrus at high temporal resolution. Brain Struct Funct 228(1):7–46
Shrout PE (1998) Measurement reliability and agreement in psychiatry. Stat Methods Med Res 7(3):301–317
Siebner HR, Conde V, Tomasevic L, Thielscher A, Bergmann TO (2019) Distilling the essence of TMS-evoked EEG potentials (TEPs): A call for securing mechanistic specificity and experimental rigor. Brain Stimul 12(4):1051–1054. https://doi.org/10.1016/j.brs.2019.03.076
Siebner HR, Funke K, Aberra AS, Antal A, Bestmann S, Chen R, Classen J, Davare M, Di Lazzaro V, Fox PT et al (2022) Transcranial magnetic stimulation of the brain: What is stimulated?–a consensus and critical position paper. Clin Neurophysiol. https://doi.org/10.1016/j.clinph.2022.04.022
Stenroos M, Nummenmaa A (2016) Incorporating and compensating cerebrospinal fluid in surface-based forward models of magneto- and electroencephalography. PLoS ONE 11(7):e0159595
Tremblay S, Rogasch NC, Premoli I, Blumberger DM, Casarotto S, Chen R, Di Lazzaro V, Farzan F, Ferrarelli F, Fitzgerald PB, Hui J, Ilmoniemi RJ, Kimiskidis VK, Kugiumtzis D, Lioumis P, Pascual-Leone A, Pellicciari MC, Rajji T, Thut G, Daskalakis ZJ (2019) Clinical utility and prospective of TMS–EEG. Clin Neurophysiol 130(5):802–844. https://doi.org/10.1016/j.clinph.2019.01.001

Supplementary Material

Evoked EEG responses to TMS targeting regions outside the primary motor cortex and their test-retest reliability

Yufei Song[1,2], Pedro C. Gordon[1,2], Johanna Metsomaa[1,2,3], Maryam Rostami[4], Paolo Belardinelli[1,2,5], Ulf Ziemann[1,2*]

[1]Department of Neurology & Stroke, University of Tübingen, Germany
[2]Hertie Institute for Clinical Brain Research, University of Tübingen, Germany
[3]Department of Neuroscience and Biomedical Engineering, Aalto University School of Science, Finland
[4]Faculty of Electrical and Computer Engineering, University of Tehran, Iran
[5]CIMeC, Center for Mind/Brain Sciences, University of Trento, Italy

[*]Corresponding Author:
Prof. Dr. Ulf Ziemann
Department of Neurology & Stroke
Hoppe-Seyler-Straße 3, 72076 Tübingen, Germany
Email: ulf.ziemann@uni-tuebingen.de

1 Supplementary method

1.1 Decay artifact removal

The decay artifact was addressed using a first-degree exponential function (a+b∗exp(c∗x) applied to the time series of each epoch and channel. Here, x represented time in milliseconds, ranging from 14 to 1000 ms, and a,b, and c were the associated parameters. The fit solution was optimized using the weighted least squares method, with greater weight assigned to the initial samples after the pulse artifact to prioritize error minimization and improve accurate estimation. This weighting strategy was based on the observation that the initial samples were more likely affected by the decay artifact. The decay-corrected data were obtained by subtracting the fitted exponential model from each time series. Finally, a detrending step was applied to the epochs to minimize sudden signal drops or jumps, ensuring the signal centered around zero as much as possible.

1.2 Test-retest reliability at the individual level

For each cortical target, we calculated the evoked EEG potential matrix for every participant in each session (i.e., 24x3=72 matrices). Each matrix has 64 rows, one for each channel, and 280 columns, one for each time point, from 20 - 300ms post-stimulation. We then flattened the matrix into a vector and calculated the inter-session CCC between each pair of sessions using the formula (2). The results were structured into a 72 x 72 symmetric matrix (left matrix in Fig. S3a), where the rows and columns indexed 24 participants in 3 sessions. Thus, each entry in the matrix contained the CCC value calculated between a specific combination of sessions and participants. We then grouped the entries by participants, excluded the diagonal entries (self-correlation), and averaged the CCC values within every block. This produced a new 24 x 24 symmetric matrix (right matrix in Fig. S3a) where diagonal entries showed the within-participant CCCs, while off-diagonal entries indicated the between-participant CCCs.

1.3 Inverse estimation

We used minimum-norm estimation (MNE) to obtain source amplitudes J as

$$J = \Lambda \mathrm{L}^{\mathrm{T}}(\mathrm{L}\Lambda\mathrm{L}^{\mathrm{T}} + \Sigma)^{-1}Y \quad \text{(S. 1)}$$

where L is the lead-field matrix, and Λ and Σ are the source and noise covariance matrices, respectively. Y is the EEG signal after preprocessing. As noise covariance matrix, we used the identity matrix $\Sigma = \delta \mathrm{I}$, which means that noise is uncorrelated across sensors with constant variances, and the regularization parameter δ corresponds to the noise-to-signal ratio (inverse of the signal-to-ratio) of EEG signal. As a regularization parameter, we used 0.01. The lead-field matrix here was computed for fixed orientations of source dipoles, which means that each dipole position corresponds to one element in J, and one respective column in L. The source covariance matrix is often chosen as a scaled identity matrix, similar to the noise covariance matrix above, corresponding to independently activating sources across the cortical surface. Here, we assumed that the source amplitudes are likely to be correlated if they are near each other, and the correlation between two sources i and j decreases as a function of the distance between their locations r_i and r_j. Specifically, the element in the ith the row and jth column of the covariance matrix was chosen to obey the Gaussian-like function:

$$\Lambda(i,j) = \exp\left[(r_i - r_j)^2/d^2\right] \quad \text{(S. 2)}$$

where d is the constant describing how fast the correlation decreases. A high value of d will lead to the assumption of roughly uncorrelated sources, whereas decreasing values correspond to the assumption of correlated sources within enlarging patches of cortical neurons. Note that, in the diagonal, the entries will always be 1, but this exact number is irrelevant since the scaling is indirectly controlled by the regularization factor δ (i.e., the assumed signal-to-noise ratio).

2 Supplementary results

2.1 Within- and between-participant test-retest reliability

On average, inter-session CCCs for the EEG responses elicited by both sham and active TMS were evidently high both within- and between- participants (Fig. S4 and Table. S1). Similar to the results at the group level, the test-retest reliability for the 'cleaned' TEPs decreased after removing PEPs. Notably, the within-participant CCCs remained higher than the pre-stimulation baseline EEG for all cortical targets. But the between-participant reliability of the 'cleaned' TEPs in mPFC was generally poor compared to AG and SMA, as indicated by the CCC values distributed around zero.

Supplementary Figures and Figure captions

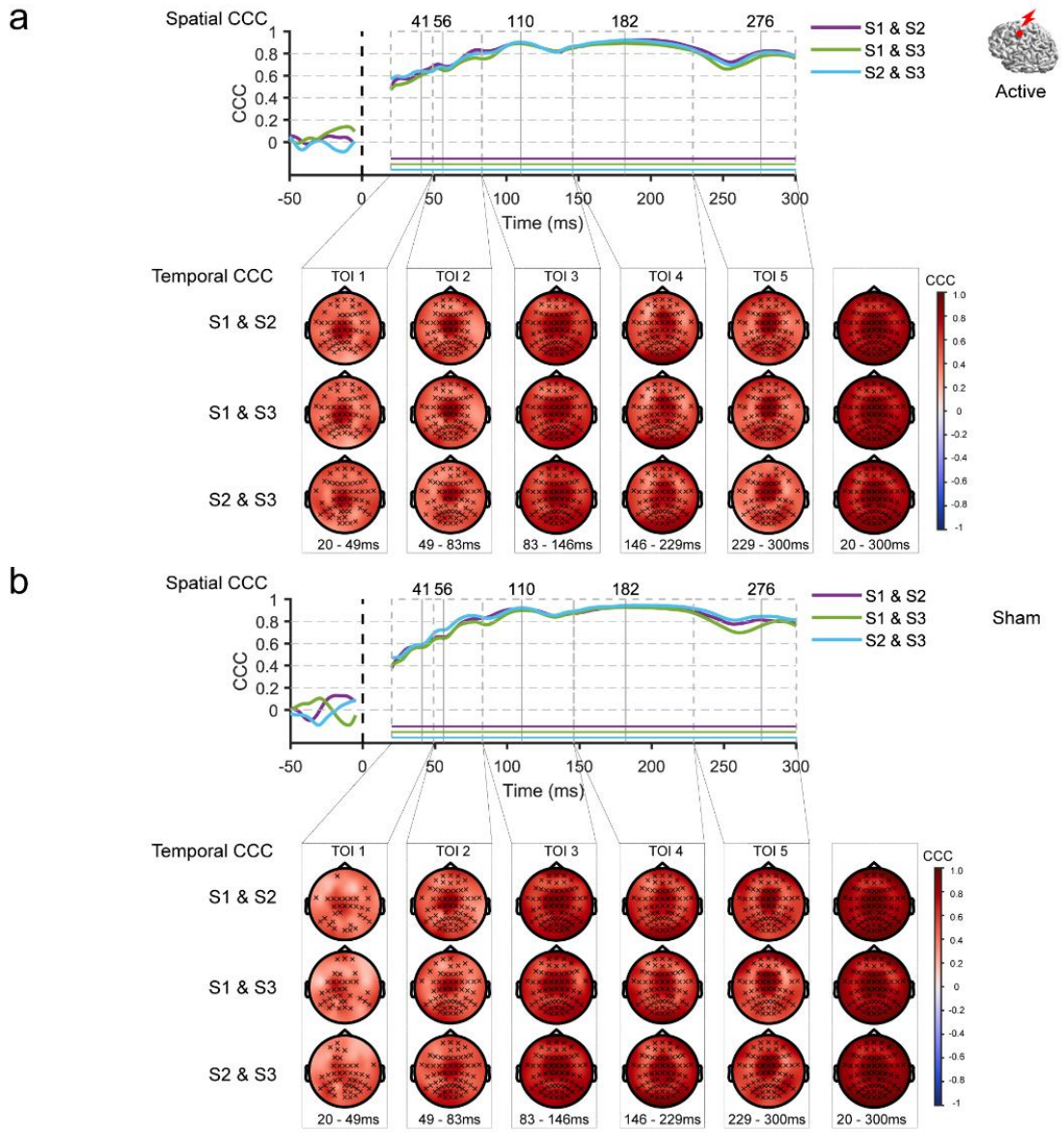

Fig. S1 Test-retest reliability of the evoked EEG potentials by active TMS (a) and sham TMS (b) of SMA. The red dot on a template brain indicates the cortical target. The upper panel shows the spatial inter-session CCCs, with traces (purple, green, and blue) representing the group averages of CCCs for each pair of sessions. Horizontal lines indicate time points where CCCs significantly differ from zero. The lower panel displays topography of the temporal CCCs within each TOI, x indicating electrodes with CCCs significantly different from zero. Abbreviations: CCC, concordance correlation coefficient; S1, S2, S3, sessions 1-3; SMA, supplementary motor area; TMS, transcranial magnetic stimulation; TOI, time window of interest.

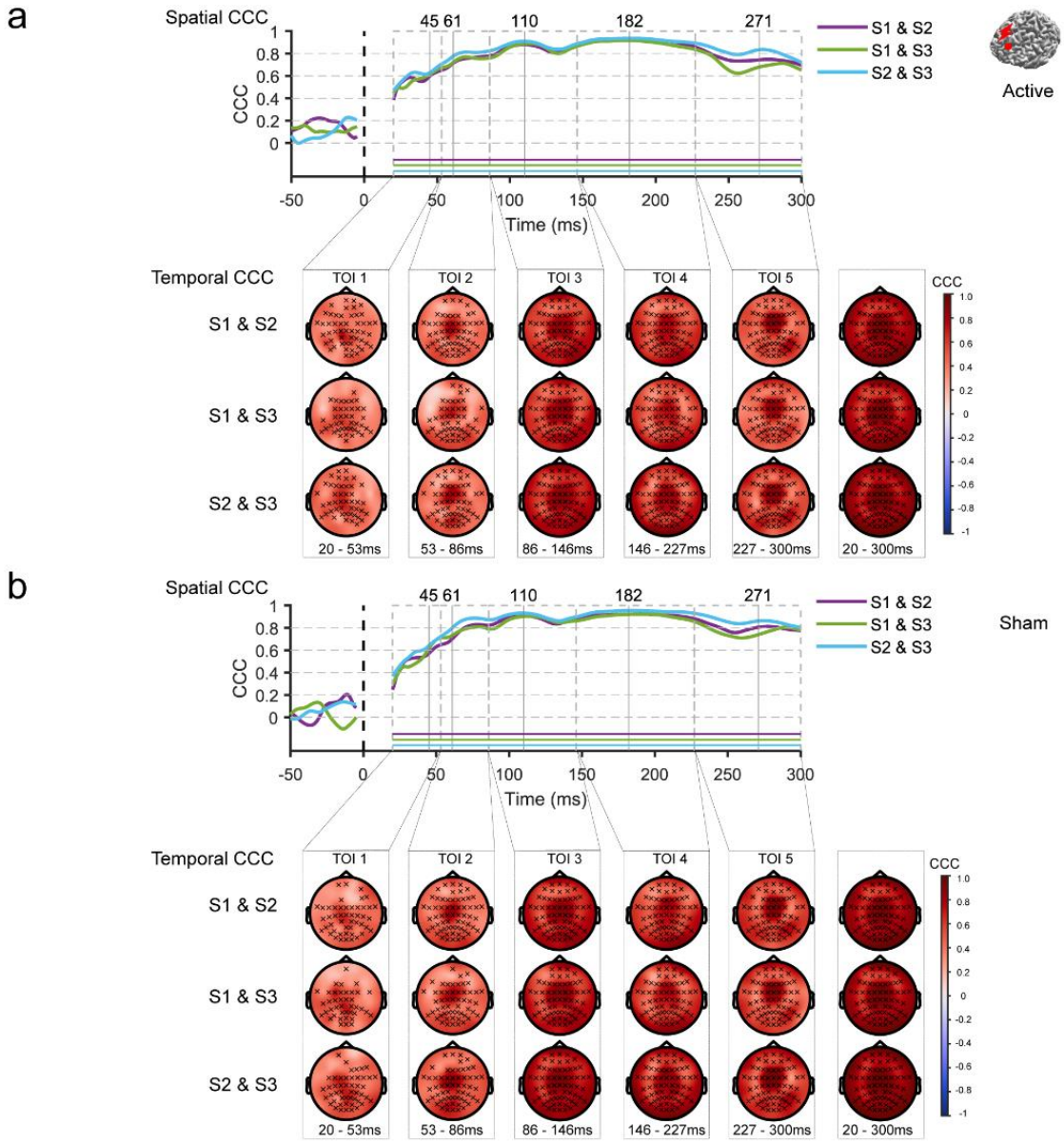

Fig. S2 Test-retest reliability of the evoked EEG potentials by active TMS (a) and sham TMS (b) of mPFC. The red dot on a template brain indicates the cortical target. The upper panel shows the spatial inter-session CCCs, with traces (purple, green, and blue) representing the group means of CCCs for each pair of sessions. Horizontal lines indicate time points where CCCs significantly differ from zero. The lower panel displays topography of the temporal CCCs within each TOI, x indicating electrodes with CCCs significantly different from zero. Abbreviations: CCC, concordance correlation coefficient; mPFC, medial prefrontal cortex; S1, S2, S3, sessions 1-3; TMS, transcranial magnetic stimulation; TOI, time window of interest.

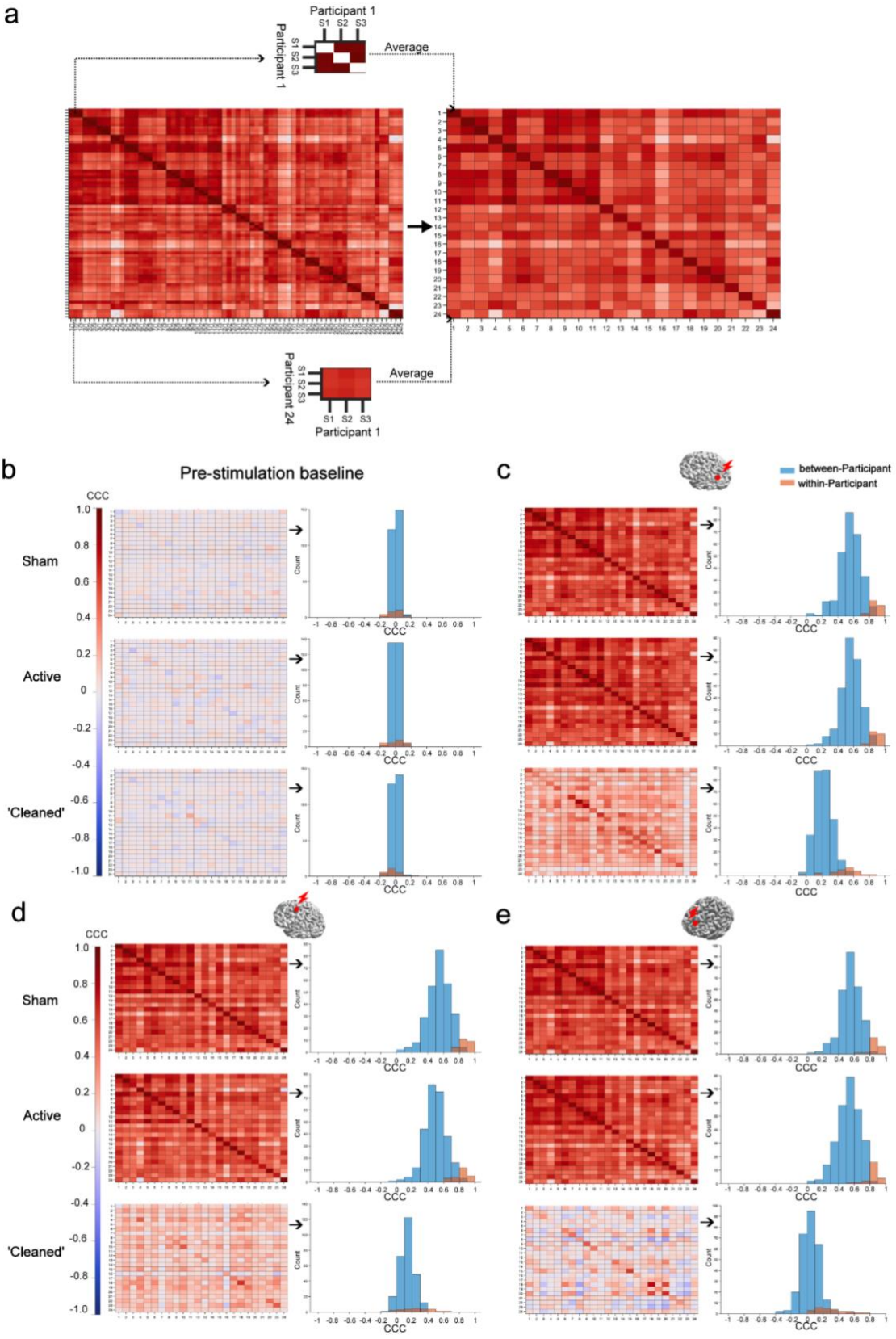

Fig. S3 Individual-level test-retest reliability. (a) The inter-session CCC Matrices. Each entry in the matrix (72 x 72; left) represents the inter-session CCC values calculated between a specific combination of sessions and participants. The entries were then

grouped by participants, and the CCC values within each block were averaged, transforming into a 24 x 24 matrix (right). The diagonal entries represent the within-participant CCCs, and the off-diagonal entries are the between-participant CCCs. Two representative blocks illustrate the transformation: the within-participant 1 CCC (excluding the diagonal), and the between participant 1 and participant 24 CCC. Within- and between-participant CCCs for the pre-stimulation baseline EEG (b) and the evoked EEG potentials by TMS of AG (c), SMA (d), and mPFC (e) in three conditions: sham (top row), active (middle row), and 'cleaned' (active – sham; bottom row). The red dot on a template brain indicates the cortical target. The CCC matrix and the distribution of the within- and between-participant CCCs are shown for each condition. *Abbreviations*: AG, angular gyrus; CCC, concordance correlation coefficient; mPFC, medial prefrontal cortex; S1, S2, S3, sessions 1-3; SMA, supplementary motor area.

	Active		**Sham**		**'Cleaned'**	
	Within-	Between-	Within-	Between-	Within-	Between-
Pre-stim baseline	0.02 [-0.17 0.14]	0.00 [-0.07 0.07]	0.00 [-0.12 0.12]	0.01[-0.06 0.07]	-0.03 [-0.14 0.16]	0.00 [-0.07 0.06]
AG	0.87 [0. 77 0.95]	0.58 [0.33 0.77]	0.98 [0.76 0.96]	0.56 [0. 29 0.77]	0.52 [0.08 0.77]	0.22 [0.03 0.41]
SMA	0.86 [0. 64 0.94]	0.49 [0.26 0.71]	0.86 [0.64 0.94]	0.49 [0. 26 0.71]	0.26 [-0.04 0.54]	0.13 [-0.01 0.30]
mPFC	0.86 [0. 64 0.93]	0.54 [0.25 0.74]	0.89 [0.72 0.96]	0.56 [0. 31 0.76]	0.28 [0.08 0.67]	0.04 [-0.15 0.22]

Table S1 Within- and between- participant inter-session CCCs. NB: value in every cell every cell represents the median, and the interval from the 5th percentile to the 95th percentile (given as: "median [q(0.05), q(0.95)]"). *Abbreviations*: AG, angular gyrus; CCC, concordance correlation coefficient; mPFC, medial prefrontal cortex; SMA, supplementary motor area.

Supplementary animations and animation captions

Animation_S1 (separate file). Propagation of source activation following TMS of mPFC. The top row displays the spatial distribution from three different perspectives. The plot on the bottom right shows the time series of normalized current density, averaged within the ROI (blue) shown to the left. The solid line represents the group average, and the shaded area is the standard error. *Abbreviations*: mPFC, medial prefrontal gyrus; ROI, region of interest; TMS, transcranial magnetic stimulation.

Animation_S2 (separate file). Propagation of source activation following TMS of SMA. The top row displays the spatial distribution from three different perspectives. The plot on the bottom right shows the time series of normalized current density, averaged within the ROI (yellow) shown to the left. The solid line represents the group average, and the shaded area is the standard error. *Abbreviations*: SMA, supplementary motor area; ROI, region of interest; TMS, transcranial magnetic stimulation.

Animation_S3 (separate file). Propagation of source activation following TMS of AG. The top row displays the spatial distribution from three different perspectives. The plot on the bottom right shows the time series of normalized current density, averaged within the ROI (red) shown to left. The solid line represents the group average, and the shaded area is the standard error. *Abbreviations*: AG, angular gyrus; ROI, region of interest; TMS, transcranial magnetic stimulation.

2.2 Involvement of muscarinic acetylcholine receptor-mediated cholinergic neurotransmission in TMS–EEG responses (Song et al., 2025)

Progress in Neuropsychopharmacology & Biological Psychiatry 136 (2025) 111167

Contents lists available at ScienceDirect

Progress in Neuropsychopharmacology & Biological Psychiatry

journal homepage: www.elsevier.com/locate/pnp

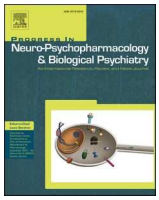

Involvement of muscarinic acetylcholine receptor-mediated cholinergic neurotransmission in TMS–EEG responses

Yufei Song [a,b], Pedro C. Gordon [a,b], Olivier Roy [a,b,c,d], Johanna Metsomaa [e], Paolo Belardinelli [a,b,f], Maryam Rostami [g], Ulf Ziemann [a,b,*]

[a] Department of Neurology & Stroke, University of Tübingen, Germany
[b] Hertie Institute for Clinical Brain Research, University of Tübingen, Germany
[c] CERVO Brain Research Centre, Quebec, Canada
[d] Department of Psychiatry and Neurosciences, Université Laval, Quebec, Canada
[e] Department of Neuroscience and Biomedical Engineering, Aalto University School of Science, Finland
[f] CIMeC, Center for Mind/Brain Sciences, University of Trento, Italy
[g] Faculty of Electrical and Computer Engineering, University of Tehran, Iran

ARTICLE INFO

Keywords:
Transcranial magnetic stimulation-electroencephalography
Pharmacological TMS–EEG
mAChR
Evoked-potentials
Oscillations

ABSTRACT

The combination of transcranial magnetic stimulation and electroencephalography (TMS–EEG) is emerging as a valuable tool for investigating brain functions in health and disease. However, the detailed neural mechanisms underlying TMS–EEG responses, including TMS-evoked EEG potentials (TEPs) and TMS-induced EEG oscillations (TIOs), remain largely unknown. Combining TMS–EEG with pharmacological interventions provides a unique opportunity to elucidate the roles of specific receptor-mediated neurotransmissions in these responses. Here, we investigated the involvement of muscarinic acetylcholine receptor (mAChR)-mediated cholinergic neurotransmission in TMS–EEG responses by evaluating the effects of mAChR antagonists on TEPs and TIOs in twenty-four healthy participants using a randomized, placebo-controlled crossover design. TEPs and TIOs were measured before and after administering a single oral dose of scopolamine (a non-selective mAChR antagonist), biperiden (an M1 mAChR antagonist), or placebo, with TMS targeting the left medial prefrontal cortex (mPFC), angular gyrus (AG), and supplementary motor area (SMA). The results indicated that mAChR-mediated cholinergic neurotransmission played a role in TEPs, but not TIOs, in a target-specific manner. Specifically, scopolamine significantly increased the amplitude of a local TEP component between approximately 40 and 63 ms post-stimulus when TMS was applied to the SMA, but not the mPFC or AG. Biperiden produced a similar but less pronounced effect. Importantly, the effects of these mAChR antagonists on TEPs were independent of those on sensory-evoked EEG potentials caused by TMS-associated sensory stimulation. These findings expand our understanding of TMS–EEG physiology, providing insights for its application in physiological and clinical research.

1. Introduction

Transcranial magnetic stimulation coupled with electroencephalography (TMS–EEG) is an effective, non-invasive tool for investigating brain functions, such as excitability and connectivity (Ilmoniemi et al., 1997). Two commonly used outcome measures in TMS–EEG studies are TMS-evoked EEG potentials (TEPs) and TMS-induced EEG oscillations (TIOs). Both measures are time-locked responses to direct cortical activation elicited by single-pulse TMS targeting specific brain regions. TEPs capture phase-locked brain activity and are typically analyzed in the time domain, revealing a sequence of positive (P) and negative (N) peaks sensitive to stimulation parameters such as site and intensity (Cohen, 2014; Hernandez-Pavon et al., 2023). In contrast, TIOs are often assessed using time-frequency decomposition techniques, enabling the extraction of non-phase-locked oscillatory power (Belardinelli et al., 2021; Gordon et al., 2021; Pellicciari et al., 2017; Premoli et al., 2017). A typical time-frequency representation (TFR) of TIOs shows synchronization (power increase) and desynchronization (power decrease) as functions of frequency and time. Changes in these TMS–EEG measures have been described in various neurological and psychiatric disorders compared to healthy controls, highlighting their potential as biomarkers for diagnosis and treatment monitoring (reviewed in (Tremblay et al.,

* Corresponding author at: Department of Neurology & Stroke, Hoppe-Seyler-Straße 3, 72076 Tübingen, Germany.
E-mail address: ulf.ziemann@uni-tuebingen.de (U. Ziemann).

https://doi.org/10.1016/j.pnpbp.2024.111167
Received 24 June 2024; Received in revised form 1 October 2024; Accepted 3 October 2024
Available online 9 October 2024

2019)). However, translating TMS–EEG measures into clinical practice requires a deeper understanding of their physiological underpinnings.

TMS induces action potentials by depolarizing axons of a mixed neural population in the stimulated cortex (Hernandez-Pavon et al., 2023; Siebner et al., 2022). The initial current travels along axons, producing local excitation or inhibition within the targeted area as well as remote effects on interconnected cortical and subcortical regions. The synchrony of postsynaptic potentials generated along this route results in measurable EEG signals (Jackson and Bolger, 2014). This chain of electrical activity is mediated through neurotransmitter-mediated processes. Glutamate and GABA are the primary excitatory and inhibitory neurotransmitters in the brain, respectively. Recent pharmacological TMS–EEG studies have demonstrated the involvement of GABAergic and glutamatergic neurotransmission in TMS–EEG responses in healthy participants (Belardinelli et al., 2021; Cash et al., 2017; Darmani et al., 2016; Gordon et al., 2023b; Hui et al., 2020; Premoli et al., 2014, 2017; Salavati et al., 2018). The intake of diazepam (a GABAA receptor positive allosteric modulator) increased the amplitude of the N45 TEP and decreased the amplitude of the P60, N100, and P150 TEP when applying single-pulse TMS to the primary motor cortex (M1) (Gordon et al., 2023b; Premoli et al., 2014). Diazepam also enhanced the TMS-induced EEG alpha power and, conversely, suppressed beta power (Gordon et al., 2023b; Premoli et al., 2017). Moreover, the intake of the anti-glutamatergic drug dextromethorphan (an NMDA receptor antagonist) also increased N45 amplitude, with a similar EEG topology as diazepam (Belardinelli et al., 2021). In contrast, the alpha5-GABAA receptor antagonist compound S44819 decreased N45 amplitude (Darmani et al., 2016). This body of evidence suggests TMS–EEG responses reflect the balance of excitatory and inhibitory neurotransmission. In addition, neuromodulators like acetylcholine (ACh) and dopamine regulate the excitatory and inhibitory transmission initiated by glutamate and GABA in neural circuits (Nadim and Bucher, 2014; Tsuboi et al., 2024). However, the involvement of neuromodulator-mediated neurotransmission in TMS–EEG responses remains largely unexplored.

ACh plays a crucial role in modulating cognitive (Bentley et al., 2011) and motor (Maurice et al., 2015) functions. Deficits in ACh-mediated cholinergic signaling have been implicated in neurodegenerative diseases, such as Alzheimer's disease (AD), Lewy body dementia, and Parkinson's disease (PD) (Bohnen et al., 2018). Therefore, exploring the involvement of cholinergic neurotransmission in TMS–EEG responses is potentially clinically valuable. If TEPs and TIOs are sensitive to the manipulation of cholinergic signaling, they may serve as non-invasive indicators of cholinergic system (dys)function. In the brain, ACh is primarily released from cholinergic projection neurons in the basal forebrain nuclei (BF), the brainstem, and local cholinergic interneurons in the striatum (Ballinger et al., 2016; Picciotto et al., 2012; Thiele, 2013). ACh acts on muscarinic ACh receptors (mAChRs) and nicotinic receptors (nAChRs). mAChRs are metabotropic G-protein coupled receptors with five subtypes (M1–M5), with M1-M4 receptors being abundant in both the cortex and striatum. At the cellular level, presynaptic M2 and M4 receptors act as inhibitory autoreceptors on cholinergic terminals and heteroreceptors on GABAergic and glutamatergic terminals, suppressing neurotransmitter release (Colangelo et al., 2019; Thiele, 2013). Conversely, postsynaptic M1 and M3 receptors, expressed on both interneurons and pyramidal cells, influence neuronal excitability by modulating ion channels. Consequently, mAChR-mediated neurotransmission finely tunes the information flow by influencing neuronal excitability and synaptic efficacy. Similar to mAChRs, nAChRs have multiple subtypes and are expressed in diverse neural populations. Though nAChRs function as excitatory cation channels, the activation of nAChRs in the brain is largely modulatory as well.

In this study, we investigated whether and how TEPs and TIOs are affected by the inhibition of cholinergic neurotransmission. nAChR antagonists are not commonly used in healthy populations due to the transient paralysis caused by blocking nicotinic activity at the neuromuscular junction (Kunnath et al., 2023). Therefore, we employed two mAChR antagonists, scopolamine and biperiden, to inhibit muscarinic cholinergic transmission. Scopolamine is a non-selective receptor antagonist, while biperiden selectively blocks the M1 receptor (Bakker et al., 2021; Klinkenberg and Blokland, 2010). For TMS targets, we chose the left medial prefrontal cortex (mPFC), angular gyrus (AG), and supplementary motor area (SMA). The mPFC and AG are integral to brain networks critical for cognitive functions, where the cholinergic system plays an important role (Bentley et al., 2011; Klinkenberg et al., 2011). The SMA is involved in motor control, which is regulated by neuromodulatory systems including cholinergic signaling (Maurice et al., 2015). We conducted a randomized, placebo-controlled crossover study in which healthy participants received a single oral dose of scopolamine (SCO), biperiden (BIP), or placebo (PLA) in three separate sessions. During each session, we measured TEPs and TIOs in response to TMS of the three brain regions before and after drug administration. We hypothesized that scopolamine and biperiden, but not placebo, would significantly alter TEPs and TIOs. Additionally, we anticipated differential effects between scopolamine and biperiden due to their receptor selectivity.

2. Methods

2.1. Participants

The study was approved by the ethics committee of the medical faculty of Tübingen University (protocol number 638/2020BO1) and was conducted in accordance with the Declaration of Helsinki. All participants provided written informed consent prior to the inclusion in the study. The inclusion criteria required that participants had no prior history of illnesses such as cardiovascular, hepatic, renal, pulmonary, gastrointestinal, neurological, or psychiatric disorders, nor were they taking any medication with effects on the central nervous system (CNS). All participants underwent a medical screening to check for any contraindications to TMS and study drugs, including a 12-lead electrocardiogram (ECG). Twenty-eight healthy participants (mean age ± SD, 26.0 ± 4.8 years; 16 females) were included in the study, and twenty-four participants (mean age ± SD, 25.7 ± 4.8 years; 14 females) completed all the sessions: three participants dropped out, and one participant did not comply with the experimenting procedures. Therefore, the final analysis was based on twenty-four participants.

2.2. Experimental design and procedure

We conducted a placebo-controlled cross-over study, which involved three experimental sessions per participant, each separated by at least one week (Fig. 1). During each session, participants were administered a single oral dose of either scopolamine (0.9 mg, Kwells®, Dexcel® pharma GmbH), biperiden (4 mg, Akineton®, Desma GmbH), or placebo (PTabletten 8 mm Lichtenstein, Zentiva Pharma GmbH). The drug order was randomized and balanced over the three sessions across participants. Each session included three blocks of TMS–EEG recordings targeting the mPFC, AG, and SMA, respectively. This was followed by a simple reaction time (SRT) task. These measurements were repeated 60 min after drug intake. To control for TMS-associated sensory inputs, a sham procedure was used during TMS–EEG recordings, involving both *active* TMS and *sham* TMS conditions (Methods: Section 2.3).

2.3. TMS–EEG setup

TMS–EEG recordings contain EEG responses to TMS-associated peripheral sensory inputs (somatosensory and auditory), which can introduce ambiguity when interpreting results in pharmacological TMS–EEG studies. This ambiguity arises because CNS-active drugs may alter not only the genuine TMS–EEG responses resulting from direct cortical activation elicited by TMS but also the EEG responses caused by

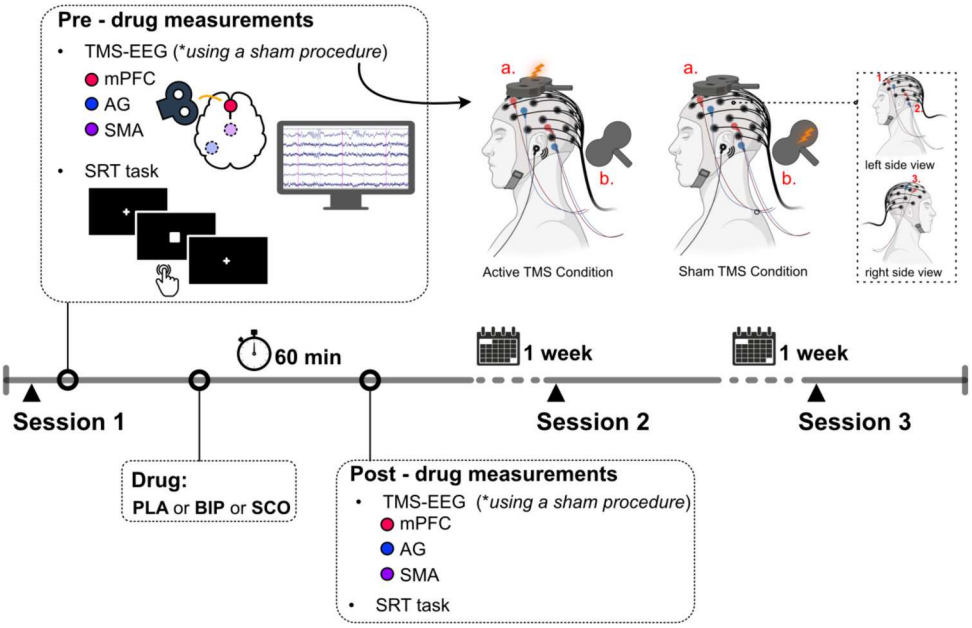

Fig. 1. Study timeline. This randomized, placebo-controlled cross-over study consisted of three sessions (PLA, BIP, SCO), each separated by one week. Each session included three blocks of TMS-EEG recordings targeting the mPFC, AG, and SMA, followed by a SRT task. Measurements were repeated 60 min after drug intake. To control for TMS-associated sensory inputs, a sham procedure was used, involving both active TMS and sham TMS conditions. The upper panel shows the experimental setup for targeting the SMA (adapted with permission from Song et al., 2023). Two identical TMS coils (a and b) were used: Coil a delivered TMS pulses to the SMA in the active condition, while Coil b produced the 'click' sound in the sham condition. ES pulses were delivered concomitantly with TMS pulses via three pairs of bipolar electrodes in both conditions. Masking noise was played throughout the recording. Abbreviations: AG: angular gyrus; BIP, biperiden; ES: electrical stimulation; mPFC: medial prefrontal cortex; PLA, placebo; SCO, scopolamine; SMA, supplementary motor area; SRT: simple reaction time; TMS-EEG, Transcranial magnetic stimulation-Electroencephalography.

sensory inputs (Gordon et al., 2023b). Consequently, it becomes challenging to determine to what extent observed changes in TMS–EEG signals following the drug administration are due to drug effects on direct cortical activation or sensory processing. A common approach to address these sensory confounds is to include a sham stimulation that replicates TMS-associated sensory inputs. Several studies have attempted to mimic TMS-associated auditory inputs with TMS 'click' generated by a TMS coil placed at an angle or a distance from the head and recreate somatosensory inputs using scalp electrical stimulation (ES) (Chowdhury et al., 2022; Conde et al., 2019; Fernandez et al., 2021). However, due to the distinct biophysical mechanisms involved in ES and TMS, precisely matching sensory-related EEG responses between sham and active conditions remains challenging (Conde et al., 2019). To mitigate this, we employed a sham procedure developed and validated in our previous work, which involves applying high-intensity ES to both *sham* and *active* TMS conditions (Gordon et al., 2021, 2023a). This approach aims to saturate the EEG response to sensory inputs, thereby minimizing the impact of any additional somatosensory inputs caused by TMS in the active condition. As a result, the sensory components between the two conditions become closely matched, allowing for reliable subtraction of *sham* EEG from the *active* condition and facilitating the identification of direct cortical activation by TMS.

Fig. 1 illustrates an example of applying TMS to the SMA. In the *active* TMS condition, a TMS stimulator (Magstim® 200^2, monophasic mode, UK) equipped with a figure-of-eight coil (external diameter = 90 mm) was used. To estimate and monitor coil positions during TMS–EEG recordings, we used a navigation system (TMS Navigator, Localite GmbH, Germany). Magnetic resonance imaging (MRI) with a T1-weighted anatomical sequence for each participant was recorded prior to TMS–EEG sessions. We aligned the individual T1w image with the Talairach coordinate system. The cortical targets were defined by the Montreal Neurological Institute (MNI) coordinates (left mPFC: −4, 52, 36; left AG: −42, −69, 31; left SMA: −2, −7, 55). Aiming to target the desired cortical locations, we positioned the *active* TMS coil perpendicular to the underlying gyrus. The induced current ran approximately from lateral to medial for targeting the mPFC and SMA and from posterior-medial to anterior-lateral for targeting the AG. The intensity in the *active* TMS condition was set to 120 % resting motor threshold (RMT). To determine the RMT, we attached bipolar surface electromyographic (EMG) electrodes to the abductor pollicis brevis (APB), and first dorsal interosseus (FDI) muscles of the participant's right hand, EMG signals were sampled at 5 kHz (device filter DC-1250 Hz). We targeted the hotspot of M1, defining RMT as the lowest intensity that produced an MEP over 50 μV in at least 5 out of 10 consecutive pulses (Groppa et al., 2012). In the *sham* TMS condition, to generate the TMS associated 'click' sound, we used a second TMS setup identical to the one in the *active* TMS condition. The second TMS coil was placed near the participant's head, with the intensity set to 1.6 x *active* TMS to account for the increased distance (Gordon et al., 2021). To mimic TMS-associated somatosensory inputs, we delivered ES pulses (Digitimer DS7A, Digitimer Ltd.UK) through short-distance bipolar electrodes attached to the EEG cap with the following montage: pair 1 (frontal: AFF1H, AFF5H) and pair 2 (parietal: TPP7H, TPP9H) in the left hemisphere, and pair 3 (central: FFC4H, FCC4H) in the right hemisphere. These positions were chosen to be near the three TMS sites, respectively. To closely approximate sensory-related EEG responses in both *sham* TMS and *active* TMS conditions, we aimed to saturate the EEG response to sensory inputs. This was done by delivering ES pluses to both *sham* and *active* conditions using a high intensity of 24 mA (width 200 μs, maximum voltage of 400 V) through the three pairs of electrodes. ES pulses were concomitant with TMS pulses, and the three pairs of electrodes were fired together. The current polarity was switched after each pulse. Additionally, masking noise was played throughout the recording for both *sham* and *active* TMS conditions (Massimini et al., 2005).

2.4. TMS–EEG data recording

EEG signals were recorded with a TMS-compatible system (NeurOne,

Bittium, Kuopio, Finland). 64 Ag/AgCl sintered ring electrodes were placed according to the International 10–5 system in an elastic cap (EasyCap BC-TMS-64, EasyCap, Germany). We used electrode CPz as the online reference and placed the ground at PPO1h. EEG signals were sampled at 5 kHz (device filter DC-1250 Hz), and EEG electrode impedances were maintained below 5 kΩ. We digitized the electrodes' positions from the navigation system for source reconstruction purposes. We recorded 150 *active* TMS pulses and 50 *sham* TMS pulses in each TMS–EEG block, with the *sham* TMS pulses randomly interleaved within the *active* TMS pulses. This resulted in a total of 150 pulses for the *sham* conditions across the three TMS–EEG blocks. The ISI was 3 s (±1 s jitter; 2–4 s range).

2.5. TMS–EEG data preprocessing

Offline EEG preprocessing and analysis were performed in a Matlab environment (version 2022b, MathWorks Inc.). EEGLAB (Delorme and Makeig, 2004), FieldTrip (Oostenveld et al., 2011), and customized scripts were used. We employed the preprocessing pipeline established in our previous work (Metsomaa et al., 2024; Song et al., 2023). The TMS–EEG signals were preprocessed individually, one TMS site at a time. We first epoched the continuous signal into 3000 ms trials (−1500 to 1500 ms around stimuli) and corrected the baseline with respect to the −1000 to −5 ms pre-stimulus time window. We next grouped *sham* and *active* TMS trials, as well as pre- and post-drug conditions from the same session, to ensure consistent artifact rejection along the pipeline. Following a robust detrending (3rd-order polynomial fitting), we re-epoched the data into shorter trials (−1000 to 1000 ms). Decay artifacts were removed with a customized function (Supplementary Materials: Section 1.1) on a trial-by-trial basis. Subsequently, pulse artifacts (−4 to 17 ms) were eliminated and cubic-interpolated. We then resampled to 1 kHz ('resample' function in Matlab, including low-pass filtering at the Nyquist frequency). Channels and trials heavily contaminated by noise or artifacts were manually excluded. We next applied FastICA to identify ocular artifact topographies, which were removed using a beamforming filter in a later step. The SSP–SOUND joint algorithm was employed to estimate the signal subspace containing TMS-related artifacts and suppress them from EEG signals (Metsomaa et al., 2024). Data were re-referenced to the average, and ocular artifacts were suppressed. Removed channels were interpolated using spherical interpolation based on surrounding channels. Lastly, TMS–EEG trials from the same session were sorted according to experimental conditions: *sham* TMS pre-drug, *active* TMS pre-drug, *sham* TMS post-drug, *active* TMS post-drug.

2.6. SRT task

Scopolamine and biperiden could produce a sedative effect (Bakker et al., 2021). To assess this, we included an SRT task before and after drug administration. The SRT task measures how quickly a participant can respond when no other mental processing is required and is sensitive in detecting sedation (Baakman et al., 2017). During the task, a white square was displayed at the center of a screen at random intervals. Participants were instructed to press a button on a response box as quickly as possible whenever the square appeared. The inter-stimulus interval (ISI) was jittered between 500 and 1500 ms and uniformly distributed. We recorded reaction times from 40 trials per participant. Trials without button presses were excluded from further processing (1.3 % of trials across all participants). Additionally, we removed extreme values with SRTs shorter than 150 ms or longer than 700 ms (5.4 % of trials across all participants) (Karamacoska et al., 2018).

2.7. Data analysis

2.7.1. TEPs and sensory inputs-evoked EEG potentials (SEPs)

For each TMS target, we averaged TMS–EEG trials by experimental conditions per participant, resulting in *sham* TMS-evoked and *active* TMS-evoked EEG potentials separately for pre- and post-drug conditions. As previously reported (Gordon et al., 2023b; Song et al., 2023), the difference between *sham* TMS-evoked and *active* TMS-evoked EEG potentials reveals responses most likely due to direct cortical activation elicited by TMS. Therefore, in this study, we used the cleaned TEPs, obtained by subtracting the *sham* TMS-evoked from the *active* TMS-evoked EEG potentials, to represent genuine TEPs. Since the *sham* TMS consisted solely of multi-sensory inputs, the corresponding evoked EEG potential represented SEPs. Additionally, we projected the evoked sensor-level EEG potentials to source space using the L2-minimum-norm estimation (MNE) approach. More details are provided in Supplementary Materials: Section 1.2.

2.7.2. TIOs and sensory inputs-induced EEG oscillations (SIOs)

For each TMS target, we used the time-frequency representation (TFR) to obtain the power of stimulation-induced oscillations for each participant. We began by calculating trial-wise TFRs for each TMS–EEG trial and then averaged them by experimental conditions: *sham* TMS or *active* TMS, pre-drug or post-drug. These condition-averaged TFRs represented the total oscillatory power. Next, we computed TFRs for *sham* TMS-evoked and *active* TMS-evoked EEG potentials separately for pre-drug and post-drug conditions, which provided the *sham* TMS-evoked and *active* TMS-evoked oscillatory power, respectively. The *sham* TMS-induced and *active* TMS-induced oscillatory power were obtained by subtracting the evoked oscillatory power from the total power (Pellicciari et al., 2017). Specifically, for TFR calculation, we applied complex Morlet wavelet convolution to decompose the frequency band ranging from 4 to 40 Hz. The width of wavelets increased as a function of frequencies, with 2.6 cycles at 4 Hz and 7.1 cycles at 40 Hz linearly spaced by 0.12. We z-transformed the trial-wise TFRs using the mean and standard deviation of the full-length trial and performed baseline correction by subtracting the mean value of a pre-stimulus time window (−500 to −200 ms), following an established methodology (Belardinelli et al., 2021; Gordon et al., 2023b; Grandchamp and Delorme, 2011; Premoli et al., 2017). This ensured that the average pre-stimulation values did not differ from zero, allowing the z-values to be interpreted as modulation of the pre-stimulation oscillatory activity. To isolate the genuine TMS-induced oscillatory power, we used the cleaned TMS-induced oscillatory power, which was obtained by subtracting *sham* TMS-induced from *active* TMS-induced oscillatory power. As the *sham* TMS consisted solely of multisensory inputs, the corresponding oscillations represented SIOs.

2.7.3. Statistical analysis

Our study employed a within-subject 2-by-3 factorial design with two factors: *Time* (two levels: *PRE* and *POST*) and *Drug* (three levels: *PLA*, *BIP*, *SCO*) per TMS target.

Drug effects on TMS–EEG responses: Given the absence of strong prior hypotheses about the time/electrode/frequency window for analyzing the effects of anti-cholinergic drugs on TMS–EEG data, we chose the non-parametric cluster-based permutation test (Maris and Oostenveld, 2007). This method detects effects without being overly constrained by pre-specified theories and preserves the richness of high-dimensional EEG data (Fields and Kuperberg, 2020; Meyer et al., 2021). We incorporated cluster-based permutation tests into our multi-factorial design through a multi-step process. The pipeline was applied to TEPs, SEPs, TIOs, and SIOs separately. Fig. 2 illustrates an example in TEPs. We denoted the two levels of *Time* as T1 and T2 and the three levels of *Drug* as D1, D2, and D3. This created a six-cell data structure per TMS site (Fig. 2a): T1D1, T2D1, T1D2, T2D2, T1D3, and T2D3, and we assigned the condition-specific TEPs accordingly.

Our primary interest was the interaction effect of *Time* x *Drug*, i.e., whether the change in TEPs (ΔTEPs; Δ denotes *POST-PRE* difference) depended on the drug conditions. By iteratively subtracting TEPs in T2 from TEPs in T1, we reduced our design to one factor *Drug* with a three-

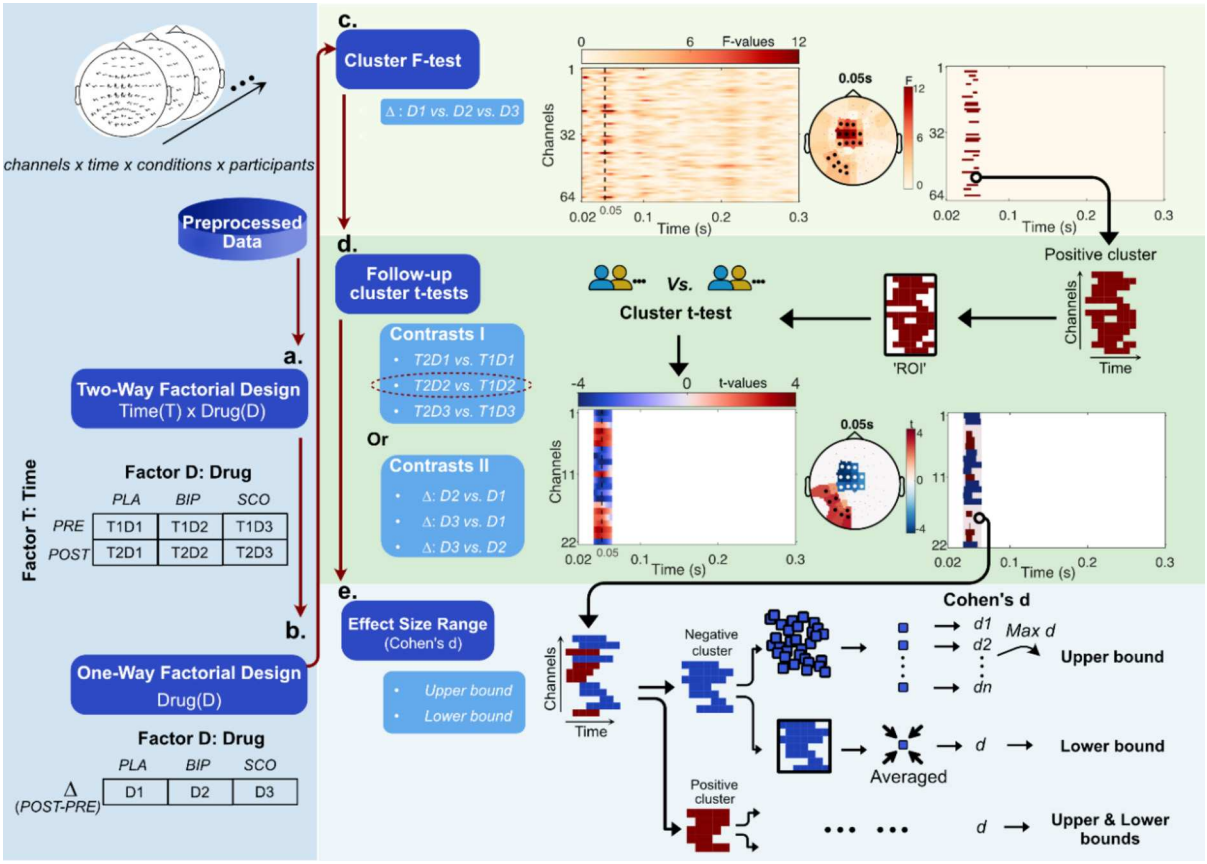

Fig. 2. Statistical analysis of TEPs. TEPs were derived by subtracting *sham* TMS-evoked potentials from *active* TMS-evoked EEG potentials, organized as channels x time x conditions x participants. (a) TEPs were sorted according to a Two-way factorial design: Factor A (Time) with levels T1 (PRE) and T2 (POST). Factor D (Drug) with levels D1 (PLA), D2 (BIP), and D3 (SCO). (b) Data was transformed into ΔTEP by subtracting PRE TEP from POST TEP, reducing the study into a One-way factor design: Factor D with levels D1 (PLA), D2 (BIP), and D3 (SCO). (c) A cluster-based permutation F-test was conducted on ΔTEPs among D1, D2, and D3. This assessed whether the change in TEPs (ΔTEPs) depended on the drug conditions, equivalent to testing a Time x Drug interaction effect. Sub-panels show F-values over time and channels (left), the F-value topography at 0.05 s with channels comprising the significant cluster marked in black (middle), and the spatiotemporal extent of the cluster (right). (d) Follow-up cluster-based permutation *t*-tests were performed within an ROI defined by the cluster identified in the F-test. Sub-panels display an example of the t-test result comparing T2D2 vs. T1D2: t-values showing over time and channels (left), the t-value topography at 0.05 s with channels comprising positive and negative clusters marked in black and white (middle), and the spatiotemporal extents of positive (in red) and negative (in blue) clusters (right). (e) Effect size range. For the upper bound, Cohen's d was calculated for each channel and time point within the cluster, and the largest value was eventually selected. For the lower bound, the cluster was circumscribed with a rectangular shape and Cohen's d was calculated for the averaged data within this shape. *Abbreviations: BIP, biperiden; PLA, placebo; PRE: pre-drug; POST: post-drug; SCO, scopolamine; ROI: region of interest; TEPs: TMS evoked EEG potentials.* (For interpretation of the references to colour in this figure legend, the reader is referred to the web version of this article.)

cell data structure (Fig. 2b): ΔTEPs for D1, D2, and D3. Conceptually, testing an interaction effect was equivalent to conducting an F-test on ΔTEPs among D1, D2, and D3, with the null hypothesis that ΔTEPs did not differ across conditions (Fields and Kuperberg, 2020). We employed the non-parametrical cluster-based permutation F-test, including all channels and a 20 to 300 ms post-stimulus time window (cluster threshold: $p < .025$ dependent F-test, critical $\alpha < 0.05$ one-tailed; randomization = 2000) (Fig. 2c). We chose $p < .025$ as cluster inclusion criteria, as TEPs, particularly in early latency, are short-lived and sharply peaked, and a more stringent criterion enhances sensitivity to focal effects (Fields and Kuperberg, 2020).

If a significant interaction effect was detected, we examined which drug condition primarily drove the interaction by testing planned contrasts (Fig. 2d: Contrast I). For instance, we compared T2D2 to T1D2 with the null hypothesis that they were not different. Importantly, these follow-up analyses were constrained to data within a region of interest (ROI), defined by a rectangular shape circumscribing the cluster identified by the F-test (Sassenhagen and Draschkow, 2019). For these follow-up analyses, we used non-parametric cluster-based permutation *t*-tests (cluster threshold: $p < .025$ dependent t-test, critical $\alpha < 0.05$ two-tailed; randomization = 2000) and corrected the critical alpha level for multiple comparisons using the Bonferroni approach (Tabachnick and Fidell, 2007). In the case of SEP, a significant difference between *POST* and *PRE* was identified in all drug conditions, including the placebo. This suggested that some time-varying factors, such as fatigue, might influence SEP over the course of the experiment (Boksem et al., 2005). To control this confounding effect, we directly compared ΔSEPs between drug conditions (Fig. 2d: Contrast II). For instance, we compared ΔSEPs under D2 to ΔSEPs under D1, with the null hypothesis that changes in SEPs were comparable between D1 and D2. To quantify the significant effects identified by cluster t-tests, we estimated the effect size using Cohen's d, which measures the standardized difference between means (Sawilowsky, 2009). Following Meyer et al. (Meyer et al., 2021), we reported an effect size range with an upper and lower bound (Fig. 2e). More details are provided in the Supplementary Materials: Section 1.3.

Similarly, we applied this pipeline to TIOs and SIOs, adjusting the parameters for the cluster-based F/t-tests to accommodate the three-dimensional data: channel x time x frequency. To examine if there was a *Time* x *Drug* interaction on oscillatory power, we conducted the cluster-based permutation F-test on Δpower (changes in oscillatory power; Δ denotes *POST-PRE* difference), including all channels, a time window of

50–650 ms and a frequency range of 4–40 Hz (cluster threshold: $p < .05$ dependent F-test, critical $\alpha < 0.05$ one-tailed; randomization = 2000). If a significant interaction effect was detected, we proceeded with follow-up analyses using cluster-based permutation t-tests (cluster threshold: $p < .05$ dependent t-test, critical $\alpha < 0.05$ two-tailed; randomization = 2000), and corrected the critical alpha level for multiple comparisons using the Bonferroni approach.

Drug effects on reaction time: We conducted a linear mixed-effects analysis on reaction time in R (version 4.3.2) using the lmer function from the lmerTest package:

$$1/\mathrm{SRT} \sim \mathrm{Time} + \mathrm{Drug} + \mathrm{Time} : \mathrm{Drug} + (1|\mathrm{participant})$$

Given that the data distribution of SRT was positively skewed, we applied a reciprocal transformation (−1/SRT) to the raw SRT data (Balota et al., 2013). The fixed effects in the model included the factors *Time* and *Drug*, as well as their interaction term *Time:Drug*. For random effects, we included intercepts for participants. If a significant *Time* x *Drug* interaction was found, we proceeded to test planned contrasts by comparing the estimated marginal means from *POST* versus *PRE* at each level of *Drug*. Multiple comparisons were controlled using the Bonferroni approach.

3. Results

3.1. Effects of drugs on reaction time

Visual inspection of residual plots from the model revealed mild deviations from normality. As outliers in the data may cause stress in the model, we further trimmed the data to exclude those with absolute standardized residuals exceeding 2.5 standard deviations (2.1 % of trials across all participants) (Baayen and Milin, 2010). The model built on the trimmed data had residuals that approximated normality more closely. The *Time* x *Drug* interaction effect on the transformed reaction time (−1/SRT) was significant ($p < .05$). Follow-up comparisons revealed that the interaction was driven by biperiden (*POST* vs. *PRE*, $p < .0001$, Cohen's d = 0.29) and scopolamine (*POST* vs. *PRE*, $p < .0001$, Cohen's d = 0.41) (Fig. 3).

3.2. Effects of drugs on TEPs

When stimulating the SMA, *POST-PRE* difference waveforms (ΔTEPs) and their respective topographies revealed prominent EEG features for the biperiden and scopolamine conditions (Fig. 4). The cluster-based permutation F-test revealed a significant difference in ΔTEPs among *PLA*, *BIP* and *SCO* (Table 1), suggesting a *Time* x *Drug* interaction. The difference was driven by the largest positive cluster ($p = .0351$, critical $\alpha = 0.05$), which approximately extended from 40 to 63 ms after the TMS pulse and covered 22 channels. Fig. 5a illustrates the cluster extent in time and channels, showing that the effect was more prominent at left parietal-central channels.

Given the presence of an interaction effect, we next investigated whether the interaction was driven more by scopolamine, biperiden, or both. Cluster-based permutation *t*-tests revealed that *POST* TEPs significantly differed from *PRE* only under the scopolamine condition (Table 2). The difference was driven by the largest negative cluster ($p = .0003$, corrected critical $\alpha = 0.0083$), approximately extending from 40 to 63 ms and spanning central channels (Fig. 5b). The estimated effect size range was large (Cohen's d = [0.82, 0.94]), yet relatively localized and short-lived, with its upper bound estimated at channel FC3 at 47 ms. As shown in Fig. 5b, the TEP at channel FC3 had a larger amplitude for *POST* scopolamine compared to *PRE* during the 40 to 63 ms window. Spatially, TEPs in the central areas were more negative after scopolamine administration, evident at both the sensor and source levels.

To assess if changes in TEPs correlated to changes in SRT under scopolamine at the group level, we used Spearman's correlation to calculate the relationship between the two variables. Changes in TEPs were averaged over the channels composing the cluster identified in the t-test, and changes in SRT were computed as means averaged over pre- and post-drug trials. We found no significant correlation between changes in SRT and changes in TEPs ($R_s = -0.28$, $p = .18$) (Supplementary Fig. 1).

The cluster-based permutation F-tests revealed no significant difference in ΔTEPs among *PLA*, *BIP* and *SCO* following either mPFC or AG stimulation (Table 1). This suggests an absence of *Time* x *Drug* interaction in TEPs when targeting these cortical areas (Supplementary Figs. 2 and 3). Consequently, no follow-up analyses were performed.

3.3. Effects of drugs on TIOs

We first aimed to characterize the TMS-induced oscillatory power for each TMS target by subtracting the effect of sensory inputs from the oscillatory response before any drug intervention (details of statistical analysis in Supplementary Materials: Section 1.4).

When stimulating the SMA, TMS-induced oscillatory power before drug administration was not significantly different across the three sessions (all identified clusters, $p > .05$). Therefore, we averaged the induced oscillator power before drug administration across three sessions to increase the signal-to-noise ratio (SNR). TMS over the SMA produced a power increase in the beta band at the left central channels, lasting up to around 200 ms (Fig. 6a). The cluster-based permutation *t*-test revealed that, when targeting the SMA, TMS-induced oscillatory power significantly differed from zero. The difference was driven by the positive cluster ($p = .0025$, Cohen's d = [0.61, 1.08], critical $\alpha = 0.025$), approximately extending from 11 to 40 Hz, 50 to 260 ms and spanning

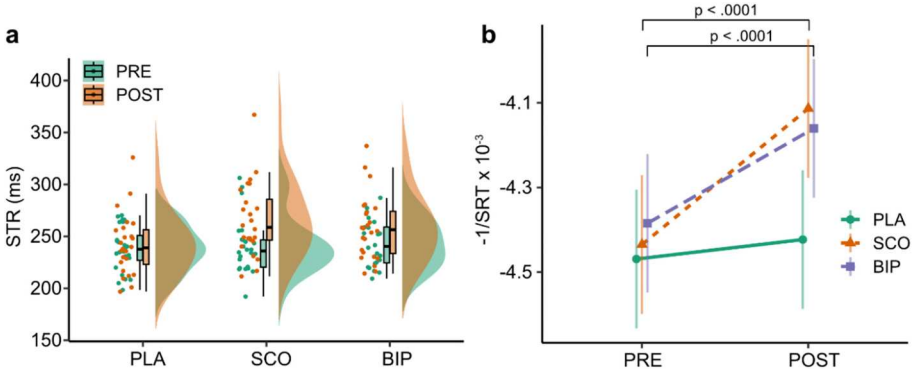

Fig. 3. Effects of drugs on reaction time. (a) Raincloud plot showing mean SRTs averaged across trials for each participant, with accompanying boxplots and probability densities for each condition. (b) Results from the linear mixed model on transformed trial-level data (−1/SRT), with estimated marginal means and 95 % confidence intervals for each condition. Significant *P*-values for the POST vs. PRE contrast are shown for SCO and BIP conditions. *Abbreviations: BIP, biperiden; PLA, placebo; SCO, scopolamine; PRE: pre-drug; POST: post-drug; SRT: simple reaction time.*

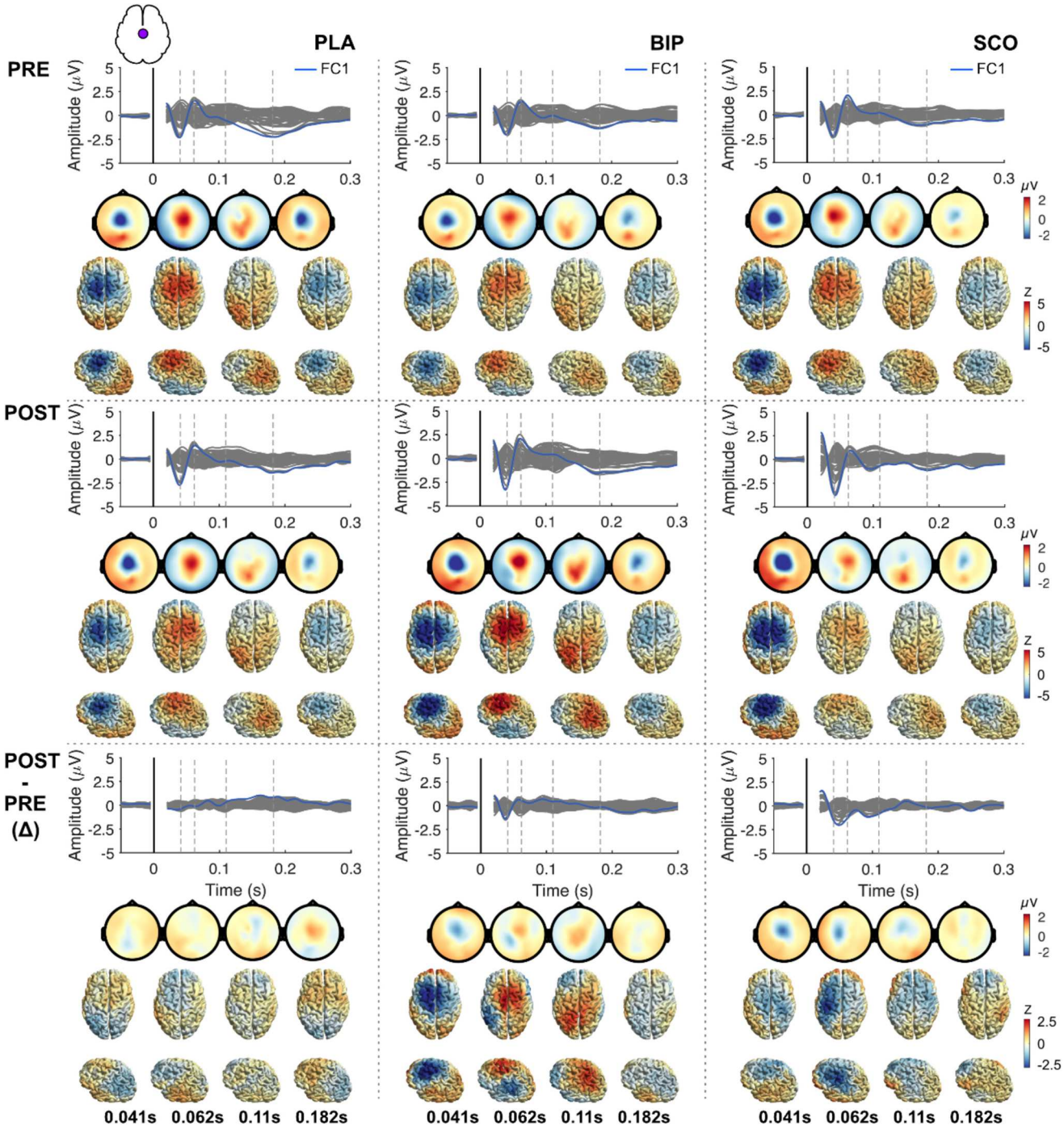

Fig. 4. TEPs in response to TMS of the SMA pre- and post-drug administration. TEPs were obtained by subtracting *sham* TMS-evoked from *active* TMS-evoked EEG potentials, averaged across participants. Each condition is shown by multi-channel TEP plots with topography time series displayed at both sensor and source levels. Rows: PRE, POST, and POST-PRE (Δ); Columns: PLA, BIP, and SCO. *Abbreviations: BIP, biperiden; PLA, placebo; PRE: pre-drug; POST: post-drug; SCO, scopolamine; SMA: supplementary motor area; TEPs: TMS evoked EEG potentials.*

54 channels (Fig. 6b). The estimated effect size was relatively large (Cohen's d = [0.61, 1.08]), with its upper bound estimated at 19 Hz, 60 ms, and channel FC3. However, when evaluating the drug effects on the TMS-induced power, the cluster-based permutation F-test revealed no significant difference in Δpower among *PLA*, *BIP,* and *SCO*, indicating the absence of *Time* x *Drug* interaction. Consequently, no follow-up analyses were performed.

When targeting the mPFC and AG, the corresponding TMS-induced oscillatory power before drug administration was not significantly different from zero (all identified clusters, $p > .025$). This indicates that TMS did not elicit robust oscillatory power in these cortical regions (Supplementary Fig. 4). Consequently, we did not proceed with further analyses of drug effects on TIOs from mPFC and AG stimulations.

3.4. Effects of drugs on SEPs

SEPs before drug administration were not significantly different among the three sessions (all identified clusters, $p > .05$). SEP waveforms and topographies were similar across sessions, with the typical N100–P200 complex evident at the frontal-central channels (Fig. 7).

Table 1
Cluster-based permutation F-test results on ΔTEPs among PLA, BIP, and SCO, separately for TMS of the SMA, AG, and mPFC.

	Cluster		Approximate extent	
SMA	Polarity	P-value	Time [ms]	Space [N channels]
Δ: PLA vs. BIP vs. SCO	+	**0.0351**	40–63	22
AG				
Δ: PLA vs. BIP vs. SCO	+	0.3986		
mPFC				
Δ: PLA vs. BIP vs. SCO	+	0.0898		

Only clusters with the smallest p-value are listed. The cluster with a *p*-value less than the critical **α (= 0.05)** is highlighted in bold, along with its approximate spatiotemporal extent. ΔTEP represents the changes in TEPs between post- and pre-drug administrations. TEPs were obtained by subtracting *sham* TMS-evoked from *active* TMS-evoked EEG potentials. *Abbreviations: AG: angular gyrus; BIP, biperiden; mPFC: medial prefrontal cortex; PLA, placebo; SCO, scopolamine; SMA, supplementary motor area; TEPs: TMS evoked EEG potentials.*

POST-PRE difference waveforms (ΔSEPs) and their corresponding topographies resembled N100–P200 but with reversed polarities, indicating that N100 was less negative and P200 was less positive after drug administration. This pattern was observed across all drug conditions, including the placebo. The cluster-based permutation F-test revealed significant differences in ΔSEPs among *PLA*, *BIP* and *SCO* (Table 3). These differences were driven by two positive clusters identified in the observed data (Table 3). The largest cluster ($p = .0001$, critical $\alpha = 0.05$) indicated a late-onset interaction effect from about 208 to 300 ms post-stimulus. The second largest cluster ($p = .0006$, critical $\alpha = 0.05$) indicated a relatively early interaction effect from around 34 to 120 ms (Fig. 8a). In follow-up analyses, we compared ΔSEPs between drugs (Table 4) separately within the two time windows.

During the early time window, ΔSEPs caused by scopolamine differed significantly from placebo, while no significant differences were found between biperiden and placebo or between scopolamine and biperiden (Table 4). The differences were driven by a negative and a positive cluster (Neg: $p = .0001$, Cohen's d = [1.24, 1.35]; Pos: $p = .0001$, Cohen's d = [1.06, 1.08], corrected critical $\alpha = 0.0042$), occurring from about 38 to 118 ms (Fig. 8b). During the late time window, ΔSEPs caused by biperiden differed significantly from both placebo and scopolamine (Table 4). The biperiden vs. placebo contrast revealed significant differences driven by a negative and a positive cluster (Neg: $p = .0001$, Cohen's d = [0.96, 1.08]; Pos: $p = .0015$, Cohen's d = [0.91, 1.06], corrected critical $\alpha = 0.0042$), occurring from about 208 to 263 ms (Fig. 8c). Similarly, the biperiden vs. scopolamine contrast revealed significant differences driven by a negative and a positive cluster (Neg: $p = .0012$, Cohen's d = [1.09, 1.17]; Pos: $p = .0005$, Cohen's d = [0.69, 1.13], corrected critical $\alpha = 0.0042$), occurring from around 208 to 300 ms (Fig. 8d).

3.5. Effects of drugs on SIOs

The sensory inputs-induced oscillatory power before drug administration was not significantly different across the three sessions (all identified clusters, $p > .05$). Fig. 9a illustrates the induced power before drug administration averaged across sessions, revealing a triphasic pattern: a brief power increase (enhancement) in broadband oscillations, followed by a decrease (suppression) and a subsequent rebound in

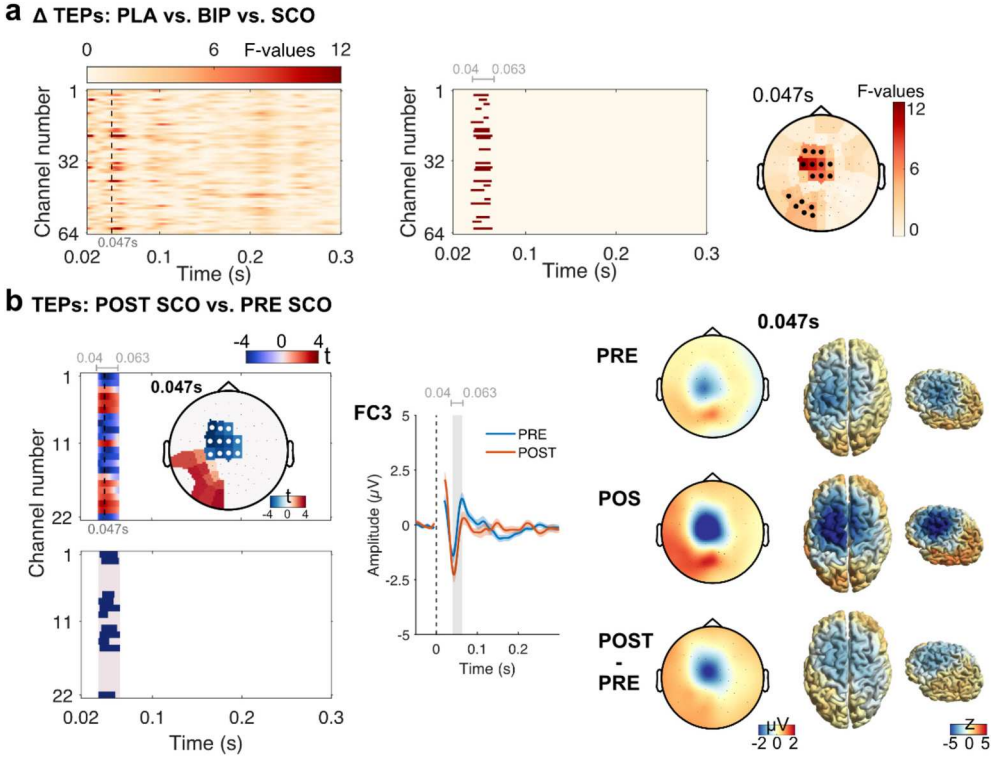

Fig. 5. Effects of drugs on TEPs in response to TMS of the SMA. (a) Cluster F-test results on ΔTEPs among PLA, BIP, and SCO. Sub-panels show F-values over time and channels (left), the spatiotemporal extent of the significant cluster (middle), and the F-value topography at 0.047 s with channels comprising the significant cluster marked in black (right). (b) Cluster *t*-test results comparing TEPs for POST SCO vs. PRE SCO. The left sub-panel displays t-values over time and channels and the t-value topography at 0.047 s, with channels comprising the significant cluster marked in white (top) and the spatiotemporal extent of the significant cluster (bottom). The middle sub-panel shows the TEP from channel FC3 with ±standard error of the means. The right sub-panel shows the topography of TEPs at 0.047 s at both sensor and source levels. The selected timepoint and channel correspond to the sample yielding the upper bound of effect size (Table 2). *Abbreviations: BIP, biperiden; PLA, placebo; PRE: pre-drug; POST: post-drug; SCO, scopolamine; SMA: supplementary motor area; TEPs: TMS evoked EEG potentials.*

Table 2
Cluster-based permutation t-test results comparing SMA TEPs for POST vs. PRE, separately for each drug condition.

Within 40–63 ms						
	Clusters		Approximate extent		Effect size	
Contrasts I	Polarity	P-value	Time [ms]	Space [N channels]	Range	Channel-time pair
PLA: POST vs. PRE	+	0.0487				
BIP: POST vs. PRE	+	0.0466				
	−	0.0098				
SCO: POST vs. PRE	+	0.0116				
	−	**0.0003**	40–63	11	0.82–0.94	FC3; 47 ms

Only clusters with the smallest p-value are listed. The cluster with a p-value less than the critical **α (= 0.0083**, Bonferroni corrected**)** is highlighted in bold, along with its approximate spatiotemporal extent and effect size range. The channel-time pair corresponds to the sample yielding the upper bound of the effect size. TEPs were obtained by subtracting evoked EEG potentials to *sham* from those to *active* TMS. *Abbreviations: BIP, biperiden; PLA, placebo; PRE: pre-drug; POST: post-drug; SCO, scopolamine; SMA, supplementary motor area; TEPs: TMS evoked EEG potentials.*

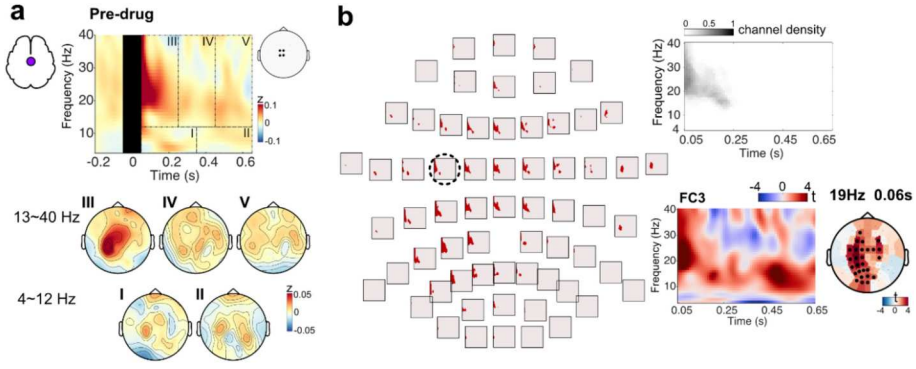

Fig. 6. TMS-induced oscillatory power in response to SMA stimulation pre-drug administration. The power was derived by subtracting *sham* TMS-induced from *active* TMS-induced EEG oscillatory power. (a) TFRs pre-drug administration were averaged across participants, channels underneath the coil (FCz, FC1, Cz, C1), and the three sessions. The black box masks the time window (−0.05 to 0.05 s) potentially contaminated by TMS-related artifacts. The bottom rows show topographies of the induced power, averaged across five time-frequency regions of interest chosen based on visual inspection (I: 0.05–0.35 s; II: 0.36–0.65 s; III: 0.05–0.25 s; IV: 0.26–0.45 s; V: 0.46–0.65 s). (b) Cluster t-test results comparing TMS-induced oscillatory power pre-drug administration against zero. The left sub-panel shows the spectral-temporal extent of the significant cluster according to electrode layout. The right sub-panel shows the ratio of channels comprising the significant cluster to the total number of channels (top), t-values over time and frequencies at channel FC3, and the t-value topography at 19 Hz, 0.06 s (bottom). The selected time point, channel, and frequency correspond to the sample yielding the upper bound of effect size. *Abbreviations: SMA, supplementary motor area; TFRs: time-frequency representations.*

power (enhancement), more prominently in the higher frequency range.

Following drug administrations, the induced power showed distinct alterations (Fig. 9b). The cluster-based permutation F-test revealed a significant difference in Δpower among *PLA*, *BIP,* and *SCO* (Table 5). This difference was driven by a positive cluster ($p = .0005$, critical $\alpha = 0.05$), indicating a *Time* x *Drug* interaction effect extending globally from 4 to 40 Hz, 50 to 650 ms and encompassing all channels. To determine whether the interaction was driven more by scopolamine, biperiden, or both, we conducted cluster-based permutation *t*-tests. We found that, unlike placebo, both scopolamine and biperiden significantly increased the induced oscillatory power (Table 6). Specifically, the *POST* vs. *PRE* contrast under biperiden revealed a significant difference driven by a positive cluster ($p = .0010$, Cohen's d = [0.5, 1.23], corrected critical $\alpha = 0.0083$), approximately extending from 4 to 33 Hz, 50 to 650 ms, and covering all channels (Fig. 9c). Similarly, the *POST* vs. *PRE* contrast under scopolamine revealed a significant difference driven by a positive cluster ($p = .0005$, Cohen's d = [0.89, 1.53], corrected critical $\alpha = 0.0083$), extending globally from 4 to 33 Hz, 50 to 650 ms, and converging all channels (Fig. 9d). While both scopolamine and biperiden had widespread effects on induced oscillatory power in terms of spatial and spectral distribution, their effects displayed distinct features. Biperiden primarily reversed the power suppression induced by sensory stimulation, whereas scopolamine appeared to augment power enhancements in both the early low-frequency and later higher-frequency ranges.

4. Discussion

The involvement of neuromodulator-mediated neurotransmission in TMS–EEG responses remains largely unexplored. In this study, we investigated how the inhibition of mAChR-mediated cholinergic neurotransmission through the intake of mAChR antagonists scopolamine and biperiden affects TEPs and TIOs. There are three main findings in this study: 1) TEPs are affected by the inhibition of cholinergic neurotransmission, with significant effects observed specifically when scopolamine is used and TMS targets the SMA. 2) While cholinergic inhibition also modulates SEPs, its effects on TEPs are independent of those on SEPs. 3) The power of SIOs, but not TIOs, is increased by the inhibition of cholinergic neurotransmission. Both scopolamine and biperiden significantly enhance broadband synchronization, each with distinct profiles.

4.1. mAChR-mediated cholinergic transmission in TMS–EEG responses when targeting the SMA

In our study, TMS over the SMA produces an N45-like TEP component near the stimulation site. Its amplitude increased significantly following scopolamine administration, with biperiden showing a similar but less robust effect (Fig. 4). The N45 component is thought to reflect the balance of excitatory and inhibitory neurotransmission, as supported by previous pharmacological TMS–EEG studies targeting the M1. These studies have shown that the amplitude of N45 increases by diazepam, a

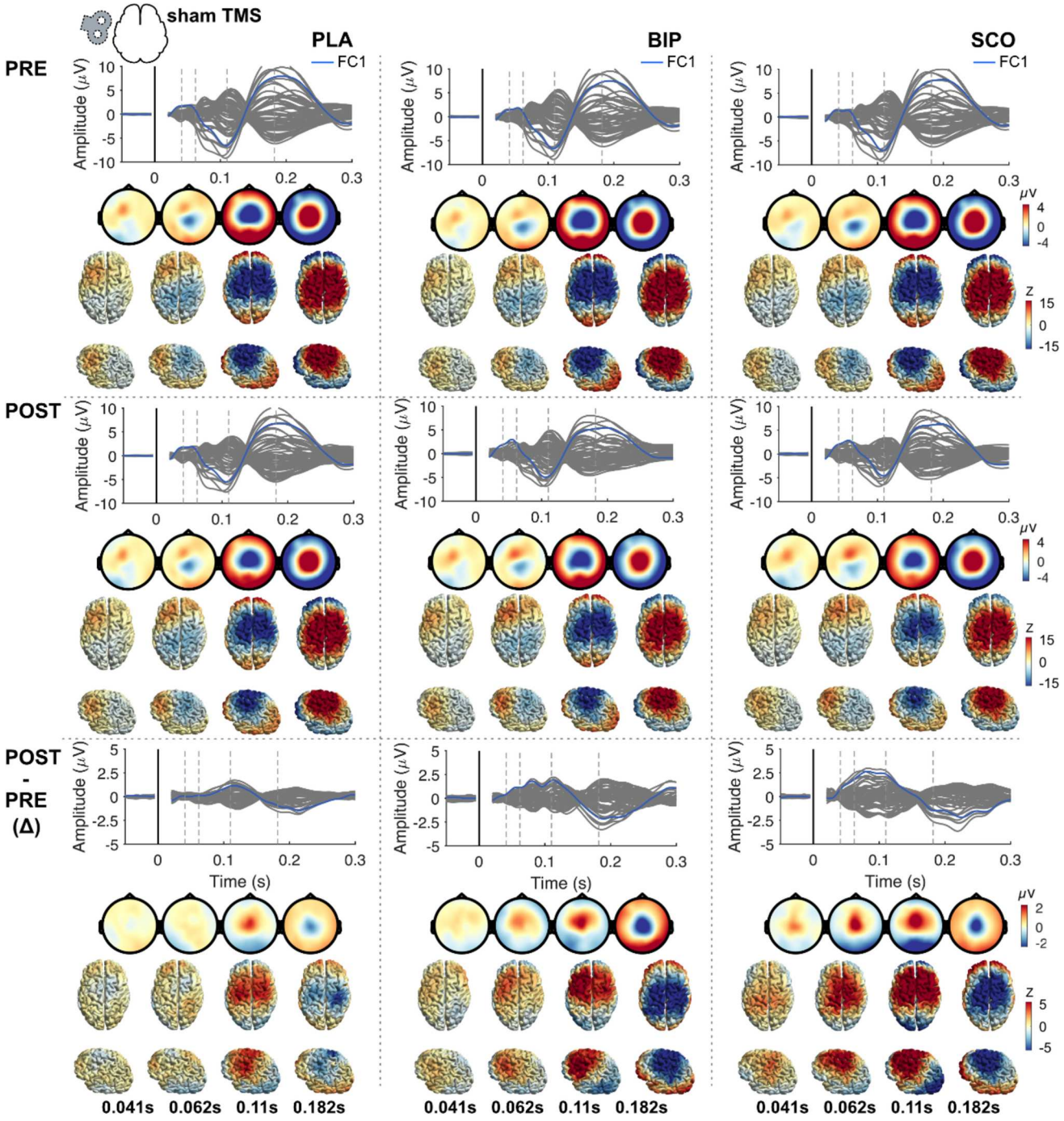

Fig. 7. SEPs in response to *sham* TMS stimulation. SEPs were averaged across participants. Each condition is shown by multi-channel SEP plots with topography time series displayed at both sensor and source levels. Rows: PRE, POST, and POST-PRE (Δ); Columns: PLA, BIP, and SCO. *Abbreviations: BIP, biperiden; PLA, placebo; PRE: pre-drug; POST: post-drug; SCO, scopolamine; SEPs: sensory inputs evoked EEG potentials.*

Table 3
Cluster-based permutation F-test result on ΔSEPs among PLA, BIP, and SCO.

	Clusters		Approximate extent	
	Polarity	P-value	Time [ms]	Space [N channels]
Δ: PLA vs. BIP vs. SCO	+	**0.0001**	208–300	50
	+	**0.0006**	34–120	37

Clusters with *p*-values less than the critical **α (= 0.05)** are listed, along with their approximate spatiotemporal extents. ΔSEP represents the changes in SEPs between post- and pre-drug administrations. *Abbreviations: BIP, biperiden; PLA, placebo; SCO, scopolamine; SEPs: sensory inputs evoked EEG potentials.*

positive allosteric modulator at GABAARs, and dextromethorphan, a competitive antagonist at the NMDAR (Belardinelli et al., 2021; Premoli et al., 2014), while it decreases by compound S44819, an experimental compound acting as specific antagonist at the alpha5-GABAAR (Darmani et al., 2016). Therefore, the increased N45 amplitude in our study likely indicates a shift of the excitation / inhibition balance, possibly toward more inhibition, following anti-cholinergic intervention.

While other cortical regions may also contribute, N45 is likely caused by activation of a cortical-subcortical motor circuit (Ziemann et al., 2015), such as the corticobasal ganglia-thalamo-cortical loop. Cortical

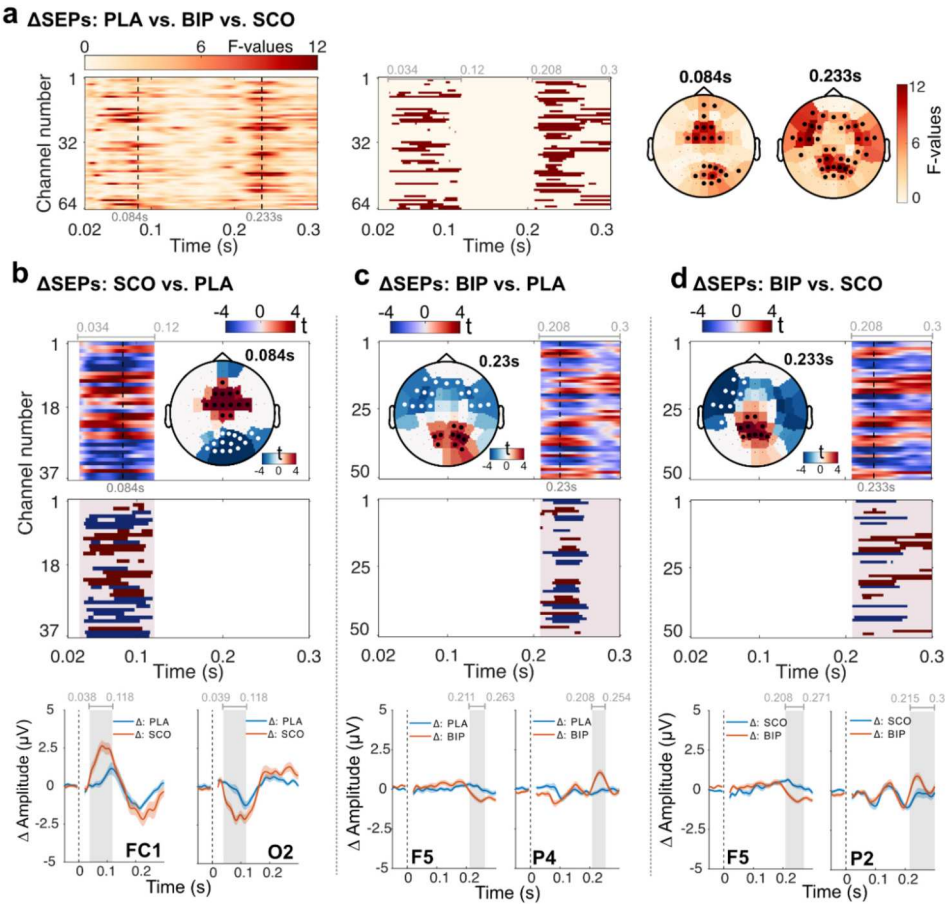

Fig. 8. Effects of drugs on SEPs in response to *sham* TMS stimulation. (a) Cluster F-test results on ΔSEPs among PLA, BIP, and SCO. Sub-panels show F-values over time and channels (left), the spatiotemporal extent of the two significant clusters (middle), and the F-value topography at 0.084 s and 0.233 s with channels comprising the significant clusters marked in black (right). Cluster t-test results comparing ΔSEPs for (b) SCO vs. PLA, (c) BIP vs. PLA, and (d) BIP vs. SCO. Within each panel, the top sub-panel shows t-values over time and channels and the t-value topography at a selected time point, with channels comprising the significant positive and negative clusters marked in black and white. The middle sub-panel shows the spatiotemporal extent of the significant positive (in red) and negative (in blue) clusters. The bottom sub-panel shows grand average ΔSEPs from selected channels with ±standard error of the means. The selected timepoint and channel correspond to the sample yielding the upper bound of effect size (Table 4); *Abbreviations: BIP, biperiden; PLA, placebo; SCO, scopolamine; SEPs: sensory inputs evoked EEG potentials.* (For interpretation of the references to colour in this figure legend, the reader is referred to the web version of this article.)

motor areas are interconnected with basal ganglia (BG) structures, such as the striatum and the subthalamic nucleus (STN). In these regions, synapses are formed with glutamatergic inputs from the cortex and dopaminergic inputs from the midbrain, which then relay information back to the cortex via the thalamus (Nakano et al., 2000; Utter and Basso, 2008). The SMA is a primary target of this BG motor circuit through the thalamus (Utter and Basso, 2008). During deep brain stimulator implantation surgery in PD patients, single-pulse TMS over the M1 altered the firing rate of STN neurons (Strafella et al., 2004), and TMS over the SMA and M1 produced evoked local field potentials recorded at the level of the STN (Doyle Gaynor et al., 2008). These studies confirm that excitation from stimulated motor areas can descend through cortical-subcortical tracts. Furthermore, ascending information from subcortical to motor cortical areas is supported by deep brain stimulation studies, where evoked EEG potentials were recorded from scalp electrodes in the motor cortical area following basal ganglia stimulation (STN or internal globus pallidus) (Kuriakose et al., 2010; Ni et al., 2018; Walker et al., 2012), with positive or negative peaks at varied latencies (<10 ms or 20–25 ms).

This circuitry is a complex network where glutamatergic (excitatory) and GABAergic (inhibitory) neurotransmission transsynaptically convey information, finely regulated by multiple neuromodulators (Augustine and Singer, 2018). Among these, AChR-mediated cholinergic transmission plays an important modulating role. Striatal cholinergic interneurons are tonically active, releasing ACh spontaneously in the absence of synaptic input (Abudukeyoumu et al., 2019). mAChRs are highly expressed by axon terminals of major afferents to the striatum (glutamatergic and dopaminergic terminals) and by striatal neurons, including (GABAergic) medium spiny projection neurons and other interneurons (Ztaou and Amalric, 2019). The diverse distribution of mAChRs and the autonomous firing feature of cholinergic interneurons underpin cholinergic regulation of striatal output, affecting medium spiny projection neurons directly and indirectly by modulating dopamine, glutamate, and GABA release (Abudukeyoumu et al., 2019; Ztaou and Amalric, 2019). One pharmacological TMS–EEG study investigated whether the acute intake of the dopamine precursor levodopa affected TEPs when targeting the SMA (Casarotto et al., 2019). They quantified TEPs using local mean field power in channels near the SMA within a time window of about 15 to 60 ms. Their findings showed that levodopa increased the size of TEPs, similar to the effect of the mAChR antagonist scopolamine observed in our study. These observations align with the known interplay between cholinergic and dopaminergic systems in basal ganglia function, where cholinergic tone increases as striatal dopamine levels decline, and vice versa (Aosaki et al., 2010). While delineating the exact neurotransmission processes affected by cholinergic inhibition is beyond the scope of our study, our findings suggest that striatal cholinergic signaling likely regulates the BG-thalamo-cortical pathway, thereby tuning excitatory and inhibitory transmission and, ultimately,

Table 4
Cluster-based permutation *t*-test results comparing ΔSEPs between drugs within two time windows.

Within 34–120 ms						
	Clusters		Approximate extent		Effect size	
Contrasts II	Polarity	P-value	Time [ms]	Space [N channels]	Range	Channel-time pair
Δ: SCO vs. PLA	+	**0.0001**	38–118	16	1.06–1.08	FC1; 84 ms
	−	**0.0001**	39–118	17	1.24–1.35	O2; 88 ms
Δ: BIP vs. PLA	+	0.0310				
	−	0.0224				
Δ: SCO vs. BIP	+	0.1937				
	−	0.0217				

Within 208–300 ms						
	Clusters		Approximate extent		Effect size	
Contrasts II	Polarity	P-value	Time [ms]	Space [N channels]	Range	Channel-time pair
Δ: SCO vs. PLA	+	0.1418				
	−	0.0504				
Δ: BIP vs. PLA	+	**0.0015**	208–254	15	0.91–1.06	P4; 230 ms
	−	**0.0001**	211–263	17	0.96–1.08	F5; 242 ms
Δ: BIP vs. SCO	+	**0.0005**	215–300	18	0.69–1.13	P2; 233 ms
	−	**0.0012**	208–271	9	1.09–1.17	F5; 248 ms

Only clusters with the smallest p-value are listed. The clusters with p-values less than the critical **α (= 0.0042**, Bonferroni corrected**)** are highlighted in bold, along with their approximate spatiotemporal extent and effect size range. The channel-time pair corresponds to the sample yielding the upper bound of the effect size. ΔSEP represents the changes in SEPs between post- and pre-drug administrations. *Abbreviations: BIP, biperiden; PLA, placebo; SCO, scopolamine; SEPs: sensory inputs evoked EEG potentials.*

influencing the excitability of the SMA.

In addition to these observations on TEPs, we found that TMS over the SMA induces a significant power increase in the 11–40 Hz range, representing beta/gamma band synchronization. This spectral dynamic of TIOs is consistent with a previous study that observed a similar oscillatory profile when TMS was applied to the cortical Brodmann area 6 (the middle or caudal portion of the superior frontal gyrus) (Rosanova et al., 2009). It has been suggested that such TMS-related oscillatory activity represents the natural frequency of the stimulated cortico-thalamic circuit. However, unlike TEPs, we did not observe anti-cholinergic modulation of TMS-induced oscillatory power, suggesting that mAChR-mediated cholinergic neurotransmission is less involved in TIOs. This discrepancy corroborates the notion that different neuro-physiological mechanisms underlie non-phase-locked TIOs and phase-locked TEPs.

4.2. mAChR-mediated cholinergic transmission in TMS–EEG responses when targeting the mPFC and AG

We found no significant effects of anti-cholinergic drugs on TEPs when stimulating the mPFC and AG. This suggests that mAChR-mediated cholinergic transmission likely does not contribute to TEPs when applying TMS to these regions in a task-free state (i.e., at rest). The primary source of ACh in the neocortex are BF cholinergic neurons. Although mAChRs are widespread across the cortex, ACh release from the BF to the cortex is region-specific and context-dependent. This specificity is possibly due to BF cholinergic neurons being organized in groups and active according to both topographical and functional principles, resulting in the spatiotemporal precision of BF cholinergic signaling (Muñoz and Rudy, 2014; Záborszky et al., 2018). Animal studies using microdialysis have shown that ACh release in the mPFC and parietal regions is specifically associated with cue detection and goal-oriented processes but not with basic behavioral operations that are not explicitly attention-demanding (Arnold et al., 2002; Himmelheber et al., 1997; Parikh et al., 2007). Similarly, in a human fMRI study, it was demonstrated that scopolamine intake can reduce brain activation in the left superior and middle frontal regions during an attentional reorienting task (Thienel et al., 2009). It is also possible that nAChR-mediated, rather than mAChR-mediated, cholinergic transmission might play a significant role. Hyperactivations in medial frontoparietal regions secondary to nicotine (a nAChR agonist) intake were observed in the resting state and in a task with low attention requirements (Lawrence et al., 2002; Stein et al., 1998). Future research may explore to what extent mAChR-mediated or nAChR-mediated cholinergic neurotransmission is involved in TMS–EEG responses in the context of attention tasks. Lastly, as we previously reported (Song et al., 2023), TMS over the mPFC resulted in a higher degree of variability in TEPs between individuals and across repeated sessions in the same individuals than the SMA and AG, which may have hindered the discovery of drug effects. However, this explanation does not entirely account for the absence of drug effects during AG stimulation.

4.3. mAChR-mediated cholinergic transmission in sensory-related EEG responses

Our study shows that the inhibition of cholinergic transmission affects cortical EEG responses to auditory and somatosensory stimuli associated with TMS. Moreover, these effects vary depending on the specific mAChRs being blocked, as evidenced by the distinct changes in SEPs and SIOs by scopolamine and biperiden.

The impact of cholinergic signaling on sensory processing is often examined in the context of cognitive functions such as attention and memory, where sensory stimuli can be either relevant or irrelevant to a task (Bentley et al., 2011). Previous studies on the effects of scopolamine or biperiden on event-related potentials in response to sensory stimuli have shown mixed results across varied task paradigms (e.g., passive exposure or attention-demanding) and sensory cues (e.g., visual, auditory, somatosensory, or multimodal) (reviewed in (Kunnath et al., 2023)). Some studies report decreases in the amplitudes of components like P50, N1, P1, P2, and P3a, while others report no changes or even opposite effects. In our study, we used cluster-based permutation F/*t*-tests to analyze changes in SEPs (ΔSEPs), rather than examining SEPs at pre-selected channels and time points, which makes direct comparisons with previous literature challenging. However, we observed that the amplitudes of the N100 and P200 components at frontal-central channels were more reduced under the influence of scopolamine and

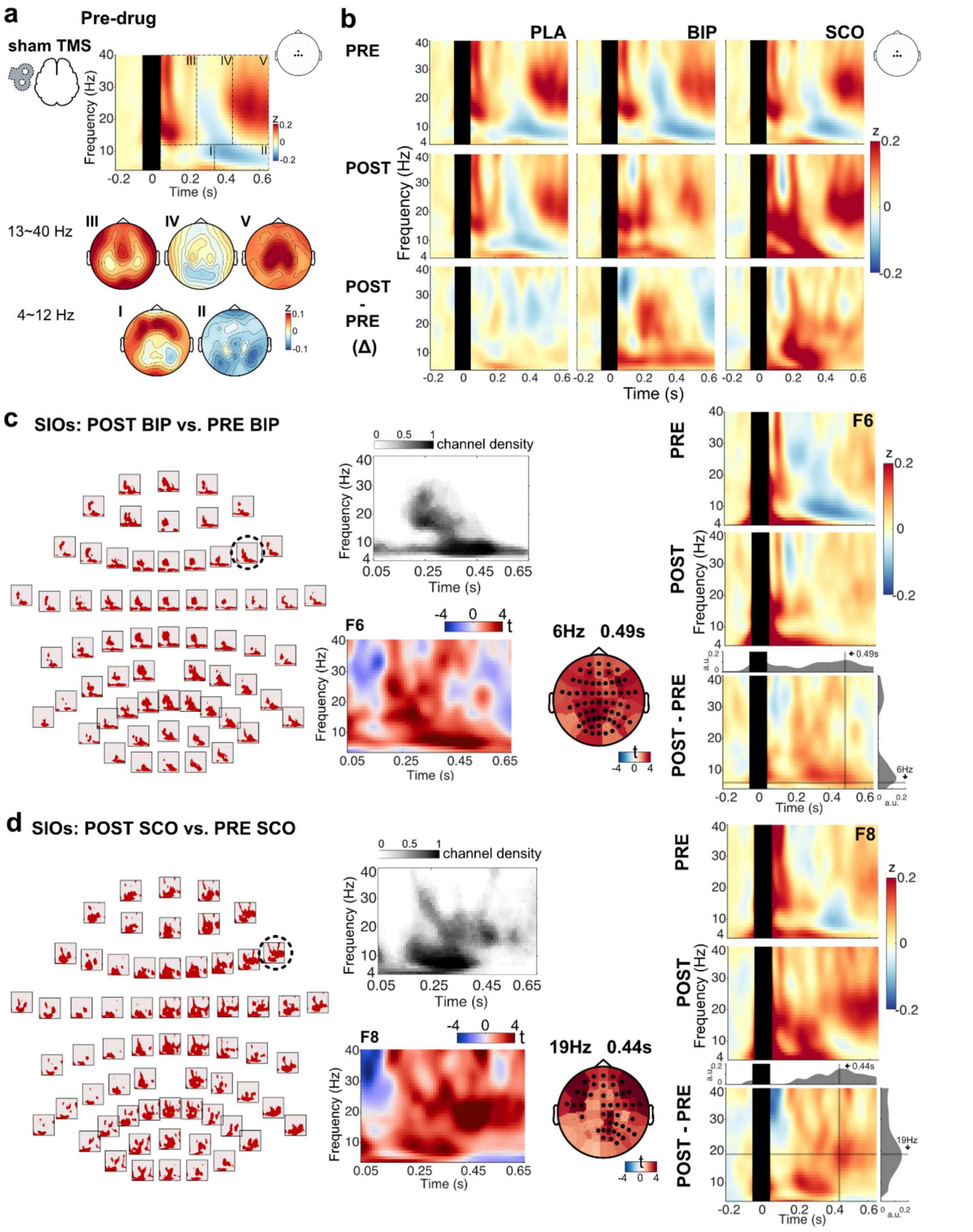

(caption on next page)

Fig. 9. Sensory inputs-induced oscillatory power in response to *sham* TMS stimulation (a) TFRs pre-drug administration were averaged across participants, channels (FCz, Cz, C1, C2), and the three sessions. The black box masks the time window (−0.05 to 0.05 s) potentially contaminated by stimulation-related artifacts. The bottom rows show topographies of the induced power, averaged across five time-frequency regions of interest chosen based on visual inspection (I: 0.05–0.35 s; II: 0.36–0.65 s; III: 0.05–0.25 s; IV: 0.26–0.45 s; V: 0.46–0.65 s). (b) Condition-specific TFRs, averaged across participants and channels (FCz, Cz, C1, C2). Rows: PRE, POST, and POST-PRE (Δ); Columns: PLA, BIP, and SCO. Cluster t-test results comparing the induced oscillatory power for (c) BIP: POST vs. PRE and (d) SCO: POST vs. PRE. Within each panel, the left sub-panel shows the spectral-temporal extent of the significant positive cluster according to electrode layout. The middle sub-panel shows the ratio of channels comprising the significant cluster to the total number of channels (top), t-values over time and frequencies at a selected channel, and the t-value topography at a selected frequency-time (bottom). The right sub-panel shows TFRs from a selected channel at PRE, POST, and POST-PRE. Marginal plots in the POST-PRE plot depict the power of a selected frequency change over time (top), and the power at a selected time point change over frequency (right). The selected time points, channels, and frequencies correspond to the sample yielding the upper bound of effect size (Table 6). *Abbreviations: BIP, biperiden; PLA, placebo; PRE: pre-drug; POST: post-drug; SCO, scopolamine; SIOs: sensory inputs-induced EEG oscillations; TFRs: time-frequency representations.*

Table 5
Cluster-based permutation F-test result on Δsensory inputs-induced oscillatory power among PLA, BIP, and SCO.

	Clusters		Approximate extent		
	Polarity	P-value	Freq [Hz]	Space [N channels]	Time [ms]
Δ: PLA vs. BIP vs. SCO	+	**0.0005**	4–40	64	50–650

The cluster with a p-value less than the critical **α (= 0.05)** is listed, along with its approximate spectral-spatial-temporal extent. Δ represents the changes in oscillatory power between post- and pre-drug administrations. *Abbreviations: BIP, biperiden; PLA, placebo; SCO, scopolamine.*

biperiden compared to the placebo (Fig. 7), aligning with studies reporting decreased N1 and P2 amplitudes (Caldenhove et al., 2017; Curran et al., 1998).

Regarding SIOs, we observed a typical pattern of oscillatory power elicited by sensory inputs: a brief broadband synchronization, followed by alpha/beta band desynchronization, and a subsequent rebound (synchronization) in the beta band. This spectral profile is commonly observed in magnetoencephalography (M/EEG) studies, with variations depending on stimulus modality and time-frequency analysis methods (Andersen and Lundqvist, 2019; Bauer et al., 2006; Novembre et al., 2019). We found that anticholinergic drugs significantly alter spectral dynamics (Fig. 9): biperiden primarily reverses alpha/beta band desynchronization, while scopolamine appears to enhance synchronization in both the alpha band early after stimulation and the beta band at a later period. Consistent with our findings, optogenetic studies in animals demonstrated that cholinergic signaling activation from the BF to sensory cortices causes desynchronization, while inhibition of cholinergic signaling enhances synchronization (Kim et al., 2016; Pinto et al., 2013).

Overall, our results support the notion that ACh in the sensory cortex influences sensory processing by altering neuronal responses to specific stimuli, shifting cortical dynamics from synchronous to asynchronous (Colangelo et al., 2019; Záborszky et al., 2018). Moreover, we found that sensory-related responses are differentially affected by scopolamine and biperiden. Biperiden differs from scopolamine in its binding specificity to M1 mAChR, compared to scopolamine's non-selective action on mAChRs. While M1–M4 mAChRs are widely expressed in the cortex, their distributions are layer- and cell-type specific. Such specificity is believed to be one reason that neural populations receiving the same sensory input could respond differentially (Colangelo et al., 2019; Thiele, 2013). Thus, distinct changes in sensory responses could be observed depending on which mAChR was blocked.

4.4. Control for TMS-associated sensory inputs

Anti-cholinergic drugs affect sensory-related EEG responses to *sham* TMS, a control condition that includes TMS-associated somatosensory and auditory inputs. These changes could be misinterpreted as anti-cholinergic modulation of genuine TEPs if sensory EEG components are not isolated before evaluating drug effects. To address this, we evaluated drug effects on cleaned TMS–EEG responses by subtracting the *sham* TMS-related EEG responses from those in the *active* TMS condition. The necessity of controlling sensory input in pharmacological TMS–EEG studies was highlighted in our recent study (Gordon et al., 2023b), where the N100 component identified in both *sham* and *active* TMS-evoked EEG potentials was affected by diazepam intake. However, in the cleaned TEPs, where the *sham* TMS-evoked EEG potentials were removed, the N100 component was largely attenuated and insensitive to diazepam. This suggests that the N100 component originates from sensory activation, and its modulation by diazepam should be interpreted as drug effects on sensory processing.

Furthermore, the profile of sensory input-induced oscillatory power, as shown in TFR plots (Fig. 9), can also be observed in the *sham* TMS condition (Gordon et al., 2023b), as well as in several TMS–EEG studies where TMS was applied to different cortical regions (Biondi et al., 2022; Casula et al., 2016; Premoli et al., 2017). This similarity suggests that some of the oscillatory power observed in these studies may stem from TMS-associated sensory inputs rather than direct cortical responses.

Controlling for TMS-associated sensory inputs is necessary for studies using TMS–EEG to measure cortical responsiveness before and after an intervention. Despite constant stimulation parameters before and after the intervention on the same participant, sensory processing can be modulated by the intervention itself, complicating the interpretation of EEG responses. Without proper sensory control, it becomes challenging to determine to what extent observed changes in EEG responses are due to the intervention's effect on direct cortical activation

Table 6
Cluster-based permutation *t*-test results comparing the sensory inputs-induced oscillatory power for POST vs. PRE for each drug condition.

	Clusters		Approximate extent			Effect size	
Contrasts I	Polarity	P-value	Freq [Hz]	Space [N channels]	Time [ms]	Range	Channel-freq-time triplet
PLA: POST vs. PRE	+	0.7206					
	−	0.0785					
BIP: POST vs. PRE	+	**0.0010**	4–33	64	50–650	0.50–1.23	F6; 6 Hz; 490 ms
	−	0.0725					
SCO: POST vs. PRE	+	**0.0005**	4–40	64	50–650	0.89–1.53	F8; 19 Hz; 440 ms
	−	0.1754					

Only clusters with the smallest p-value are listed. The clusters with *p*-values less than the critical **α (= 0.0083**, Bonferroni corrected**)** are highlighted in bold, along with their approximate spectral-spatial-temporal extent and effect size range. The channel-freq-time triplet corresponds to the sample yielding the upper bound of the effect size. *Abbreviations: BIP, biperiden; PLA, placebo; PRE: pre-drug; POST: post-drug; SCO, scopolamine.*

elicited by TMS, sensory processing, or both.

4.5. Limitations

One possible limitation of the present study is the choice of the sham procedure, which involved applying high-intensity ES in both *sham* and *active* TMS conditions. This approach deviates from previous studies, where ES is administered only in the *sham* TMS condition (Chowdhury et al., 2022; Rocchi et al., 2021). Our rationale was to closely approximate sensory-related EEG responses in both conditions by saturating sensory inputs with high-intensity ES. By subtracting *sham* from *active* TMS–EEG responses, we aimed to eliminate common sensory responses, thereby revealing the direct cortical activation elicited by TMS, as described in our previous study (Gordon et al., 2021). However, concerns arise regarding the use of high-intensity ES in the *active* TMS condition, as it may alter cortical responsiveness to TMS due to neurophysiological interactions. This raises doubts about the reliability of isolating genuine TMS–EEG responses through subtraction. Despite these concerns, we have reported that TEPs obtained through this sham procedure remained largely unchanged despite varying ES intensity used for saturation (Gordon et al., 2023a). Therefore, there is currently no evidence for a significant interaction between sensory responses and direct cortical responses from TMS measured by EEG. Additionally, using this sham procedure, we were able to successfully obtain distinct EEG responses with unique topographies that were likely due to direct cortical activation by TMS of specific brain regions, i.e., mPFC, AG, and SMA (Song et al., 2023).

Another limitation is the high inter-individual and inter-session variability of TEPs elicited with mPFC stimulation (Song et al., 2023), which may have hindered the discovery of modulation of TEPs by cholinergic transmission inhibition. The low signal-to-noise ratio may contribute to this variability, as suggested by the low amplitude of TEPs when applying TMS to the mPFC. While increasing TMS intensity may result in stronger direct cortical responses, as reported in a previous study (Kähkönen et al., 2005), it could also amplify unwanted signals, such as somatosensory and auditory EEG responses. Future studies may investigate strategies to optimize TMS–EEG measures in frontal regions while carefully controlling for TMS-associated sensory inputs.

Additionally, our study did not include the short-latency afferent inhibition (SAI) paradigm, which previous studies have linked to the central cholinergic system (Tremblay et al., 2019; Ziemann et al., 2015). While combining SAI with TMS–EEG has the potential to probe cholinergic neurotransmission in non-motor regions (Noda et al., 2016), the complexity of controlling for sensory contamination in the SAI TMS–EEG paradigm led us to focus on single-pulse TMS–EEG in this study. Lastly, while the order of TMS–EEG measurements targeting the mPFC, AG, and SMA was randomized, it was not fully counterbalanced across participants. Future studies should employ a fully counterbalanced design to minimize potential biases related to time-varying factors.

5. Conclusion

Our study demonstrates the involvement of mAChR-mediated cholinergic neurotransmission in TEPs but not in TIOs. Notably, this involvement is target-specific, as cholinergic inhibition through scopolamine, a non-selective mAChR antagonist, significantly increased the amplitude of a local TEP component between approximately 40 and 63 ms post-stimulus when TMS was applied to the SMA, but not to the mPFC or AG. The selective M1 mAChR antagonist biperiden tended to produce a similar effect as scopolamine, but this was less pronounced. Moreover, cholinergic inhibition also affected SEPs but, importantly, its effects on TEPs were independent of those on SEPs. These findings add to the understanding of neuromodulator-mediated transmission in TMS–EEG responses, supporting their potential use in further physiological and clinical research.

Ethical statement

The study was approved by the ethics committee of the medical faculty of Tübingen University (protocol number 638/2020BO1) and was conducted in accordance with the Declaration of Helsinki. Informed consent was obtained from all individual participants included in the study.

Funding

The study was funded by the European Research Council (ERC Synergy) under the European Union's Horizon 2020 research and innovation program (ConnectToBrain, grant number 810377).

Declaration of generative AI in scientific writing

During the preparation of this work, the first author used ChatGPT-4o (freely available at https://chatgpt.com/) solely for grammar correctness, word choice, and semantics improvement. After using this tool, the first author and all co-authors reviewed and edited the content as needed and take full responsibility for the content of the publication.

CRediT authorship contribution statement

Yufei Song: Conceptualization, Methodology, Formal analysis, Investigation, Data curation, Writing – original draft, Writing – review & editing, Visualization, Project administration. **Pedro C. Gordon:** Conceptualization, Methodology, Writing – review & editing, Supervision, Project administration. **Olivier Roy:** Methodology, Writing – review & editing, Visualization. **Johanna Metsomaa:** Software, Methodology, Writing – review & editing. **Paolo Belardinelli:** Software, Methodology, Writing – review & editing. **Maryam Rostami:** Software, Methodology, Writing – review & editing. **Ulf Ziemann:** Conceptualization, Methodology, Validation, Resources, Writing – review & editing, Supervision, Project administration, Funding acquisition.

Declaration of competing interest

The authors declare no conflicts of interest.

Data availability

The code used is available in GitHub: https://github.com/Song-Yufei/anti-cholinergic-drugs-on-TMS-EEG-responses. The preprocessed TMS–EEG data, individual head models and lead field matrices that support the findings of the manuscript are deposited in the repository FDAT: https://doi.org/10.57754/FDAT.d0ms3-z0v09 with access granted under specified conditions, i.e., EULA (End User License Agreement) signed by the user.

Appendix A. Supplementary data

Supplementary data to this article can be found online at https://doi.org/10.1016/j.pnpbp.2024.111167.

References

Abudukeyoumu, N., Hernandez-Flores, T., Garcia-Munoz, M., Arbuthnott, G.W., 2019. Cholinergic modulation of striatal microcircuits. Eur. J. Neurosci. 49, 604–622.
Andersen, L.M., Lundqvist, D., 2019. Somatosensory responses to nothing: an MEG study of expectations during omission of tactile stimulations. NeuroImage 184, 78–89.
Aosaki, T., Miura, M., Suzuki, T., Nishimura, K., Masuda, M., 2010. Acetylcholine–dopamine balance hypothesis in the striatum: an update. Geriatr Gerontol Int 10, S148–S157.
Arnold, H., Burk, J., Hodgson, E., Sarter, M., Bruno, J., 2002. Differential cortical acetylcholine release in rats performing a sustained attention task versus behavioral control tasks that do not explicitly tax attention. Neuroscience 114, 451–460.

Augustine, F., Singer, H.S., 2018. Merging the pathophysiology and pharmacotherapy of tics. Tremor Other Hyperkinet. Mov. 8.
Baakman, A.C., Alvarez-Jimenez, R., Rissmann, R., Klaassen, E.S., Stevens, J., Goulooze, S.C., den Burger, J.C., Swart, E.L., van Gerven, J.M., Groeneveld, G.J., 2017. An anti-nicotinic cognitive challenge model using mecamylamine in comparison with the anti-muscarinic cognitive challenge using scopolamine. Br. J. Clin. Pharmacol. 83, 1676–1687.
Baayen, R.H., Milin, P., 2010. Analyzing reaction times. Int. J. Psychol. Res. 3, 12–28.
Bakker, C., van Esdonk, M.J., Stuurman, R.F.E., Borghans, L.G., de Kam, M.L., van Gerven, J.M., Groeneveld, G.J., 2021. Biperiden challenge model in healthy elderly as proof-of-pharmacology tool: a randomized, placebo-controlled trial. J. Clin. Pharmacol. 61, 1466–1478.
Ballinger, E.C., Ananth, M., Talmage, D.A., Role, L.W., 2016. Basal forebrain cholinergic circuits and signaling in cognition and cognitive decline. Neuron 91, 1199–1218.
Balota, D.A., Aschenbrenner, A.J., Yap, M.J., 2013. Additive effects of word frequency and stimulus quality: the influence of trial history and data transformations. J. Exp. Psychol. Learn. Mem. Cogn. 39, 1563.
Bauer, M., Oostenveld, R., Peeters, M., Fries, P., 2006. Tactile spatial attention enhances gamma-band activity in somatosensory cortex and reduces low-frequency activity in parieto-occipital areas. J. Neurosci. 26, 490–501.
Belardinelli, P., König, F., Liang, C., Premoli, I., Desideri, D., Müller-Dahlhaus, F., Gordon, P.C., Zipser, C., Zrenner, C., Ziemann, U., 2021. TMS-EEG signatures of glutamatergic neurotransmission in human cortex. Sci. Rep. 11, 8159.
Bentley, P., Driver, J., Dolan, R.J., 2011. Cholinergic modulation of cognition: insights from human pharmacological functional neuroimaging. Prog. Neurobiol. 94, 360–388.
Biondi, A., Rocchi, L., Santoro, V., Rossini, P., Beatch, G., Richardson, M., Premoli, I., 2022. Spontaneous and TMS-related EEG changes as new biomarkers to measure anti-epileptic drug effects. Sci. Rep. 12, 1919.
Bohnen, N.I., Grothe, M.J., Ray, N.J., Müller, M.L., Teipel, S.J., 2018. Recent advances in cholinergic imaging and cognitive decline—revisiting the cholinergic hypothesis of dementia. Curr. Geriatr. Rep. 7, 1–11.
Boksem, M.A., Meijman, T.F., Lorist, M.M., 2005. Effects of mental fatigue on attention: an ERP study. Cogn. Brain Res. 25, 107–116.
Caldenhove, S., Borghans, L., Blokland, A., Sambeth, A., 2017. Role of acetylcholine and serotonin in novelty processing using an oddball paradigm. Behav. Brain Res. 331, 199–204.
Casarotto, S., Turco, F., Comanducci, A., Perretti, A., Marotta, G., Pezzoli, G., Rosanova, M., Isaias, I.U., 2019. Excitability of the supplementary motor area in Parkinson's disease depends on subcortical damage. Brain Stimul. 12, 152–160.
Cash, R.F.H., Noda, Y., Zomorrodi, R., Radhu, N., Farzan, F., Rajji, T.K., Fitzgerald, P.B., Chen, R., Daskalakis, Z.J., Blumberger, D.M., 2017. Characterization of glutamatergic and GABAA-mediated neurotransmission in motor and dorsolateral prefrontal cortex using paired-pulse TMS–EEG. Neuropsychopharmacology 42, 502–511. https://doi.org/10.1038/npp.2016.133.
Casula, E.P., Pellicciari, M.C., Picazio, S., Caltagirone, C., Koch, G., 2016. Spike-timing-dependent plasticity in the human dorso-lateral prefrontal cortex. Neuroimage 143, 204–213.
Chowdhury, N.S., Rogasch, N.C., Chiang, A.K., Millard, S.K., Skippen, P., Chang, W.-J., Bilska, K., Si, E., Seminowicz, D.A., Schabrun, S.M., 2022. The influence of sensory potentials on transcranial magnetic stimulation–electroencephalography recordings. Clin. Neurophysiol. 140, 98–109.
Cohen, M.X., 2014. Analyzing Neural Time Series Data: Theory and Practice. MIT press.
Colangelo, C., Shichkova, P., Keller, D., Markram, H., Ramaswamy, S., 2019. Cellular, synaptic and network effects of acetylcholine in the neocortex. Front. Neural Circuits 13, 24.
Conde, V., Tomasevic, L., Akopian, I., Stanek, K., Saturnino, G.B., Thielscher, A., Bergmann, T.O., Siebner, H.R., 2019. The non-transcranial TMS-evoked potential is an inherent source of ambiguity in TMS-EEG studies. Neuroimage 185, 300–312.
Curran, H., Pooviboonsuk, P., Dalton, J., Lader, M., 1998. Differentiating the effects of centrally acting drugs on arousal and memory: an event-related potential study of scopolamine, lorazepam and diphenhydramine. Psychopharmacology 135, 27–36.
Darmani, G., Zipser, C.M., Böhmer, G.M., Deschet, K., Müller-Dahlhaus, F., Belardinelli, P., Schwab, M., Ziemann, U., 2016. Effects of the selective α5-GABAAR antagonist S44819 on excitability in the human brain: a TMS–EMG and TMS–EEG phase I study. J. Neurosci. 36, 12312–12320.
Delorme, A., Makeig, S., 2004. EEGLAB: an open source toolbox for analysis of single-trial EEG dynamics including independent component analysis. J. Neurosci. Methods 134, 9–21.
Doyle Gaynor, L., Kühn, A., Dileone, M., Litvak, V., Eusebio, A., Pogosyan, A., Androulidakis, A., Tisch, S., Limousin, P., Insola, A., others, 2008. Suppression of beta oscillations in the subthalamic nucleus following cortical stimulation in humans. Eur. J. Neurosci. 28, 1686–1695.
Fernandez, L., Biabani, M., Do, M., Opie, G.M., Hill, A.T., Barham, M.P., Teo, W.-P., Byrne, L.K., Rogasch, N.C., Enticott, P.G., 2021. Assessing cerebellar-cortical connectivity using concurrent TMS-EEG: a feasibility study. J. Neurophysiol. 125, 1768–1787.
Fields, E.C., Kuperberg, G.R., 2020. Having your cake and eating it too: flexibility and power with mass univariate statistics for ERP data. Psychophysiology 57, e13468.
Gordon, P.C., Jovellar, D.B., Song, Y., Zrenner, C., Belardinelli, P., Siebner, H.R., Ziemann, U., 2021. Recording brain responses to TMS of primary motor cortex by EEG–utility of an optimized sham procedure. Neuroimage 245, 118708.
Gordon, P.C., Song, Y., Jovellar, B., Belardinelli, P., Ziemann, U., 2023a. No evidence for interaction between TMS-EEG responses and sensory inputs. Brain Stimul. 16, 25–27.
Gordon, P.C., Song, Y.F., Jovellar, D.B., Rostami, M., Belardinelli, P., Ziemann, U., 2023b. Untangling TMS-EEG responses caused by TMS versus sensory input using optimized sham control and GABAergic challenge. J. Physiol. 601, 1981–1998.
Grandchamp, R., Delorme, A., 2011. Single-trial normalization for event-related spectral decomposition reduces sensitivity to noisy trials. Front. Psychol. 2, 236.
Groppa, S., Oliviero, A., Eisen, A., Quartarone, A., Cohen, L., Mall, V., Kaelin-Lang, A., Mima, T., Rossi, S., Thickbroom, G., others, 2012. A practical guide to diagnostic transcranial magnetic stimulation: report of an IFCN committee. Clin. Neurophysiol. 123, 858–882.
Hernandez-Pavon, J.C., Veniero, D., Bergmann, T.O., Belardinelli, P., Bortoletto, M., Casarotto, S., Casula, E.P., Farzan, F., Fecchio, M., Julkunen, P., others, 2023. TMS combined with EEG: recommendations and open issues for data collection and analysis. Brain Stimul. 16, 567–593.
Himmelheber, A.M., Sarter, M., Bruno, J.P., 1997. Operant performance and cortical acetylcholine release: role of response rate, reward density, and non-contingent stimuli. Cogn. Brain Res. 6, 23–36.
Hui, J., Zomorrodi, R., Lioumis, P., Salavati, B., Rajji, T.K., Chen, R., Blumberger, D.M., Daskalakis, Z.J., 2020. Pharmacological mechanisms of interhemispheric signal propagation: a TMS-EEG study. Neuropsychopharmacology 45, 932–939. https://doi.org/10.1038/s41386-019-0468-7.
Ilmoniemi, R.J., Virtanen, J., Ruohonen, J., Karhu, J., Aronen, H.J., Näätänen, R., Katila, T., 1997. Neuronal responses to magnetic stimulation reveal cortical reactivity and connectivity. Neuroreport 8, 3537–3540.
Jackson, A.F., Bolger, D.J., 2014. The neurophysiological bases of EEG and EEG measurement: a review for the rest of us. Psychophysiology 51, 1061–1071.
Kähkönen, S., Komssi, S., Wilenius, J., Ilmoniemi, R.J., 2005. Prefrontal transcranial magnetic stimulation produces intensity-dependent EEG responses in humans. Neuroimage 24, 955–960.
Karamacoska, D., Barry, R.J., Steiner, G.Z., 2018. Electrophysiological underpinnings of response variability in the Go/NoGo task. Int. J. Psychophysiol. 134, 159–167.
Kim, J.-H., Jung, A.-H., Jeong, D., Choi, I., Kim, K., Shin, S., Kim, S.J., Lee, S.-H., 2016. Selectivity of neuromodulatory projections from the basal forebrain and locus ceruleus to primary sensory cortices. J. Neurosci. 36, 5314–5327.
Klinkenberg, I., Blokland, A., 2010. The validity of scopolamine as a pharmacological model for cognitive impairment: a review of animal behavioral studies. Neurosci. Biobehav. Rev. 34, 1307–1350.
Klinkenberg, I., Sambeth, A., Blokland, A., 2011. Acetylcholine and attention. Behav. Brain Res. 221, 430–442.
Kunnath, A.J., Gifford, R.H., Wallace, M.T., 2023. Cholinergic modulation of sensory perception and plasticity. Neurosci. Biobehav. Rev. 152, 105323.
Kuriakose, R., Saha, U., Castillo, G., Udupa, K., Ni, Z., Gunraj, C., Mazzella, F., Hamani, C., Lang, A.E., Moro, E., others, 2010. The nature and time course of cortical activation following subthalamic stimulation in Parkinson's disease. Cereb. Cortex 20, 1926–1936.
Lawrence, N.S., Ross, T.J., Stein, E.A., 2002. Cognitive mechanisms of nicotine on visual attention. Neuron 36, 539–548.
Maris, E., Oostenveld, R., 2007. Nonparametric statistical testing of EEG-and MEG-data. J. Neurosci. Methods 164, 177–190.
Massimini, M., Ferrarelli, F., Huber, R., Esser, S.K., Singh, H., Tononi, G., 2005. Breakdown of cortical effective connectivity during sleep. Science 309, 2228–2232.
Maurice, N., Liberge, M., Jaouen, F., Ztaou, S., Hanini, M., Camon, J., Deisseroth, K., Amalric, M., Kerkerian-Le Goff, L., Beurrier, C., 2015. Striatal cholinergic interneurons control motor behavior and basal ganglia function in experimental parkinsonism. Cell Rep. 13, 657–666.
Metsomaa, J., Song, Y., Mutanen, T.P., Gordon, P.C., Ziemann, U., Zrenner, C., Hernandez-Pavon, J.C., 2024. Adapted beamforming: a robust and flexible approach for removing various types of artifacts from TMS–EEG data. Brain Topogr. 1–25.
Meyer, M., Lamers, D., Kayhan, E., Hunnius, S., Oostenveld, R., 2021. Enhancing reproducibility in developmental EEG research: BIDS, cluster-based permutation tests, and effect sizes. Dev. Cogn. Neurosci. 52, 101036.
Muñoz, W., Rudy, B., 2014. Spatiotemporal specificity in cholinergic control of neocortical function. Curr. Opin. Neurobiol. 26, 149–160.
Nadim, F., Bucher, D., 2014. Neuromodulation of neurons and synapses. Curr. Opin. Neurobiol. 29, 48–56.
Nakano, K., Kayahara, T., Tsutsumi, T., Ushiro, H., 2000. Neural circuits and functional organization of the striatum. J. Neurol. 247, V1–V15.
Ni, Z., Kim, S.J., Phielipp, N., Ghosh, S., Udupa, K., Gunraj, C.A., Saha, U., Hodaie, M., Kalia, S.K., Lozano, A.M., others, 2018. Pallidal deep brain stimulation modulates cortical excitability and plasticity. Ann. Neurol. 83, 352–362.
Noda, Y., Cash, R.F.H., Zomorrodi, R., Dominguez, L.G., Farzan, F., Rajji, T.K., Barr, M.S., Chen, R., Daskalakis, Z.J., Blumberger, D.M., 2016. A combined TMS-EEG study of short-latency afferent inhibition in the motor and dorsolateral prefrontal cortex. J. Neurophysiol. 116, 938–948. https://doi.org/10.1152/jn.00260.2016.
Novembre, G., Pawar, V.M., Kilintari, M., Bufacchi, R.J., Guo, Y., Rothwell, J.C., Iannetti, G.D., 2019. The effect of salient stimuli on neural oscillations, isometric force, and their coupling. NeuroImage 198, 221–230.
Oostenveld, R., Fries, P., Maris, E., Schoffelen, J.-M., 2011. FieldTrip: open source software for advanced analysis of MEG, EEG, and invasive electrophysiological data. Comput. Intell. Neurosci. 2011, 1–9.
Parikh, V., Kozak, R., Martinez, V., Sarter, M., 2007. Prefrontal acetylcholine release controls cue detection on multiple timescales. Neuron 56, 141–154.
Pellicciari, M.C., Veniero, D., Miniussi, C., 2017. Characterizing the cortical oscillatory response to TMS pulse. Front. Cell. Neurosci. 11, 38.
Picciotto, M.R., Higley, M.J., Mineur, Y.S., 2012. Acetylcholine as a neuromodulator: cholinergic signaling shapes nervous system function and behavior. Neuron 76, 116–129.

Pinto, L., Goard, M.J., Estandian, D., Xu, M., Kwan, A.C., Lee, S.-H., Harrison, T.C., Feng, G., Dan, Y., 2013. Fast modulation of visual perception by basal forebrain cholinergic neurons. Nat. Neurosci. 16, 1857–1863.
Premoli, I., Castellanos, N., Rivolta, D., Belardinelli, P., Bajo, R., Zipser, C., Espenhahn, S., Heidegger, T., Müller-Dahlhaus, F., Ziemann, U., 2014. TMS-EEG signatures of GABAergic neurotransmission in the human cortex. J. Neurosci. 34, 5603–5612.
Premoli, I., Bergmann, T.O., Fecchio, M., Rosanova, M., Biondi, A., Belardinelli, P., Ziemann, U., 2017. The impact of GABAergic drugs on TMS-induced brain oscillations in human motor cortex. Neuroimage 163, 1–12.
Rocchi, L., Di Santo, A., Brown, K., Ibáñez, J., Casula, E., Rawji, V., Di Lazzaro, V., Koch, G., Rothwell, J., 2021. Disentangling EEG responses to TMS due to cortical and peripheral activations. Brain Stimul. 14, 4–18.
Rosanova, M., Casali, A., Bellina, V., Resta, F., Mariotti, M., Massimini, M., 2009. Natural frequencies of human corticothalamic circuits. J. Neurosci. 29, 7679–7685.
Salavati, B., Rajji, T.K., Zomorrodi, R., Blumberger, D.M., Chen, R., Pollock, B.G., Daskalakis, Z.J., 2018. Pharmacological manipulation of cortical inhibition in the dorsolateral prefrontal cortex. Neuropsychopharmacology 43, 354–361. https://doi.org/10.1038/npp.2017.104.
Sassenhagen, J., Draschkow, D., 2019. Cluster-based permutation tests of MEG/EEG data do not establish significance of effect latency or location. Psychophysiology 56, e13335.
Sawilowsky, S.S., 2009. New effect size rules of thumb. J. Mod. Appl. Stat. Methods 8, 26.
Siebner, H.R., Funke, K., Aberra, A.S., Antal, A., Bestmann, S., Chen, R., Classen, J., Davare, M., Di Lazzaro, V., Fox, P.T., others, 2022. Transcranial magnetic stimulation of the brain: what is stimulated?–a consensus and critical position paper. Clin. Neurophysiol. 140, 59–97.
Song, Y., Gordon, P.C., Metsomaa, J., Rostami, M., Belardinelli, P., Ziemann, U., 2023. Evoked EEG responses to TMS targeting regions outside the primary motor cortex and their test–retest reliability. Brain Topogr. 1–18.
Stein, E.A., Pankiewicz, J., Harsch, H.H., Cho, J.-K., Fuller, S.A., Hoffmann, R.G., Hawkins, M., Rao, S.M., Bandettini, P.A., Bloom, A.S., 1998. Nicotine-induced limbic cortical activation in the human brain: a functional MRI study. Am. J. Psychiatry 155, 1009–1015.
Strafella, A.P., Vanderwerf, Y., Sadikot, A.F., 2004. Transcranial magnetic stimulation of the human motor cortex influences the neuronal activity of subthalamic nucleus. Eur. J. Neurosci. 20, 2245–2249.
Tabachnick, B.G., Fidell, L.S., 2007. Experimental Designs Using ANOVA. Thomson/Brooks/Cole Belmont, CA.
Thiele, A., 2013. Muscarinic signaling in the brain. Annu. Rev. Neurosci. 36, 271–294.
Thienel, R., Kellermann, T., Schall, U., Voss, B., Reske, M., Halfter, S., Sheldrick, A.J., Radenbach, K., Habel, U., Shah, N.J., others, 2009. Muscarinic antagonist effects on executive control of attention. Int. J. Neuropsychopharmacol. 12, 1307–1317.
Tremblay, S., Rogasch, N.C., Premoli, I., Blumberger, D.M., Casarotto, S., Chen, R., Di Lazzaro, V., Farzan, F., Ferrarelli, F., Fitzgerald, P.B., others, 2019. Clinical utility and prospective of TMS–EEG. Clin. Neurophysiol. 130, 802–844.
Tsuboi, D., Nagai, T., Yoshimoto, J., Kaibuchi, K., 2024. Neuromodulator regulation and emotions: insights from the crosstalk of cell signaling. Front. Mol. Neurosci. 17, 1376762.
Utter, A.A., Basso, M.A., 2008. The basal ganglia: an overview of circuits and function. Neurosci. Biobehav. Rev. 32, 333–342.
Walker, H.C., Huang, H., Gonzalez, C.L., Bryant, J.E., Killen, J., Cutter, G.R., Knowlton, R.C., Montgomery, E.B., Guthrie, B.L., Watts, R.L., 2012. Short latency activation of cortex during clinically effective subthalamic deep brain stimulation for Parkinson's disease. Mov. Disord. 27, 864–873.
Záborszky, L., Gombkoto, P., Varsanyi, P., Gielow, M.R., Poe, G., Role, L.W., Ananth, M., Rajebhosale, P., Talmage, D.A., Hasselmo, M.E., others, 2018. Specific basal forebrain–cortical cholinergic circuits coordinate cognitive operations. J. Neurosci. 38, 9446–9458.
Ziemann, U., Reis, J., Schwenkreis, P., Rosanova, M., Strafella, A., Badawy, R., Müller-Dahlhaus, F., 2015. TMS and drugs revisited 2014. Clin. Neurophysiol. 126, 1847–1868.
Ztaou, S., Amalric, M., 2019. Contribution of cholinergic interneurons to striatal pathophysiology in Parkinson's disease. Neurochem. Int. 126, 1–10.

Supplementary Material

Involvement of muscarinic acetylcholine receptor-mediated cholinergic neurotransmission in TMS–EEG responses

Yufei Song[1,2], Pedro C. Gordon[1,2], Olivier Roy[1,2,3,4], Johanna Metsomaa[5], Paolo Belardinelli[1,2,6], Maryam Rostami[7], Ulf Ziemann[1,2*]

[1]Department of Neurology & Stroke, University of Tübingen, Germany
[2]Hertie Institute for Clinical Brain Research, University of Tübingen, Germany
[3]CERVO Brain Research Centre, Quebec, Canada
[4]Department of Psychiatry and Neurosciences, Université Laval, Quebec, Canada
[5]Department of Neuroscience and Biomedical Engineering, Aalto University School of Science,
Finland
[6]CIMeC, Center for Mind/Brain Sciences, University of Trento, Italy
[7]Faculty of Electrical and Computer Engineering, University of Tehran, Iran

[*]Corresponding Author:
Prof. Dr. Ulf Ziemann
Department of Neurology & Stroke
Hoppe-Seyler-Straße 3, 72076 Tübingen, Germany
Email: ulf.ziemann@uni-tuebingen.de

1 Supplementary method

1.1 Decay Artifact Removal

To address the decay artifact, we applied a first-degree exponential function (a+b∗exp(c∗x) to the time series of each trial and channel, where x represented the time in ms, ranging from 14 to 1000 ms, and a, b, and c were the model parameters. The optimal fit was achieved using the weighted least squares method, giving higher weight to the initial samples following the pulse artifact to prioritize error minimization and enhance estimation accuracy. This weighting strategy was based on the observation that initial samples were more likely to be affected by the decay artifact. The decay-corrected data were obtained by subtracting the fitted exponential model from each time series. Finally, a detrending step was applied to the epochs to minimize sudden signal drops or jumps, ensuring the signal centered around zero.

1.2 Source Reconstruction of Evoked EEG potentials

We followed a procedure documented in our previous work (Song et al., 2023). We processed individual T1 images through a pipeline involving Fieldtrip (Oostenveld et al., 2011), FreeSurfer (Fischl, 2012), HCP-workbench, and SPM toolboxes (Litvak et al., 2011) jointly with custom-made scripts. The source model was built on a triangulated cortical mesh with 15,684 vertices. A 3-D compartment volume conductor model was created individually with the Boundary Element Method (Stenroos and Nummenmaa, 2016). We then aligned the EEG electrode positions with the generated scalp surface. For the inverse estimation, we used minimum-norm estimation (MNE) to obtain source amplitudes **J** as

$$\mathbf{J} = \mathbf{\Lambda L}^T(\mathbf{L\Lambda L}^T + \mathbf{\Sigma})^{-1}\mathbf{Y} \quad (1)$$

Y represents the sensor-level TMS–EEG signals after preprocessing, including the *sham* TMS-evoked or *active* TMS-evoked EEG potentials. The lead-field matrix is denoted as **L**, while **Λ** and **Σ** represent the source and noise covariance matrices, respectively. For the noise covariance matrix, we utilized an identity matrix $\mathbf{\Sigma} = \delta\mathbf{I}$, implying that noise is uncorrelated across sensors with constant variances. The regularization parameter δ, set to 0.01, corresponds to the noise-to-signal ratio (inverse of the signal-to-noise ratio) of the EEG signal. The lead-field matrix **L** was computed for fixed orientations of source dipoles, with each dipole position corresponding to an element in **J** and a respective column in **L**. For the source covariance matrix **Λ**, we assumed that source amplitudes are correlated if they are spatially proximal, with the correlation between two sources i and j decreasing as a function of the distance between their locations r_i and r_j. Specifically, the element in the ith row and jth column of the covariance matrix was defined by the Gaussian-like function:

$$\Lambda(i,j) = \exp[(r_i - r_j)^2/d^2] \quad (2)$$

where d is a constant describing the rate at which correlation decreases. A high value of d suggests roughly uncorrelated sources, whereas lower values imply correlated sources

within larger patches of cortical neurons. The diagonal entries are always 1, but their exact values are irrelevant as the scaling is indirectly controlled by the regularization parameter δ.

Finally, we z-transformed the reconstructed source amplitude of evoked EEG potentials relative to a pre-stimulus time window (–600 to –100 ms) and subtracted *sham* TMS-evoked from *active* TMS-evoked responses to obtain cleaned TEPs at the source level.

1.3 Effect Size Estimation

Following the identification of a significant effect via cluster t-tests, we estimated the effect size using Cohen's d to quantify the standardized difference between means (Sawilowsky, 2009). The irregular shape of the cluster in both space and time introduced uncertainty about which data to include in the computation of the mean. To address this, we adopted the method suggested by Meyer et al. (Meyer et al., 2021) to calculate an upper and lower bound for the effect size estimate. For the lower bound, we utilized the extent of the cluster identified in the t-test. We circumscribed the cluster with a rectangular shape and calculated Cohen's d for the averaged data within this shape. This approach provided a conservative estimate of the effect size. For the upper bound, we calculated Cohen's d for each channel and time point within the cluster and eventually selected the largest value. This approach identified the maximum effect within the cluster. By reporting both upper and lower bounds, we described a range of the effect size and provided precise information about the specific data samples used for the effect size calculations.

1.4 Characterization of TIOs

For each TMS target, to examine whether TMS-induced oscillatory power before drug administration significantly differed among the three sessions, we conducted the non-parametric cluster-based permutation F-test (Maris and Oostenveld, 2007), including all channels, the 50-650 ms time window and the 4-40Hz frequency range (cluster threshold: $p < .05$ dependent F-test, $\alpha < .05$ one-tailed; randomization = 2000). If no significant difference was identified, we averaged the induced oscillatory power before drug administration across the three sessions to increase the signal-to-noise ratio. To characterize TMS-induced oscillatory power, we examined whether the induced oscillatory power significantly differed from zero. This was done by conducting the non-parametric cluster-based permutation t-test (Maris and Oostenveld, 2007), including all channels, a time window of 50 to 650 ms, and a frequency range of 4 to 40 Hz (cluster threshold: $p < .05$ dependent t-test, $\alpha < .05$ two-tailed; randomization = 2000).

References

Fischl, B., 2012. FreeSurfer. Neuroimage 62, 774–781.

Litvak, V., Mattout, J., Kiebel, S., Phillips, C., Henson, R., Kilner, J., Barnes, G., Oostenveld, R., Daunizeau, J., Flandin, G., others, 2011. EEG and MEG data analysis in SPM8. Computational intelligence and neuroscience 2011.

Maris, E., Oostenveld, R., 2007. Nonparametric statistical testing of EEG-and MEG-data. Journal of neuroscience methods 164, 177–190.

Meyer, M., Lamers, D., Kayhan, E., Hunnius, S., Oostenveld, R., 2021. Enhancing reproducibility in developmental EEG research: BIDS, cluster-based permutation tests, and effect sizes. Developmental cognitive neuroscience 52, 101036.

Oostenveld, R., Fries, P., Maris, E., Schoffelen, J.-M., 2011. FieldTrip: open source software for advanced analysis of MEG, EEG, and invasive electrophysiological data. Computational intelligence and neuroscience 2011, 1–9.

Sawilowsky, S.S., 2009. New effect size rules of thumb. Journal of modern applied statistical methods 8, 26.

Song, Y., Gordon, P.C., Metsomaa, J., Rostami, M., Belardinelli, P., Ziemann, U., 2023. Evoked EEG Responses to TMS Targeting Regions Outside the Primary Motor Cortex and Their Test–Retest Reliability. Brain Topography 1–18.

Stenroos, M., Nummenmaa, A., 2016. Incorporating and compensating cerebrospinal fluid in surface-based forward models of magneto-and electroencephalography. PLoS One 11, e0159595.

Supplementary Figures

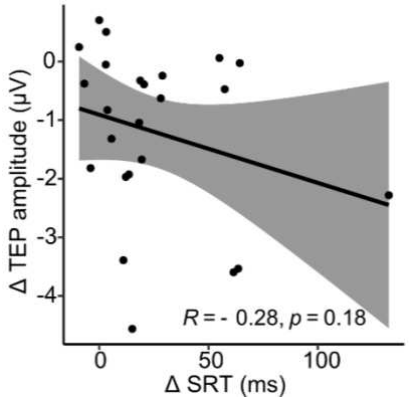

Supplementary Figure 1. Correlation between changes in SRT (POST-PRE) and changes in SMA TEPs (POST-PRE) following scopolamine administration. ΔSRT was averaged over pre- and post-drug trials for each participant. ΔTEP was averaged over the channels composing the cluster identified in the contrast: POST vs. PRE (**Table 2**) for each participant. Spearman's correlation coefficient R = – 0.28 (p = 0.18). *Abbreviations: PRE: pre-drug; POST: post-drug; SRT: simple reaction time; TEPs: TMS evoked EEG potentials.*

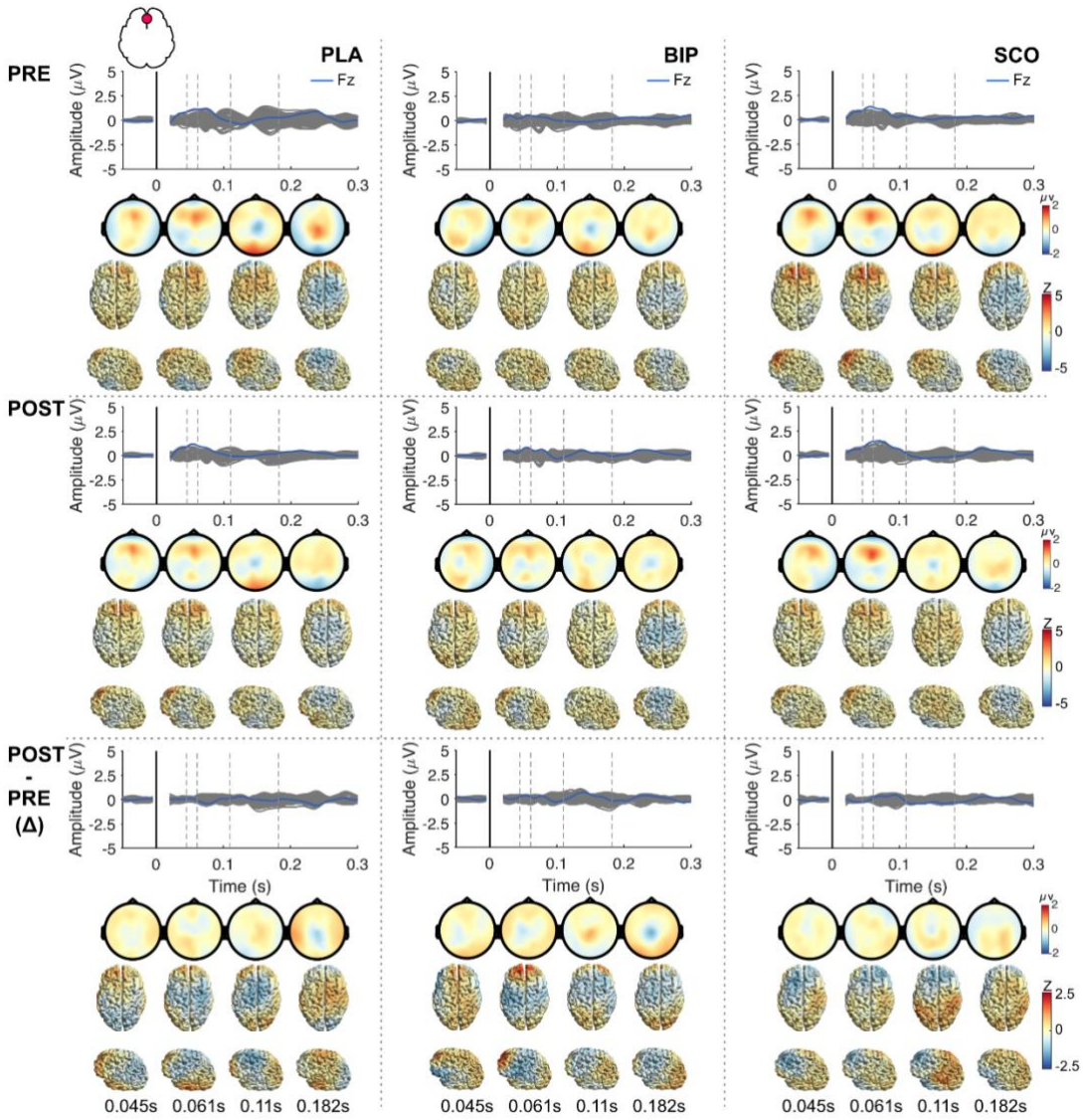

Supplementary Figure 2. TEPs in response to TMS of the mPFC Pre- and Post-drug administration. TEPs were obtained by subtracting *sham* TMS-evoked from *active* TMS-evoked EEG potentials, averaged across participants. Each condition is shown by multi-channel TEP plots with topography time series displayed at both sensor and source levels. Rows: PRE, POST, and POST-PRE (Δ); Columns: PLA, BIP, and SCO. *Abbreviations: BIP, biperiden; mPFC: medial prefrontal cortex; PLA, placebo; PRE: pre-drug; POST: post-drug; SCO, scopolamine; TEPs: TMS evoked EEG potentials.*

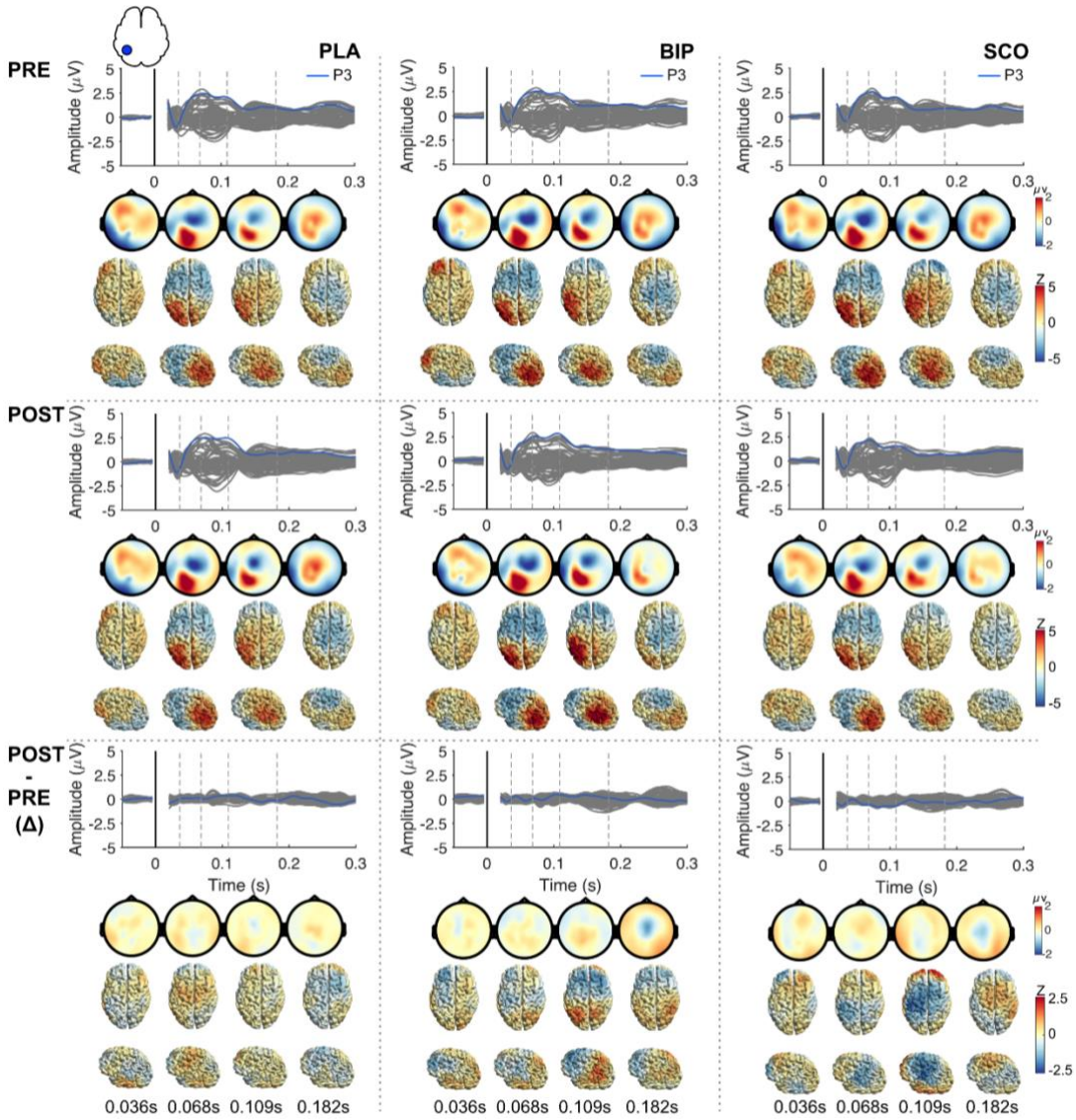

Supplementary Figure 3. TEPs in response to TMS of the AG Pre- and Post-drug administration. TEPs were obtained by subtracting *sham* TMS-evoked from *active* TMS-evoked EEG potentials, averaged across participants. Each condition is shown by multi-channel TEP plots with topography time series displayed at both sensor and source levels. Rows: PRE, POST, and POST-PRE (Δ); Columns: PLA, BIP, and SCO. *Abbreviations: AG: angular gyrus; BIP, biperiden; PLA, placebo; PRE: pre-drug; POST: post-drug; SCO, scopolamine; TEPs: TMS evoked EEG potentials.*

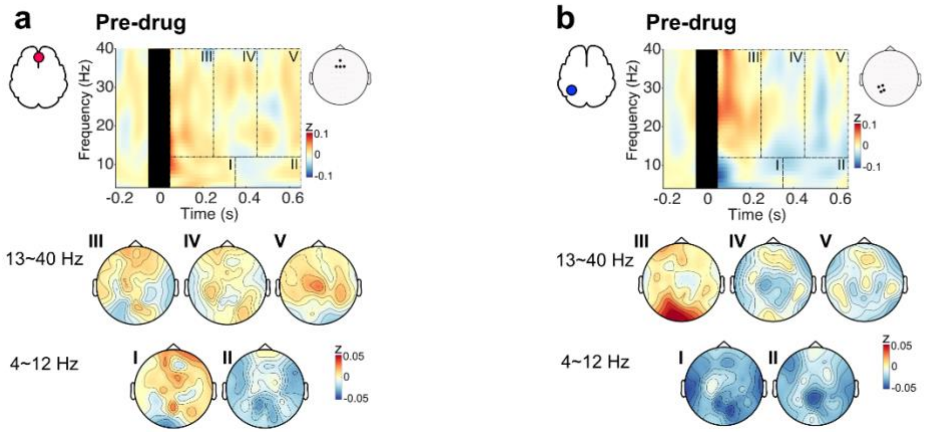

Supplementary Figure 4. TMS-induced oscillatory power in response to **(a)** mPFC and **(b)** AG stimulations Pre-drug administration. The power was derived by subtracting *sham* TMS-induced from *active* TMS-induced EEG oscillatory power. TFRs pre-drug administration were averaged across participants, channels underneath the coil (AFz, Fz, F1, F2 for mPFC; CP3, CP5, P3, P5 for AG), and the three sessions. The black box masks the time window (–0.05 to 0.05s) potentially contaminated by TMS-related artifacts. The bottom rows show topographies of the induced power, averaged across five time-frequency regions of interest chosen based on visual inspection (I: 0.05–0.35s; II: 0.36–0.65s; III: 0.05–0.25s; IV: 0.26–0.45s; V: 0.46–0.65s). *Abbreviations: AG: angular gyrus; mPFC: medial prefrontal cortex; TFRs: time-frequency representations.*

3 Discussion

We first addressed the issue of sensory confounds in single-pulse TMS–EEG responses using a sensory control procedure, which was thoroughly documented in our publication *'Evoked EEG Responses to TMS Targeting Regions Outside the Primary Motor Cortex and Their Test–Retest Reliability'* (Song et al., 2024). Specifically, our findings are twofold: 1) the significant differences in EEG responses between the *active* and *sham* conditions show temporal and spatial characteristics that are specific to the stimulation site, which strongly suggests cortical activation by TMS. These features are effectively captured by the 'cleaned' TEPs, obtained by subtracting the *sham* EEG from the *active*. 2) The test-retest reliability of EEG responses evoked by the *active* is substantially high, but it significantly decreases for 'cleaned' TEPs following the removal of SEPs, particularly during late latencies (i.e., beyond 80 ms). Moreover, the reliability of 'cleaned' TEPs varies by the stimulation site, with the mPFC TEPs being the least reliable compared to the SMA and AG.

With sensory contamination being largely controlled, we next assessed the effects of cholinergic inhibition through mAChR antagonists on 'cleaned' TMS–EEG responses. This is achieved by administering mAChR antagonists scopolamine (non-selective mAChR antagonist) and biperiden (M1 mAChR antagonist) and placebo to healthy participants and comparing 'cleaned' TEPs and TIOs resulting from three brain regions stimulations (the mPFC, AG, and SMA) before and after drug intake. As shown in our publication *'Involvement of muscarinic acetylcholine receptor-mediated cholinergic neurotransmission in TMS–EEG responses'* (Song et al., 2025), we demonstrated: 1) mAChR-mediated cholinergic inhibition increases the amplitude of early-latency TEPs resulting from the SMA stimulation but not the mPFC and AG, with scopolamine but not biperiden producing significant effects. 2) While mAChR-mediated cholinergic inhibition also significantly influences SEPs, its effects on TEPs occur independently of SEPs. 3) The inhibition of mAChR-mediated cholinergic significantly increases the power of SIOs, not TIOs, with distinct spectral and temporal characteristics induced by scopolamine and biperiden, respectively.

In this chapter, I will first compare TMS–EEG characteristics identified using our sensory control procedure to those reported in the existing literature (section 3.1). This will be

followed by a discussion about their test-retest reliability (section 3.2). I will then explore possible reasons why the involvement of mAChR-mediated transmission in TEPs appears to be dependent on the stimulation site (section 3.3). In parallel, the role of mAChR-mediated transmission in sensory-related responses will be briefly discussed. Building on these discussions, I will lastly highlight the usefulness and caveats of incorporating sensory control in TMS–EEG studies (section 3.4).

3.1 Characterizing TMS–EEG responses

Evidence from numerous TMS–EEG studies targeting various brain regions has suggested that early-latency TEPs that feature site-specific topography and time course primarily reflect direct cortical activation by TMS (Biabani et al., 2019, 2024; Conde et al., 2019; Farzan & Bortoletto, 2022; Freedberg et al., 2020; Gordon et al., 2021; Rogasch et al., 2020). In contrast, later responses, which often converge on a frontocentral N100-P200 component irrespective of stimulation site and intensity, are likely of sensory origin due to peripheral co-stimulation. Our study, using a sensory control procedure to effectively mitigate sensory confounds, provides further evidence to support this notion. Notably, because of the high ES intensity used for saturation, the early-latency SEPs (<60 ms) from the *sham* condition in our study are more pronounced than previously reported (Biabani et al., 2024; Conde et al., 2019; Raffin et al., 2020; Rocchi et al., 2021). Nevertheless, the temporal and spatial characteristics of early-latency 'cleaned' TEPs exhibit stimulation site specificity, strongly implying direct cortical activation by TMS rather than a shared common sensory activity. When stimulating the SMA, our findings are consistent with recent studies targeting the SMA (Casarotto et al., 2019) and pre-SMA (Biabani et al., 2024; Leodori et al., 2022, 2024), showing a prominent N45-like component (around 30–50 ms) at frontocentral channels near the stimulated site. In addition, we observed a late TEP component (>100 ms) in the central area, slightly left-lateralized, indicating the activation of left SMA. This signal may have been obscured by the dominant sensory component N100-P200 if sensory control is absent.

For the mPFC or AG stimulation, we compare our results to previous research that targeted brain areas near the mPFC or AG. For instance, Rogasch and colleagues conducted a study that applied single-pulse TMS to the left superior frontal gyrus and left superior parietal lobule (Rogasch et al., 2020). Similar to our results, they found that early

latency TEPs (~83 m) from both targets showed stimulation site specificity. In addition, they found a high correlation between the TEPs at later latencies following frontal and parietal stimulations. The similarity in late-latency TEPs may indicate a shared sensory activation. This hypothesis is further supported by a subsequent experiment from the same group, where a sensory control condition (TMS 'click' plus concomitant scalp ES) was incorporated when stimulating three different brain regions (Biabani et al., 2024). They showed that late-latency TEPs, regardless of stimulation site, were strongly correlated with SEPs from the sensory control condition.

In addition to TEPs, we also observed that SMA stimulation induces significant changes in oscillatory activity: an increased power (synchronization) in the beta and gamma frequency bands (~11–40 Hz) up to around 260 ms post-stimulus. The temporal and spectral pattern is effectively captured by the 'cleaned' TIOs obtained by subtracting the *sham* EEG from the *active*. Similar oscillatory patterns have been described in TMS–EEG studies targeting brain regions such as the M1 and premotor cortex (Belardinelli et al., 2021; Canali et al., 2017; Fecchio et al., 2017; Gordon et al., 2021; Premoli et al., 2017; Rosanova et al., 2009; Van Der Werf & Paus, 2006). It is proposed that a shared common underlying mechanism, such as the activation of the cortico-thalamic circuit, may account for spectral dynamics following TMS (Rosanova et al., 2009; Van Der Werf & Paus, 2006). Notably, unlike our earlier studies targeting the M1 (Belardinelli et al., 2021; Premoli et al., 2017), our current results do not show a prominent power decrease in the alpha/beta frequency band after 200 ms post-stimulus. While this discrepancy could be partially explained by stimulating different brain regions, sensory confounds control in our current study suggest another possible reason. A TMS–EEG study by Fecchio et al. showed that desynchronization in the alpha/beta frequency band was pronounced only when stronger finger muscular activation through the cortico-spinal tract was triggered (Fecchio et al., 2017). This links the origin of desynchronization to sensory feedback caused by the finger movement. Along with this, tactile stimuli through ES over the median nerve and index finger (Andersen & Lundqvist, 2019; Bauer et al., 2012; Novembre et al., 2019), as well as acoustic stimuli through a loudspeaker, can also lead to significant desynchronization in the alpha/beta frequency band. Therefore, the absence of such desynchronization in our current work may indicate an effective sensory control in TMS–EEG data.

The sham procedure appears more effective when stimulating the SMA than the AG and mPFC regarding matching perceptions. For the SMA, participants reported similar perceptions between *active* and *sham* stimulation conditions. This is accompanied by closely matched sensory-related EEG responses (indicated by N100-P200 amplitude). Together, this allows for a more reliable removal of sensory confounds from *active* EEG. In contrast, mPFC stimulation results in greater discomfort and stronger scalp perceptions compared to the sham condition. However, in our study, the difference in sensory perception does not lead to a significant difference in the N100-P200 component between *active* and *sham* conditions. Conversely, *active* AG stimulation causes stronger scalp perceptions and sensory responses with larger amplitudes than *sham* stimulation. Consequently, some sensory confounds likely remain in the 'cleaned' TEPs, as implied by the topographical resemblance of late-latency AG TEPs to the sensory N100-P200 complex. These results suggest that there may not be a direct correspondence between sensory experience and sensory-related EEG responses. This finding is consistent with the observation that the ability to differentiate *sham* stimulation from *active* did not significantly influence the characterization of TEPs (Gordon et al., 2021). While matching perceptions certainly assist in developing effective sham stimulation, the ultimate characterization of TEPs requires a careful assessment of the topographical patterns (Bergmann et al., 2024; Farzan & Bortoletto, 2022).

3.2 Test-retest Reliability of TEPs

3.2.1 Are TEPs Reliable?

The reliability of TEPs has been studied in various studies (Bertazzoli et al., 2021; Kerwin et al., 2018; Lioumis et al., 2009; Moffa et al., 2022). Late-latency TEPs are considered more reliable and reproducible between repeated measures compared to early TEPs. Lioumis et al. conducted a study that stimulated the M1 and dorsal lateral prefrontal cortex (dlPFC) at different TMS intensities and measured the similarities of TEP peaks between repeated measures one week apart (Lioumis et al., 2009). They showed overall high Pearson correlations for amplitudes and latencies of all identified peaks. Kerwin et al. assessed the reliability of TEP peaks from dlPFC stimulation between trials within a run and between different runs using the metric concordance correlation coefficient (CCC). They found the highest reliability at peaks N100 and P200. While the N40 and

P60 peaks showed substantial reliability, this was evident only within a run and not between different runs (Kerwin et al., 2018). Similarly, Moffa et al. targeted the dlPFC and reported moderate reliability for peaks N100 and P200 (CCC_{max}>0.6) based on the Shrout 1998 standard (Shrout, 1998) but minimal reliability for both peaks N40 and P60 (Moffa et al., 2022). The same observation applies to the peak amplitudes and latencies of TEPs following the inferior parietal lobe stimulation (Bertazzoli et al., 2021). Our results provide additional evidence that the reported high reliability of late-latency TEPs may be due to a common sensory activation. Specifically, we used CCC to assess the spatial and temporal test-retest reliability of TMS–EEG responses between repeated sessions. Consistent with previous research, EEG responses in the *active* condition are reproducible and stable between sessions, with CCC values gradually increasing from early on and peaking at around 100 ms and beyond. However, following the subtraction of the *sham* EEG from the *active*, CCC values for 'cleaned' TEPs during late latencies (around >50 ms) were greatly reduced. This reduced reliability suggests that the presence of SEPs significantly biases the assessment and interpretation of TEP reliability. SEPs, particularly during late latencies (e.g., frontocentral N100-P200), often feature large amplitude, prolonged duration, and widespread topography. These characteristics tend to result in high values during reliability assessment. Consequently, caution should be taken when drawing conclusions about the high reliability of late-latency TEPs, especially when the sensory confounds associated with TMS are not adequately controlled.

In addition, our results show that the spatial and temporal reliability of the 'cleaned' TEPs varies depending on the stimulated site. TEPs from the mPFC stimulation are less reproducible than those from the SMA and AG stimulation. Unlike SEPs, TEPs display rapid deflections with smaller amplitudes and distinct scalp distributions, particularly during early latencies. Moreover, they are highly sensitive to stimulation parameters such as intensity and site, and can be more easily affected by various TMS-related artifacts and preprocessing pipelines (Bertazzoli et al., 2021; Hernandez-Pavon et al., 2023; Rogasch et al., 2022). When stimulating the mPFC, the contraction of the frontalis muscle is often unavoidable. Because these muscle artifacts are time-locked to TMS and have an amplitude that is an order of magnitude larger than the neural EEG signal, aggressive algorithms are often used during offline signal preprocessing to remove them. We suspect

that these factors together likely contribute to a low signal-to-noise (SNR) ratio and, consequently, poor test-retest reliability of TEPs.

3.2.2 Improving TEPs Reliability

Reducing the 'noise' (e.g., TMS-related muscle artifacts) should naturally enhance the SNR of TMS–EEG. Casarotto and colleagues developed a graphical user interface to monitor TMS–EEG signals in real-time and showed that slight adjustments of stimulation parameters (such as TMS location, coil angle, and intensity) can prevent or minimize muscle artifacts and improve the quality of TMS–EEG data (Casarotto et al., 2022). However, this method may be less effective for brain regions located directly beneath craniofacial muscles. In our pilot test that stimulated the mPFC, we monitored the TMS–EEG signal in real-time and found that TMS-triggered blinks and frontalis muscle contraction masked the early TMS–EEG response in nearly every trial, despite making small adjustments to the coil locations and angles. Moving the coil farther away from the muscle insertions might greatly reduce muscle contraction, but this could compromise the stimulation precision, which is not desirable for our study.

Alternatively, one can consider boosting the 'signal' for the SNR. In our study, we set the TMS intensity for the mPFC, AG, and SMA based on the resting motor threshold (RMT). While this approach is well-established, it is viewed as suboptimal for non-motor areas (Hernandez-Pavon et al., 2023). The RMT-based approach assumes that the threshold for effectively exciting non-motor neurons is similar to that for M1, which may not hold. Several studies comparing TEPs resulting from TMS over different cortical regions using various intensities suggest that M1 is more excitable than non-motor regions such as the parietal, prefrontal, and premotor cortex (Fecchio et al., 2017; Kähkönen et al., 2005; Raffin et al., 2020). The differences in excitability across brain regions may be attributed to various cytoarchitectural features (including the density of pyramidal neurons and the configuration of neural populations) (Fernández-Ruiz et al., 2013), cortical thickness, and skin-cortex distance (Stokes et al., 2005). Compared to the RMT-based dosing approach, estimating the TMS-induced E-field and using it to guide stimulation is proposed to be a more effective alternative. For instance, Numssen and colleagues aimed to equalize cortical stimulation exposure across the cortex (Numssen et al., 2024). They calculated the E-field on the cortex for M1 and four non-motor brain regions (auditory,

somatomotor, inferior parietal lobe, and dlPFC). Then, they determined the stimulator intensity (in %MSO) needed to generate the same stimulation strength (in E-field strength) at the non-motor area as in M1 at the RMT. They showed that this E-field-based dosing method was more effective and reliable than RMT-based methods regarding matching cortical stimulation exposure across the cortex, both within and between participants. However, while the E-field-based approach has shown some improvements, it still fails to consider factors such as TMS pulse waveforms, duration, and underlying axonal geometry, which could also affect the cortical response to TMS (Hernandez-Pavon et al., 2023). Furthermore, additional investigations on the interaction between the TMS-induced E-field and the activation of local neural circuits are necessary to determine parameters such as intensity and orientation of the E-field for effective stimulation in non-motor areas (Hernandez-Pavon et al., 2023). Notably, in the study by Numssen et al., it was found that to achieve the same cortical E-field strength as in M1 at the RMT, the required stimulator intensity for non-motor areas needed to be around 20-50% higher than that of M1 (Numssen et al., 2024). However, such an increased stimulation intensity also amplifies TMS-related artifacts, such as muscle contractions and auditory inputs, which may not necessarily enhance the SNR. In summary, in order to maximize the potential of TMS–EEG-based measures for research and clinical use, effective methods are needed to improve the SNR and increase reliability (Julkunen et al., 2022; Parmigiani et al., 2022).

3.3 mAChR-mediated Cholinergic Transmission in single-pulse TMS–EEG

3.3.1 mAChR-mediated Cholinergic Transmission in SMA TEPs

One primary finding of our study is the involvement of mAChR-mediated cholinergic transmission in TEPs from the SMA stimulation. This is evidenced by the increased amplitude of early-latency TEPs after administering mAChR antagonists scopolamine and biperiden compared to placebo. Specifically, the effects caused by scopolamine are more pronounced at around ~40–63 ms at the central area near the stimulation site. Biperiden appears to produce similar but less robust effects. Previous pharmacologic TMS–EEG studies suggest that TEPs during this period are affected by GABAergic (inhibitory) and glutamatergic (excitatory) neurotransmission manipulation (Belardinelli et al., 2021; Darmani et al., 2016; Premoli et al., 2014). Following stimulating the M1, the amplitude of TEP component N45 was increased by the GABAergic drug diazepam

(Premoli et al., 2014) and the anti-glutamatergic drug dextromethorphan (Belardinelli et al., 2021), with a similar effect on spatial topography. Moreover, its amplitude was decreased by the anti-GABAergic compound S44819 (Darmani et al., 2016). Therefore, the TEP component N45 is considered to reflect the E/I balance controlled by glutamatergic and GABAergic transmission. We thus speculate that the increased amplitude of the N45-like TEP component caused by anticholinergic drugs might result from the shift of E/I balance, possibly in favor of inhibition.

Why is there a convergent effect on N45 TEPs while manipulating various neurotransmission systems? There is an interesting, albeit speculative, hypothesis to reconcile these observations. While other cortical and subcortical areas can contribute, the activation of the cortico-basal ganglia-thalamocortical motor circuit may play an important role in shaping the TEP component N45 or components with similar latency (Li et al., 2017; Ziemann et al., 2015). Cortical motor areas such as the M1 and SMA are highly interconnected with the subcortical structures basal (BG) ganglia and thalamus. Neurons from the motor cortex (glutamatergic) and midbrain (dopaminergic) synapse onto BG nuclei, including the striatum and the subthalamic nucleus (STN). After successive processing between the BG and thalamus, thalamic nuclei synapse back onto the motor cortex, thus completing a vast loop that originates and terminates in cortical motor areas (Figure 2a) (Nakano et al., 2000; Utter & Basso, 2008). When stimulating the M1 or SMA, TMS excites local cortical neurons, which likely transsynaptically activate the BG structures. BG then reciprocates activation back to the original cortical areas through the thalamus via polysynaptic pathways. This hypothesis is supported by deep brain stimulation (DBS) studies in patients with PD (Doyle Gaynor et al., 2008; Strafella et al., 2004). During the implantation surgery for DBS, Straffela et al. found that applying single-pulse TMS over the M1 changed the STN firing rate measured by single-unit recordings (Strafella et al., 2004). Similarly, evoked local field potentials (LFPs) can be recorded at the level of the STN following the TMS of the M1 and SMA (Doyle Gaynor et al., 2008). These studies confirm the excitation triggered by TMS over the motor cortex can descend to the subcortical structure BG. Moreover, the excitation triggered by DBS over the subcortical BG (STN or internal globus pallidus) can ascend to the motor cortex, resulting in evoked potentials that can be captured by scalp EEG (Kuriakose et al., 2010; Ni et al., 2018; Walker et al., 2012). While the temporal and

spatial characteristics of recorded EEG waveforms varied among studies, cortical EEG responses can be detected as early as ~10 ms following the DBS. The transfer of neural information along this cortico-basal ganglia-thalamocortical motor circuit is inherently complex, involving excitatory (glutamatergic) and inhibitory (GABAergic) neurotransmission, as well as regulation from multiple neuromodulators (Augustine & Singer, 2018). The cholinergic transmission mediated by ACh is one of these important modulating systems. The cholinergic interneurons (ChIs) in the striatum are tonically active, firing to release ACh without receiving synaptic input (Abudukeyoumu et al., 2019). While the ACh signals through both mAChRs and nAChRs, the activation of mAChRs tends to produce more sustainable effects. Axon terminals of major afferents to the striatum (glutamatergic and dopaminergic terminals) and striatal neurons, including GABAergic medium spiny projection neurons (MSNs) and other interneurons, all highly express mAChRs (Figure 2b) (Abudukeyoumu et al., 2019; Lester et al., 2010; Ztaou & Amalric, 2019). These are the foundations of how MSNs can be directly and indirectly modulated by cholinergic neurotransmission, which likely influences the net output of excitation and inhibition from the BG to the thalamus, ultimately changing the SMA activation by TMS.

As discussed, the striatum acts as a hub integrating various neurotransmission systems. Could N45 TEPs reflect an interplay between cholinergic and dopaminergic systems? This idea is partially supported by a recent study that stimulated the SMA of PD patients when they were not taking their dopaminergic replacement medication (Casarotto et al., 2019). In this study, Casarotto and colleagues assessed TEPs before and after an acute intake of levodopa, measuring the immediate response area, a parameter derived from LMFA, within an early time window (~15–60 ms post-stimulus) from electrodes near the stimulation site. The immediate response area was larger after taking levodopa compared to before. This increase, corresponding to an increased size of early-latency TEPs, was significant when stimulating the brain side with severe dopaminergic innervation loss. In combination with the scopolamine effect observed in our current work, the modulation of early-latency TEPs possibly reflects the counterbalance between cholinergic and dopaminergic systems in the BG, where cholinergic tone increases as striatal dopamine levels decline and vice versa (Aosaki et al., 2010; Lester et al., 2010). However, a contrasting finding was reported in a study by Leodori et al. that stimulated the pre-SMA

in patients with PD (Leodori et al., 2022). They found that, compared to healthy control, the amplitude of TEP component N40 increased for PD patients 'off' their antiparkinsonian medications, which returned to normal levels following the dopaminergic therapy. The authors suspected the conflicting finding reported by Casarotto et al. was due to the different brain regions targeted in the studies. However, it is also possible that the endogenous dopaminergic and cholinergic activity at the time of stimulation might differ due to the withdrawal of antiparkinsonian medications (Julkunen et al., 2022).

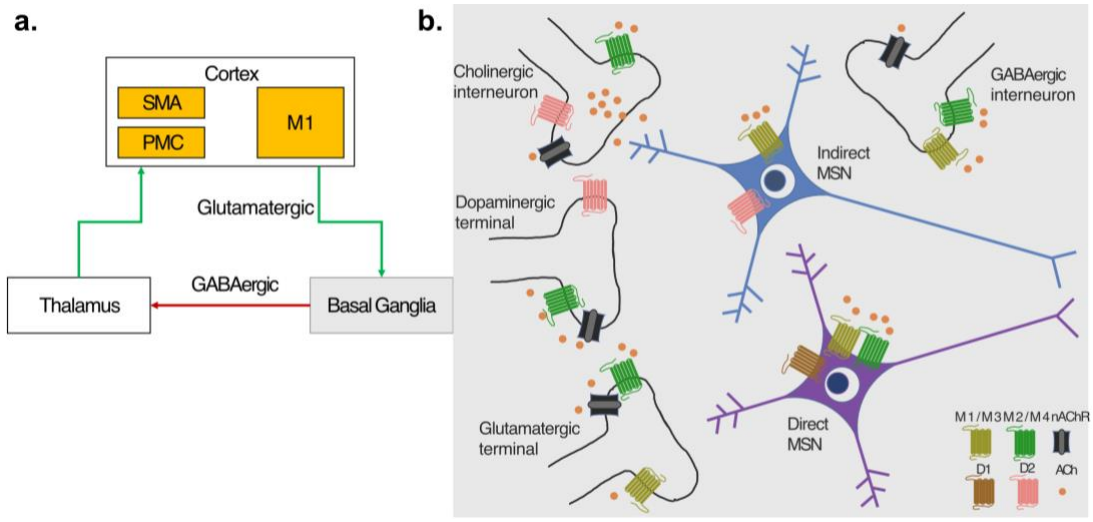

Figure 2. (a) The Cortico-Basal Ganglia-Thalamocortical Motor circuit. SMA, supplementary motor area; PMC, premotor cortex; M1, primary motor area. (b). Schematic illustration of cholinergic modulation of the striatal microcircuitry. ACh released from the striatal cholinergic interneuron can bind and activate multiple muscarinic acetylcholine receptors (mAChRs) subtypes: M1, M2, M3, M4, and nicotinic acetylcholine receptors (nAChRs). These receptors are localized in various neural elements, including glutamatergic and dopaminergic terminals, striatal medium spiny projection neurons (MSNs), and striatal GABAergic interneurons. Direct MSNs express dopamine receptor subtypes (D1), and indirect MSNs express dopamine receptor subtypes (D2). b. is adapted from Ztaou & Amalric, 2019.

3.3.2 mAChR-mediated Cholinergic Transmission in mPFC TEPs and AG TEPs

In contrast to the SMA, mAChR antagonists do not significantly alter the TEPs elicited by either the mPFC or AG stimulation. A couple of reasons may account for the absence of drug effects. First, TMS–EEG responses are dependent on the functional properties of the stimulated neural circuit and networks (Siebner et al., 2022). The observation that

TEPs remain largely unchanged indicates that the instinct functional properties of the mPFC and SMA might be insensitive to the inhibition of mAChR-mediated cholinergic transmission at the resting state. Basal forebrain (BF) cholinergic neurons are the primary source of ACh for cholinergic neurotransmission in the neocortex (Ballinger et al., 2016). While the mAChRs are widely distributed across the cortex, BF cholinergic actions are not spatially diffused; instead, they show sufficient spatial and temporal specificity necessary for regulating processes such as attention and learning (Ballinger et al., 2016; Muñoz & Rudy, 2014; Záborszky et al., 2018). For example, the innervation of BF cholinergic neurons follows a topographic, rather than diffuse, distribution. Moreover, the release of ACh is brain region specific and context-dependent. Animal studies using the microdialysis technique showed that the release of ACh in the mPFC and parietal regions is specifically linked to processes such as cue detection and goal orientation, opposite to basic behavioral processes that do not explicitly require attention (Arnold et al., 2002; Himmelheber et al., 1997; Parikh et al., 2007). In addition, a fMRI study by Thienel et al. indicated reduced activation in the left superior and middle frontal regions of participants following the intake of scopolamine during an attentional reorienting task (Thienel et al., 2009). It is thus conceivable that cholinergic transmission might shape TEPs from the mPFC and AG stimulation when participants are engaged in attention or other cognitive tasks.

Alternatively, since our present study focuses on mAChR-mediated neurotransmission, the role of nAChR-mediated transmission in TMS–EEG may have been overlooked. Previous human fMRI studies have shown that the intake of nAChR agonist nicotine can cause hyperactivations in medial frontoparietal regions during both the resting state and tasks with low attention requirements (Lawrence et al., 2002; Stein et al., 1998). This suggests that the nAChR-mediated transmission is active in the frontal and parietal brain areas in the task-free states, which might have influenced TMS–EEG outcomes when targeting these regions. Lastly, as described in section 3.2, TEPs resulting from the mPFC stimulation exhibit low reliability between repeated sessions as well as within and between participants, which may have hindered the discovery of drug effects. However, this explanation does not entirely account for the lack of drug effects on TEPs elicited by AG stimulation.

3.3.3 mAChR-mediated Cholinergic Transmission in Sensory-related EEG Responses

Incorporating a *sham* condition allows us to separately evaluate the role of mAChR-mediated cholinergic transmission in sensory-related EEG responses from TMS-associated multiple sensory stimulations. We found that mAChR antagonists have a significant impact on SEPs and SIOs. Furthermore, the modulation of these sensory-related EEG responses depends on the selectivity of mAChRs, as the effects caused by scopolamine and biperiden feature distinct temporal, spatial, and spectral characteristics.

In the field of ERPs, many studies have explored the role of central cholinergic signaling in sensory processes related to cognitive functions such as attention and memory, where sensory stimuli can be either relevant or irrelevant to a given task (Bentley et al., 2011). Previous studies in humans that involved scopolamine or biperiden as the pharmacological intervention showed mixed effects on ERPs (reviewed in (Kunnath et al., 2023). Some studies reported reduced amplitudes of ERP components such as P50, N1, P1, P2, and P3a (Caldenhove et al., 2017; Curran et al., 1998; Potter et al., 2000), while others demonstrated no changes or even opposite effects (Brown et al., 2015). This may be partly due to various task paradigms used in studies. For example, participants may passively experience or actively attend to certain sensory stimuli, resulting in different brain states across studies. Additionally, the sensory stimuli were also diverse, including auditory, visual, or even multimodal. In our study, we used cluster-based permutation F/t tests to examine changes in SEPs (ΔSEPs) to preserve the high-dimensional information conveyed by EEG signals and to address potential confounding factors such as fatigue. However, this does not necessarily prevent us from linking our SEP findings to the existing literature. For instance, the relative change in amplitudes of the frontocentral N100-P200 was greater for scopolamine and biperiden compared to the placebo. This implies a more reduced amplitude after the intake of mAChR antagonists, consistent with studies showing decreased N1 and P2 amplitudes (Caldenhove et al., 2017; Curran et al., 1998).

The power of SIOs in our *sham* condition demonstrates a specific temporal and spectral characteristic: a transient synchronization in a broad frequency range (~200 ms), followed by a prolonged desynchronization in the alpha frequency band, a brief

desynchronization and subsequent synchronization in the beta band. While some variations may occur depending on the used time-frequency decomposition methods or the type of stimulus, this dynamic in power caused by sensory stimulation is largely in line with several magnetoencephalography (M/EEG) studies (Andersen & Lundqvist, 2019; Bauer et al., 2006; Novembre et al., 2019). Evidence suggests that cholinergic signaling in the sensory cortex impacts sensory processing by altering neural responses to stimuli, leading to a shift in cortical dynamics from synchronous to asynchronous (Colangelo et al., 2019; Záborszky et al., 2018). For example, in animal studies, researchers used optogenetics to activate or inhibit cholinergic signaling from the BF to primary sensory cortices and recorded LFPs in the sensory cortices to measure oscillatory power (Kim et al., 2016; Pinto et al., 2013). They showed that optogenetic activation of cholinergic signaling led to desynchronization, while inhibition increased synchronization. Similarly, our results show that cholinergic antagonists significantly enhance the power of SIOs (synchronization), despite their spatially diffuse effects. Moreover, this synchronization exhibits distinct temporal and spectral characteristics depending on the targeted mAChR subtypes: the selective M1 mAChR antagonist biperiden tends to primarily reverse the desynchronization in the alpha/beta frequency band, while the non-selective mAChR antagonist scopolamine appears to enhance power diffusely in both the early alpha and later beta frequency bands. We suspect that the differential modulation of sensory-related EEG responses by scopolamine and biperiden is possibly related to the cell-type specific expression of mAChR subtypes and downstream signaling cascades, which could result in various responses in neural populations that receive the same sensory input (Colangelo et al., 2019; Thiele, 2013).

3.4 Sensory Control in TMS–EEG

3.4.1 Which is more Evil: Auditory or Somatosensory?

While sensory confounds are currently well-acknowledged in the field, ongoing debates continue regarding the extent to which TMS–EEG responses are contaminated and which confounding factor (auditory or somatosensory) plays a major role. Some argue that confounding SEPs are mainly of auditory origin (Ilmoniemi et al., 2015; Paus et al., 2001; Rocchi et al., 2021; ter Braack et al., 2015), while others suggest a combined contribution (Chowdhury et al., 2022; Conde et al., 2019; Ross et al., 2022). For instance, Rocchi and

colleagues used scalp ES to simulate somatosensory stimulation associated with the subthreshold TMS of M1 (Rocchi et al., 2021). The resulting SSEPs displayed very small amplitudes throughout the entire time window (∼15–270 ms), leading to the conclusion that SSEPs may contribute marginally to TEPs. Conversely, in a study that stimulated the frontal and parietal areas, Conde et al. and colleagues established a multisensory sham stimulation that consisted of TMS 'click' sound and concomitant scalp ES near the stimulation sites. They showed that the sham stimulation produced an EEG response similar to that of the active TMS for nearly the entire post-stimulus window (∼20–410 ms) (Conde et al., 2019). With a similar sham design, Chowdhury and colleagues showed a similarity between EEG responses evoked by the multisensory sham stimulation and those by active TMS of the M1 with suprathreshold intensity (%110 RMT) from 55 ms onward (Chowdhury et al., 2022). The conflicting conclusions drawn from these studies may be partially due to the various stimulation protocols. For example, although both Rocchi et al. and Conde et al. adjusted ES intensity based on the perception produced by active TMS, the TMS sites and intensities differed between the two studies. Rocchi et al. stimulated the M1 with subthreshold TMS intensity (90% RMT) (Rocchi et al., 2021). On the other hand, Conde et al. used TMS intensities comparable to 80–120% RMT to stimulate the frontal and parietal areas where TMS-related craniofacial muscle contraction is more pronounced (Conde et al., 2019; Siebner et al., 2019). As a result, the average ES intensity applied in the Conde et al. study was higher, leading to more potent somatosensory activation due to the dependence of SSEP on ES intensity (Gordon et al., 2021; Raffin et al., 2020). Therefore, the relative contaminations of auditory and somatosensory inputs to TMS–EEG responses likely vary depending on stimulation protocols. A one-size-fits-all solution to sensory confounds will inevitably fail. For instance, TMS–EEG responses from suprathreshold TMS of brain regions located directly beneath the cranial muscle insertions are more likely to contain both auditory and somatosensory contamination. As such, a well-designed multisensory control will provide strong evidence supporting the interpretation of TMS–EEG results.

3.4.2 What if Intervention Modulates Sensory Processing?

Our findings on the pharmacological modulation of sensory-related EEG responses emphasize the importance of including sensory control in studies with pre/post-intervention TMS–EEG measurements. The pre/post-study design typically involves

testing the same participants before and after an intervention with consistent TMS parameters (Hernandez-Pavon et al., 2023). The idea is that by comparing TMS–EEG outcomes before and after the intervention, any differences can be attributed to the intervention's effect on direct cortical responsiveness to TMS. However, this applies only when the intervention does not affect the sensory processing. Our current results demonstrate the contrary. mAChR antagonists significantly change the SEPs in response to sensory stimuli associated with TMS. These drug-induced changes in EEG may misinterpreted as the modulation of direct cortical responsiveness to TMS. To address this ambiguity, before evaluating drug effects, we applied a sham procedure and isolated the 'cleaned' TEPs by subtracting *sham* EEG from the *active* condition. This approach allows us to attribute drug effects on the 'cleaned' TEPs to the direct cortical responsiveness to TMS rather than sensory processing. Similarly, the GABAergic drug diazepam was found to significantly affect the frontocentral N100 component in both *active* and *sham* conditions (Gordon et al., 2023). However, further analysis showed that this modulation was not of transcranial but mainly of peripheral sensory origin, as there was no modulation of the component in the 'cleaned' TEPs. In addition, we showed that temporal and spectral characteristics of SIOs in response to TMS-associated sensory stimuli resemble those reported in TMS–EEG studies that lack a sensory control condition (Biondi et al., 2022; Casula et al., 2016; Premoli et al., 2017). This similarity indicates that some of the oscillatory features observed in these studies may arise from sensory inputs associated with TMS. Without proper sensory control, it becomes challenging to determine to what extent changes in these oscillatory responses are due to the impact of the intervention on the direct cortical responsiveness to TMS, sensory processing, or both.

3.4.3 Isolating TMS–EEG Responses by Subtraction

The challenge of establishing an effective sham control for TMS–EEG is described in the Introduction section 1.2.2. Another potential issue arises when subtracting the *sham* EEG from the *active* or statistically comparing EEG responses between the two conditions to characterize TMS–EEG responses. It might be problematic as the subtraction or comparison assumes that direct cortical activation by TMS is linearly superimposed on sensory-related activity, which may not always hold. When this assumption is violated, the resulting waveforms after subtraction may not accurately reflect neurophysiologically meaningful processes (Farzan & Bortoletto, 2022). It is important to note that the linear

assumption is not unique to the TMS–EEG field. For example, ERP difference waveforms (subtraction ERP in one condition from the other), like mismatch negativity MMN, are commonly used to represent cognitive processes (Luck, 2014). In addition, the assumption of linear superposition is often involved in TMS–EEG data preprocessing algorithms, including the commonly used independent component analysis (ICA) (Rogasch et al., 2014).

4 Summary

The combination of transcranial magnetic stimulation and electroencephalography (TMS– EEG) is a powerful, non-invasive approach for investigating brain function in both health and disease. Single-pulse TMS–EEG provides a straightforward method: a single TMS pulse stimulates a specific brain region, while concurrent EEG records the resulting cortical responses. However, applying TMS pulses during EEG recordings introduces various artifacts. Among these, sensory-related EEG responses caused by peripheral co-stimulation are particularly problematic, as they closely resemble true TMS–EEG responses and can lead to misinterpretation. Therefore, the first aim of this thesis was to assess whether a sensory control procedure, adapted from previous work, could effectively mitigate sensory confounds.

The effective application of TMS–EEG depends on a deeper understanding of its underlying neurophysiological mechanisms. Combining pharmacological interventions with TMS–EEG offers an avenue for exploring the roles of specific receptor-mediated neurotransmission in shaping TMS–EEG responses. Accordingly, the second aim of this thesis was to investigate the involvement of muscarinic acetylcholine receptor (mAChR)-mediated central cholinergic neurotransmission in TMS–EEG responses.

To achieve these aims, we conducted a randomized, placebo-controlled crossover study involving 24 healthy participants. Each participant received a single oral dose of the non-selective mAChR antagonist scopolamine, the selective mAChR antagonist biperiden, or placebo across three separate sessions. During each session, TMS–EEG responses to stimulation of three brain regions were measured before and after drug administration using the sensory control procedure designed to mitigate sensory confounds. We first

demonstrated that 'cleaned' TMS–EEG responses, with sensory responses removed through the control procedure, strongly represent direct cortical activation. Subsequently, we observed that scopolamine significantly increases the amplitude of a local TEP (TMS-evoked EEG potential) component occurring approximately 40–63 ms following the supplementary motor area stimulation. Previous pharmacological TMS–EEG studies suggest that the TEP component N45 reflects the excitation and inhibition (E/I) balance controlled by glutamatergic and GABAergic transmission. We thus speculate that the increased amplitude of the N45-like TEP component caused by anti-cholinergic drugs might result from the shift in E/I balance, possibly favoring inhibition.

Our results emphasize the importance of sensory control in TMS–EEG studies and provide new insights into the neurophysiology of single-pulse TMS–EEG. Clinically, these findings are informative for interpreting TMS–EEG abnormalities in conditions involving cholinergic deficits and may help guide and monitor therapies targeting the cholinergic system.

5 Bibliography

Aberra, A. S., Wang, B., Grill, W. M., & Peterchev, A. V. (2020). Simulation of transcranial magnetic stimulation in head model with morphologically-realistic cortical neurons. *Brain Stimulation*, *13*(1), 175–189. https://doi.org/10.1016/j.brs.2019.10.002

Abudukeyoumu, N., Hernandez-Flores, T., Garcia-Munoz, M., & Arbuthnott, G. W. (2019). Cholinergic modulation of striatal microcircuits. *European Journal of Neuroscience*, *49*(5), 604–622.

Ahn, S., & Fröhlich, F. (2021). Pinging the brain with transcranial magnetic stimulation reveals cortical reactivity in time and space. *Brain Stimulation*, *14*(2), 304–315.

Andersen, L. M., & Lundqvist, D. (2019). Somatosensory responses to nothing: An MEG study of expectations during omission of tactile stimulations. *NeuroImage*, *184*, 78–89.

Aosaki, T., Miura, M., Suzuki, T., Nishimura, K., & Masuda, M. (2010). Acetylcholine–dopamine balance hypothesis in the striatum: An update. *Geriatrics & Gerontology International*, *10*, S148–S157.

Arnold, H., Burk, J., Hodgson, E., Sarter, M., & Bruno, J. (2002). Differential cortical acetylcholine release in rats performing a sustained attention task versus behavioral control tasks that do not explicitly tax attention. *Neuroscience*, *114*(2), 451–460.

Augustine, F., & Singer, H. S. (2018). Merging the pathophysiology and pharmacotherapy of tics. *Tremor and Other Hyperkinetic Movements*, *8*.

Bakker, C., van Esdonk, M. J., Stuurman, R. (F) E., Borghans, L. G., de Kam, M. L., van Gerven, J. M., & Groeneveld, G. J. (2021). Biperiden Challenge Model in Healthy Elderly as Proof-of-Pharmacology Tool: A Randomized, Placebo-Controlled Trial. *The Journal of Clinical Pharmacology*, *61*(11), 1466–1478.

Ballinger, E. C., Ananth, M., Talmage, D. A., & Role, L. W. (2016). Basal forebrain cholinergic circuits and signaling in cognition and cognitive decline. *Neuron*, *91*(6), 1199–1218.

Barker, A. T., Jalinous, R., & Freeston, I. L. (1985). NON-INVASIVE MAGNETIC STIMULATION OF HUMAN MOTOR CORTEX. *The Lancet*, *325*(8437), 1106–1107. https://doi.org/10.1016/S0140-6736(85)92413-4

Bauer, M., Kluge, C., Bach, D., Bradbury, D., Heinze, H. J., Dolan, R. J., & Driver, J. (2012). Cholinergic enhancement of visual attention and neural oscillations in the human brain. *Current Biology*, *22*(5), 397–402.

Bauer, M., Oostenveld, R., Peeters, M., & Fries, P. (2006). Tactile spatial attention enhances gamma-band activity in somatosensory cortex and reduces low-frequency activity in parieto-occipital areas. *Journal of Neuroscience*, *26*(2), 490–501.

Belardinelli, P., Biabani, M., Blumberger, D. M., Bortoletto, M., Casarotto, S., David, O., Desideri, D., Etkin, A., Ferrarelli, F., Fitzgerald, P. B., & others. (2019). Reproducibility in TMS–EEG studies: A call for data sharing, standard procedures and effective experimental control. *Brain Stimulation: Basic, Translational, and Clinical Research in Neuromodulation*, *12*(3), 787–790.

Belardinelli, P., König, F., Liang, C., Premoli, I., Desideri, D., Müller-Dahlhaus, F., Gordon, P. C., Zipser, C., Zrenner, C., & Ziemann, U. (2021). TMS-EEG signatures of glutamatergic neurotransmission in human cortex. *Scientific Reports*, *11*(1), 8159.

Bennett, M. H., & Jannetta, P. J. (1980). Trigeminal evoked potentials in humans. *Electroencephalography and Clinical Neurophysiology*, *48*(5), 517–526. https://doi.org/10.1016/0013-4694(80)90287-4

Bentley, P., Driver, J., & Dolan, R. J. (2011). Cholinergic modulation of cognition: Insights from human pharmacological functional neuroimaging. *Progress in Neurobiology*, *94*(4), 360–388.

Bergmann, T. O., Karabanov, A., Hartwigsen, G., Thielscher, A., & Siebner, H. R. (2016). Combining non-invasive transcranial brain stimulation with neuroimaging and electrophysiology: Current approaches and future perspectives. *NeuroImage*, *140*, 4–19. https://doi.org/10.1016/j.neuroimage.2016.02.012

Bergmann, T. O., Tomasevic, L., & Siebner, H. R. (2024). Transcranial brain stimulation and EEG/MEG. In E. M. Wassermann, A. V. Peterchev, U. Ziemann, S. H. Lisanby, H. R. Siebner, & V. Walsh (Eds.), *The Oxford Handbook of Transcranial Stimulation: Second Edition* (p. 0). Oxford University Press. https://doi.org/10.1093/oxfordhb/9780198832256.013.26

Bertazzoli, G., Esposito, R., Mutanen, T. P., Ferrari, C., Ilmoniemi, R. J., Miniussi, C., & Bortoletto, M. (2021). The impact of artifact removal approaches on TMS–EEG signal. *NeuroImage*, *239*, 118272.

Biabani, M., Fornito, A., Goldsworthy, M., Thompson, S., Graetz, L., Semmler, J. G., Opie, G. M., Bellgrove, M. A., & Rogasch, N. C. (2024). Characterising the contribution of auditory and somatosensory inputs to TMS-evoked potentials following stimulation of prefrontal, premotor, and parietal cortex. *Imaging Neuroscience*, *2*, 1–23. https://doi.org/10.1162/imag_a_00349

Biabani, M., Fornito, A., Mutanen, T. P., Morrow, J., & Rogasch, N. C. (2019). Characterizing and minimizing the contribution of sensory inputs to TMS-evoked potentials. *Brain Stimulation*, *12*(6), 1537–1552.

Biondi, A., Rocchi, L., Santoro, V., Rossini, P., Beatch, G., Richardson, M., & Premoli, I. (2022). Spontaneous and TMS-related EEG changes as new biomarkers to measure anti-epileptic drug effects. *Scientific Reports*, *12*(1), 1919.

Bohnen, N. I., Grothe, M. J., Ray, N. J., Müller, M. L., & Teipel, S. J. (2018). Recent advances in cholinergic imaging and cognitive decline—Revisiting the cholinergic hypothesis of dementia. *Current Geriatrics Reports*, *7*, 1–11.

Bortoletto, M., Veniero, D., Thut, G., & Miniussi, C. (2015). The contribution of TMS–EEG coregistration in the exploration of the human cortical connectome. *Neuroscience & Biobehavioral Reviews*, *49*, 114–124.

Brown, S. B. R. E., van der Wee, N. J. A., van Noorden, M. S., Giltay, E. J., & Nieuwenhuis, S. (2015). Noradrenergic and cholinergic modulation of late ERP responses to deviant stimuli. *Psychophysiology*, *52*(12), 1620–1631. https://doi.org/10.1111/psyp.12544

Buzsáki, G., Anastassiou, C. A., & Koch, C. (2012). The origin of extracellular fields and currents—EEG, ECoG, LFP and spikes. *Nature Reviews Neuroscience*, *13*(6), 407–420. https://doi.org/10.1038/nrn3241

Caldenhove, S., Borghans, L., Blokland, A., & Sambeth, A. (2017). Role of acetylcholine and serotonin in novelty processing using an oddball paradigm. *Behavioural Brain Research*, *331*, 199–204.

Canali, P., Casarotto, S., Rosanova, M., Sferrazza-Papa, G., Casali, A. G., Gosseries, O., Massimini, M., Smeraldi, E., Colombo, C., & Benedetti, F. (2017). Abnormal brain oscillations persist after recovery from bipolar depression. *European Psychiatry: The Journal of the Association of European Psychiatrists*, *41*, 10–15. https://doi.org/10.1016/j.eurpsy.2016.10.005

Casarotto, S., Fecchio, M., Rosanova, M., Varone, G., D'Ambrosio, S., Sarasso, S., Pigorini, A., Russo, S., Comanducci, A., Ilmoniemi, R. J., & others. (2022). The rt-TEP tool: Real-time visualization of TMS-Evoked Potentials to maximize cortical activation and minimize artifacts. *Journal of Neuroscience Methods*, *370*, 109486.

Casarotto, S., Turco, F., Comanducci, A., Perretti, A., Marotta, G., Pezzoli, G., Rosanova, M., & Isaias, I. U. (2019). Excitability of the supplementary motor area in Parkinson's disease depends on subcortical damage. *Brain Stimulation*, *12*(1), 152–160.

Casula, E. P., Borghi, I., Maiella, M., Pellicciari, M. C., Bonnì, S., Mencarelli, L., Assogna, M., D'Acunto, A., Di Lorenzo, F., Spampinato, D. A., Santarnecchi, E., Martorana, A., & Koch, G. (2023). Regional Precuneus Cortical Hyperexcitability in Alzheimer's Disease Patients. *Annals of Neurology*, *93*(2), 371–383. https://doi.org/10.1002/ana.26514

Casula, E. P., Pellicciari, M. C., Picazio, S., Caltagirone, C., & Koch, G. (2016). Spike-timing-dependent plasticity in the human dorso-lateral prefrontal cortex. *Neuroimage*, *143*, 204–213.

Chowdhury, N. S., Rogasch, N. C., Chiang, A. K., Millard, S. K., Skippen, P., Chang, W.-J., Bilska, K., Si, E., Seminowicz, D. A., & Schabrun, S. M. (2022). The influence of sensory potentials on transcranial magnetic stimulation–Electroencephalography recordings. *Clinical Neurophysiology*, *140*, 98–109.

Cohen, M. X. (2014). *Analyzing neural time series data: Theory and practice*. MIT press.

Colangelo, C., Shichkova, P., Keller, D., Markram, H., & Ramaswamy, S. (2019). Cellular, synaptic and network effects of acetylcholine in the neocortex. *Frontiers in Neural Circuits*, *13*, 24.

Conde, V., Tomasevic, L., Akopian, I., Stanek, K., Saturnino, G. B., Thielscher, A., Bergmann, T. O., & Siebner, H. R. (2019). The non-transcranial TMS-evoked potential is an inherent source of ambiguity in TMS-EEG studies. *Neuroimage*, *185*, 300–312.

Curran, H., Pooviboonsuk, P., Dalton, J., & Lader, M. (1998). Differentiating the effects of centrally acting drugs on arousal and memory: An event-related potential study of scopolamine, lorazepam and diphenhydramine. *Psychopharmacology*, *135*, 27–36.

Darmani, G., Bergmann, T. O., Zipser, C., Baur, D., Müller-Dahlhaus, F., & Ziemann, U. (2019). Effects of antiepileptic drugs on cortical excitability in humans: A TMS-EMG and TMS-EEG study. *Human Brain Mapping*, *40*(4), 1276–1289.

Darmani, G., Zipser, C. M., Böhmer, G. M., Deschet, K., Müller-Dahlhaus, F., Belardinelli, P., Schwab, M., & Ziemann, U. (2016). Effects of the selective α5-GABAAR antagonist S44819 on excitability in the human brain: A TMS–EMG and TMS–EEG phase I study. *Journal of Neuroscience*, *36*(49), 12312–12320.

Doyle Gaynor, L., Kühn, A., Dileone, M., Litvak, V., Eusebio, A., Pogosyan, A., Androulidakis, A., Tisch, S., Limousin, P., Insola, A., & others. (2008). Suppression of beta oscillations in the subthalamic nucleus following cortical stimulation in humans. *European Journal of Neuroscience*, *28*(8), 1686–1695.

Du, X., Choa, F.-S., Summerfelt, A., Rowland, L. M., Chiappelli, J., Kochunov, P., & Hong, L. E. (2017). N100 as a generic cortical electrophysiological marker based on decomposition of TMS-evoked potentials across five anatomic locations. *Experimental Brain Research*, *235*(1), 69–81. https://doi.org/10.1007/s00221-016-4773-7

Esser, S. K., Huber, R., Massimini, M., Peterson, M. J., Ferrarelli, F., & Tononi, G. (2006). A direct demonstration of cortical LTP in humans: A combined TMS/EEG study. *Brain Research Bulletin*, *69*(1), 86–94. https://doi.org/10.1016/j.brainresbull.2005.11.003

Farzan, F., & Bortoletto, M. (2022). Identification and verification of a'true'TMS evoked potential in TMS-EEG. *Journal of Neuroscience Methods*, *378*, 109651.

Fecchio, M., Pigorini, A., Comanducci, A., Sarasso, S., Casarotto, S., Premoli, I., Derchi, C.-C., Mazza, A., Russo, S., Resta, F., Ferrarelli, F., Mariotti, M., Ziemann, U., Massimini, M., & Rosanova, M. (2017). The spectral features of EEG responses to transcranial magnetic stimulation of the primary motor cortex depend on the amplitude of the motor evoked potentials. *PloS One*, *12*(9), e0184910. https://doi.org/10.1371/journal.pone.0184910

Fernández-Ruiz, A., Muñoz, S., Sancho, M., Makarova, J., Makarov, V. A., & Herreras, O. (2013). Cytoarchitectonic and dynamic origins of giant positive local field potentials in the dentate gyrus. *The Journal of Neuroscience: The Official Journal of the Society for Neuroscience*, *33*(39), 15518–15532. https://doi.org/10.1523/JNEUROSCI.0338-13.2013

Ferrarelli, F., Sarasso, S., Guller, Y., Riedner, B. A., Peterson, M. J., Bellesi, M., Massimini, M., Postle, B. R., & Tononi, G. (2012). Reduced Natural Oscillatory Frequency of Frontal Thalamocortical Circuits in Schizophrenia. *Archives of General Psychiatry*, *69*(8), 766–774. https://doi.org/10.1001/archgenpsychiatry.2012.147

Ferreri, F., Guerra, A., Vollero, L., Ponzo, D., Määtta, S., Könönen, M., Vecchio, F., Pasqualetti, P., Miraglia, F., Simonelli, I., Corbetta, M., & Rossini, P. M. (2021). TMS-EEG Biomarkers of Amnestic Mild Cognitive Impairment Due to Alzheimer's Disease: A Proof-of-Concept Six Years Prospective Study. *Frontiers in Aging Neuroscience*, *13*, 737281. https://doi.org/10.3389/fnagi.2021.737281

Ferreri, F., Vecchio, F., Vollero, L., Guerra, A., Petrichella, S., Ponzo, D., Määtta, S., Mervaala, E., Könönen, M., Ursini, F., Pasqualetti, P., Iannello, G., Rossini, P. M., & Di Lazzaro, V. (2016). Sensorimotor cortex excitability and connectivity in Alzheimer's disease: A TMS-EEG Co-registration study. *Human Brain Mapping*, *37*(6), 2083–2096. https://doi.org/10.1002/hbm.23158

Freedberg, M., Reeves, J. A., Hussain, S. J., Zaghloul, K. A., & Wassermann, E. M. (2020). Identifying site- and stimulation-specific TMS-evoked EEG potentials using a quantitative cosine similarity metric. *PLOS ONE*, *15*(1), e0216185. https://doi.org/10.1371/journal.pone.0216185

Gordon, P. C., Desideri, D., Belardinelli, P., Zrenner, C., & Ziemann, U. (2018). Comparison of cortical EEG responses to realistic sham versus real TMS of human motor cortex. *Brain Stimulation*, *11*(6), 1322–1330. https://doi.org/10.1016/j.brs.2018.08.003

Gordon, P. C., Jovellar, D. B., Song, Y., Zrenner, C., Belardinelli, P., Siebner, H. R., & Ziemann, U. (2021). Recording brain responses to TMS of primary motor cortex by EEG–utility of an optimized sham procedure. *Neuroimage*, *245*, 118708.

Gordon, P. C., Song, Y. F., Jovellar, D. B., Rostami, M., Belardinelli, P., & Ziemann, U. (2023). Untangling TMS-EEG responses caused by TMS versus sensory input using optimized sham control and GABAergic challenge. *The Journal of Physiology*, *601*(10), 1981–1998.

Gordon, P. C., Song, Y., Jovellar, B., Belardinelli, P., & Ziemann, U. (2022). No evidence for interaction between TMS-EEG responses and sensory inputs. *Brain Stimulation: Basic, Translational, and Clinical Research in Neuromodulation*.

Hashimoto, I. (1988). Trigeminal evoked potentials following brief air puff: Enhanced signal-to-noise ratio. *Annals of Neurology*, *23*(4), 332–338.

Hernandez-Pavon, J. C., Veniero, D., Bergmann, T. O., Belardinelli, P., Bortoletto, M., Casarotto, S., Casula, E. P., Farzan, F., Fecchio, M., Julkunen, P., & others. (2023). TMS combined with EEG: Recommendations and open issues for data collection and analysis. *Brain Stimulation*.

Herring, J. D., Thut, G., Jensen, O., & Bergmann, T. O. (2015). Attention modulates TMS-locked alpha oscillations in the visual cortex. *Journal of Neuroscience*, *35*(43), 14435–14447.

Herrmann, C. S., Rach, S., Vosskuhl, J., & Strüber, D. (2014). Time–Frequency Analysis of Event-Related Potentials: A Brief Tutorial. *Brain Topography*, *27*(4), 438–450. https://doi.org/10.1007/s10548-013-0327-5

Himmelheber, A. M., Sarter, M., & Bruno, J. P. (1997). Operant performance and cortical acetylcholine release: Role of response rate, reward density, and non-contingent stimuli. *Cognitive Brain Research*, *6*(1), 23–36.

Hui, J., Zomorrodi, R., Lioumis, P., Salavati, B., Rajji, T. K., Chen, R., Blumberger, D. M., & Daskalakis, Z. J. (2020). Pharmacological mechanisms of interhemispheric signal propagation: A TMS-EEG study. *Neuropsychopharmacology*, *45*(6), 932–939. https://doi.org/10.1038/s41386-019-0468-7

Ilmoniemi, R. J., Hernandez-Pavon, J. C., Mäkelä, N. N., Metsomaa, J., Mutanen, T. P., Stenroos, M., & Sarvas, J. (2015). Dealing with artifacts in TMS-evoked EEG. *2015 37th Annual International Conference of the IEEE Engineering in Medicine and Biology Society (EMBC)*, 230–233. https://doi.org/10.1109/EMBC.2015.7318342

Ilmoniemi, R. J., Rogasch, N. C., & Casarotto, S. (2024). TMS measures explored by EEG recordings. In E. M. Wassermann, A. V. Peterchev, U. Ziemann, S. H. Lisanby, H. R. Siebner, & V. Walsh (Eds.), *The Oxford Handbook of Transcranial Stimulation:*

Second Edition (p. 0). Oxford University Press. https://doi.org/10.1093/oxfordhb/9780198832256.013.17

Ilmoniemi, R. J., Virtanen, J., Ruohonen, J., Karhu, J., Aronen, H. J., Näätänen, R., & Katila, T. (1997). Neuronal responses to magnetic stimulation reveal cortical reactivity and connectivity. *Neuroreport*, *8*(16), 3537–3540.

Jackson, A. F., & Bolger, D. J. (2014). The neurophysiological bases of EEG and EEG measurement: A review for the rest of us. *Psychophysiology*, *51*(11), 1061–1071.

Julkunen, P., Kimiskidis, V. K., & Belardinelli, P. (2022). Bridging the gap: TMS-EEG from lab to clinic. *Journal of Neuroscience Methods*, *369*, 109482. https://doi.org/10.1016/j.jneumeth.2022.109482

Kähkönen, S., Komssi, S., Wilenius, J., & Ilmoniemi, R. J. (2005). Prefrontal transcranial magnetic stimulation produces intensity-dependent EEG responses in humans. *Neuroimage*, *24*(4), 955–960.

Kandel, E. R., Schwartz, J. H., Jessell, T. M., Siegelbaum, S., Hudspeth, A. J., & Mack, S. (2000). *Principles of neural science* (Vol. 4). McGraw-hill New York.

Kerwin, L. J., Keller, C. J., Wu, W., Narayan, M., & Etkin, A. (2018). Test-retest reliability of transcranial magnetic stimulation EEG evoked potentials. *Brain Stimulation*, *11*(3), 536–544.

Kida, T., Tanaka, E., & Kakigi, R. (2016). Multi-Dimensional Dynamics of Human Electromagnetic Brain Activity. *Frontiers in Human Neuroscience*, *9*. https://doi.org/10.3389/fnhum.2015.00713

Kim, J.-H., Jung, A.-H., Jeong, D., Choi, I., Kim, K., Shin, S., Kim, S. J., & Lee, S.-H. (2016). Selectivity of neuromodulatory projections from the basal forebrain and locus ceruleus to primary sensory cortices. *Journal of Neuroscience*, *36*(19), 5314–5327.

Klinkenberg, I., & Blokland, A. (2010). The validity of scopolamine as a pharmacological model for cognitive impairment: A review of animal behavioral studies. *Neuroscience & Biobehavioral Reviews*, *34*(8), 1307–1350.

Klinkenberg, I., Sambeth, A., & Blokland, A. (2011). Acetylcholine and attention. *Behavioural Brain Research*, *221*(2), 430–442.

Komssi, S., Aronen, H. J., Huttunen, J., Kesäniemi, M., Soinne, L., Nikouline, V. V., Ollikainen, M., Roine, R. O., Karhu, J., Savolainen, S., & Ilmoniemi, R. J. (2002). Ipsi- and contralateral EEG reactions to transcranial magnetic stimulation. *Clinical Neurophysiology*, *113*(2), 175–184. https://doi.org/10.1016/S1388-2457(01)00721-0

Kunnath, A. J., Gifford, R. H., & Wallace, M. T. (2023). Cholinergic Modulation of Sensory Perception and Plasticity. *Neuroscience & Biobehavioral Reviews*, 105323.

Kuriakose, R., Saha, U., Castillo, G., Udupa, K., Ni, Z., Gunraj, C., Mazzella, F., Hamani, C., Lang, A. E., Moro, E., & others. (2010). The nature and time course of cortical activation following subthalamic stimulation in Parkinson's disease. *Cerebral Cortex*, *20*(8), 1926–1936.

Lawrence, N. S., Ross, T. J., & Stein, E. A. (2002). Cognitive mechanisms of nicotine on visual attention. *Neuron*, *36*(3), 539–548.

Lehmann, D., & Skrandies, W. (1980). Reference-free identification of components of checkerboard-evoked multichannel potential fields. *Electroencephalography and Clinical Neurophysiology*, *48*(6), 609–621. https://doi.org/10.1016/0013-4694(80)90419-8

Leodori, G., De Bartolo, M. I., Guerra, A., Fabbrini, A., Rocchi, L., Latorre, A., Paparella, G., Belvisi, D., Conte, A., Bhatia, K. P., Rothwell, J. C., & Berardelli, A. (2022). Motor Cortical Network Excitability in Parkinson's Disease. *Movement Disorders*, *37*(4), 734–744. https://doi.org/10.1002/mds.28914

Leodori, G., De Bartolo, M. I., Piervincenzi, C., Mancuso, M., Ojha, A., Costanzo, M., Aiello, F., Vivacqua, G., Fabbrini, G., Conte, A., Pantano, P., Berardelli, A., & Belvisi, D. (2024). Mapping Motor Cortical Network Excitability and Connectivity Changes in De Novo Parkinson's Disease. *Movement Disorders: Official Journal of the Movement Disorder Society*, *39*(9), 1523–1532. https://doi.org/10.1002/mds.29901

Lester, D. B., Rogers, T. D., & Blaha, C. D. (2010). Acetylcholine-dopamine interactions in the pathophysiology and treatment of CNS disorders. *CNS Neuroscience & Therapeutics*, *16*(3), 137–162. https://doi.org/10.1111/j.1755-5949.2010.00142.x

Li, B., Virtanen, J. P., Oeltermann, A., Schwarz, C., Giese, M. A., Ziemann, U., & Benali, A. (2017). Lifting the veil on the dynamics of neuronal activities evoked by transcranial magnetic stimulation. *Elife*, *6*, e30552.

Lioumis, P., Kičić, D., Savolainen, P., Mäkelä, J. P., & Kähkönen, S. (2009). Reproducibility of TMS—Evoked EEG responses. *Human Brain Mapping*, *30*(4), 1387–1396.

Luck, S. J. (2014). *An introduction to the event-related potential technique*. MIT press.

Maccabee, P. J., Nagarajan, S. S., Amassian, V. E., Durand, D. M., Szabo, A. Z., Ahad, A. B., Cracco, R. Q., Lai, K. S., & Eberle, L. P. (1998). Influence of pulse sequence, polarity and amplitude on magnetic stimulation of human and porcine peripheral nerve. *The Journal of Physiology*, *513 (Pt 2)*(Pt 2), 571–585. https://doi.org/10.1111/j.1469-7793.1998.571bb.x

Mancuso, M., Cruciani, A., Sveva, V., Casula, E., Brown, K., Rothwell, J., Di Lazzaro, V., Koch, G., & Rocchi, L. (2023). Somatosensory input in the context of transcranial magnetic stimulation coupled with electroencephalography: An evidence-based overview. *Neuroscience & Biobehavioral Reviews*, *155*, 105434.

Massimini, M., Ferrarelli, F., Huber, R., Esser, S. K., Singh, H., & Tononi, G. (2005). Breakdown of cortical effective connectivity during sleep. *Science*, *309*(5744), 2228–2232.

Maurice, N., Liberge, M., Jaouen, F., Ztaou, S., Hanini, M., Camon, J., Deisseroth, K., Amalric, M., Kerkerian-Le Goff, L., & Beurrier, C. (2015). Striatal cholinergic interneurons control motor behavior and basal ganglia function in experimental parkinsonism. *Cell Reports*, *13*(4), 657–666.

Moffa, A. H., Nikolin, S., Martin, D., Loo, C., & Boonstra, T. W. (2022). Reliability of transcranial magnetic stimulation evoked potentials to detect the effects of theta-burst stimulation of the prefrontal cortex. *Neuroimage: Reports*, *2*(3), 100115.

Mouraux, A., & Iannetti, G. D. (2009). Nociceptive laser-evoked brain potentials do not reflect nociceptive-specific neural activity. *Journal of Neurophysiology*, *101*(6), 3258–3269.

Muñoz, W., & Rudy, B. (2014). Spatiotemporal specificity in cholinergic control of neocortical function. *Current Opinion in Neurobiology*, *26*, 149–160.

Murakami, S., & Okada, Y. (2006). Contributions of principal neocortical neurons to magnetoencephalography and electroencephalography signals. *The Journal of Physiology*, *575*(Pt 3), 925–936. https://doi.org/10.1113/jphysiol.2006.105379

Nadim, F., & Bucher, D. (2014). Neuromodulation of neurons and synapses. *Current Opinion in Neurobiology*, *29*, 48–56. https://doi.org/10.1016/j.conb.2014.05.003

Nakano, K., Kayahara, T., Tsutsumi, T., & Ushiro, H. (2000). Neural circuits and functional organization of the striatum. *Journal of Neurology*, *247*, V1–V15.

Ni, Z., Kim, S. J., Phielipp, N., Ghosh, S., Udupa, K., Gunraj, C. A., Saha, U., Hodaie, M., Kalia, S. K., Lozano, A. M., & others. (2018). Pallidal deep brain stimulation modulates cortical excitability and plasticity. *Annals of Neurology*, *83*(2), 352–362.

Novembre, G., Pawar, V. M., Kilintari, M., Bufacchi, R. J., Guo, Y., Rothwell, J. C., & Iannetti, G. D. (2019). The effect of salient stimuli on neural oscillations, isometric force, and their coupling. *NeuroImage*, *198*, 221–230.

Numssen, O., Kuhnke, P., Weise, K., & Hartwigsen, G. (2024). Electric-field-based dosing for TMS. *Imaging Neuroscience*, *2*, 1–12. https://doi.org/10.1162/imag_a_00106

Parikh, V., Kozak, R., Martinez, V., & Sarter, M. (2007). Prefrontal acetylcholine release controls cue detection on multiple timescales. *Neuron*, *56*(1), 141–154.

Parmigiani, S., Ross, J. M., Cline, C., Minasi, C., Gogulski, J., & Keller, C. J. (2022). Reliability and validity of TMS-EEG biomarkers. *Biological Psychiatry: Cognitive Neuroscience and Neuroimaging*.

Paus, T., Sipila, P. K., & Strafella, A. P. (2001). Synchronization of Neuronal Activity in the Human Primary Motor Cortex by Transcranial Magnetic Stimulation: An EEG Study. *Journal of Neurophysiology*, *86*(4), 1983–1990. https://doi.org/10.1152/jn.2001.86.4.1983

Pellicciari, M. C., Bonnì, S., Ponzo, V., Cinnera, A. M., Mancini, M., Casula, E. P., Sallustio, F., Paolucci, S., Caltagirone, C., & Koch, G. (2018). Dynamic reorganization of TMS-evoked activity in subcortical stroke patients. *NeuroImage*, *175*, 365–378. https://doi.org/10.1016/j.neuroimage.2018.04.011

Pellicciari, M. C., Veniero, D., & Miniussi, C. (2017). Characterizing the cortical oscillatory response to TMS pulse. *Frontiers in Cellular Neuroscience*, *11*, 38.

Peterchev, A. V., Rosa, M. A., Deng, Z.-D., Prudic, J., & Lisanby, Sarah. H. (2010). ECT Stimulus Parameters: Rethinking Dosage. *The Journal of ECT*, *26*(3), 159–174. https://doi.org/10.1097/YCT.0b013e3181e48165

Picciotto, M. R., Higley, M. J., & Mineur, Y. S. (2012). Acetylcholine as a neuromodulator: Cholinergic signaling shapes nervous system function and behavior. *Neuron*, *76*(1), 116–129.

Pinto, L., Goard, M. J., Estandian, D., Xu, M., Kwan, A. C., Lee, S.-H., Harrison, T. C., Feng, G., & Dan, Y. (2013). Fast modulation of visual perception by basal forebrain cholinergic neurons. *Nature Neuroscience*, *16*(12), 1857–1863.

Potter, D. D., Pickles, C. D., Roberts, R. C., & Rugg, M. D. (2000). Scopolamine impairs memory performance and reduces frontal but not parietal visual P3 amplitude. *Biological Psychology*, *52*(1), 37–52.

Premoli, I., Bergmann, T. O., Fecchio, M., Rosanova, M., Biondi, A., Belardinelli, P., & Ziemann, U. (2017). The impact of GABAergic drugs on TMS-induced brain oscillations in human motor cortex. *NeuroImage*, *163*, 1–12. https://doi.org/10.1016/j.neuroimage.2017.09.023

Premoli, I., Castellanos, N., Rivolta, D., Belardinelli, P., Bajo, R., Zipser, C., Espenhahn, S., Heidegger, T., Müller-Dahlhaus, F., & Ziemann, U. (2014). TMS-EEG signatures of GABAergic neurotransmission in the human cortex. *Journal of Neuroscience*, *34*(16), 5603–5612.

Purves, D., Augustine, G. J., Fitzpatrick, D., Hall, W. C., LaMantia, A. S., Mooney, R. D., Platt, M. L., & White, L. E. (2018). *Neuroscience (Sixth Edit)*. Oxford University Press.

Raffin, E., Harquel, S., Passera, B., Chauvin, A., Bougerol, T., & David, O. (2020). Probing regional cortical excitability via input–output properties using transcranial magnetic stimulation and electroencephalography coupling. *Human Brain Mapping*, *41*(10), 2741–2761.

Rocchi, L., Di Santo, A., Brown, K., Ibáñez, J., Casula, E., Rawji, V., Di Lazzaro, V., Koch, G., & Rothwell, J. (2021). Disentangling EEG responses to TMS due to cortical and peripheral activations. *Brain Stimulation*, *14*(1), 4–18.

Rogasch, N. C., Biabani, M., & Mutanen, T. P. (2022). Designing and comparing cleaning pipelines for TMS-EEG data: A theoretical overview and practical example. *Journal of Neuroscience Methods*, 109494.

Rogasch, N. C., & Fitzgerald, P. B. (2013). Assessing cortical network properties using TMS–EEG. *Human Brain Mapping*, *34*(7), 1652–1669.

Rogasch, N. C., Thomson, R. H., Farzan, F., Fitzgibbon, B. M., Bailey, N. W., Hernandez-Pavon, J. C., Daskalakis, Z. J., & Fitzgerald, P. B. (2014). Removing artefacts from TMS-EEG recordings using independent component analysis: Importance for assessing prefrontal and motor cortex network properties. *NeuroImage*, *101*, 425–439. https://doi.org/10.1016/j.neuroimage.2014.07.037

Rogasch, N. C., Zipser, C., Darmani, G., Mutanen, T. P., Biabani, M., Zrenner, C., Desideri, D., Belardinelli, P., Müller-Dahlhaus, F., & Ziemann, U. (2020). The effects of NMDA receptor blockade on TMS-evoked EEG potentials from prefrontal and parietal cortex. *Scientific Reports*, *10*(1), 3168.

Rosanova, M., Casali, A., Bellina, V., Resta, F., Mariotti, M., & Massimini, M. (2009). Natural frequencies of human corticothalamic circuits. *Journal of Neuroscience*, *29*(24), 7679–7685.

Ross, J. M., Sarkar, M., & Keller, C. J. (2022). Experimental suppression of transcranial magnetic stimulation-electroencephalography sensory potentials. *Human Brain Mapping*, *43*(17), 5141–5153.

Rossi, S., Hallett, M., Rossini, P. M., Pascual-Leone, A., & Safety of TMS Consensus Group. (2009). Safety, ethical considerations, and application guidelines for the use of transcranial magnetic stimulation in clinical practice and research. *Clinical Neurophysiology: Official Journal of the International Federation of Clinical Neurophysiology*, *120*(12), 2008–2039. https://doi.org/10.1016/j.clinph.2009.08.016

Russo, S., Sarasso, S., Puglisi, G. E., Dal Palù, D., Pigorini, A., Casarotto, S., D'Ambrosio, S., Astolfi, A., Massimini, M., Rosanova, M., & others. (2022). TAAC-TMS Adaptable Auditory Control: A universal tool to mask TMS clicks. *Journal of Neuroscience Methods*, *370*, 109491.

Salavati, B., Rajji, T. K., Zomorrodi, R., Blumberger, D. M., Chen, R., Pollock, B. G., & Daskalakis, Z. J. (2018). Pharmacological Manipulation of Cortical Inhibition in the Dorsolateral Prefrontal Cortex. *Neuropsychopharmacology: Official Publication of the American College of Neuropsychopharmacology*, *43*(2), 354–361. https://doi.org/10.1038/npp.2017.104

Sarasso, S., Rosanova, M., Casali, A. G., Casarotto, S., Fecchio, M., Boly, M., Gosseries, O., Tononi, G., Laureys, S., & Massimini, M. (2014). Quantifying Cortical EEG Responses to TMS in (Un)consciousness. *Clinical EEG and Neuroscience*, *45*(1), 40–49. https://doi.org/10.1177/1550059413513723

Shrout, P. E. (1998). Measurement reliability and agreement in psychiatry. *Statistical Methods in Medical Research*, *7*(3), 301–317.

Siebner, H. R., Bergmann, T. O., Bestmann, S., Massimini, M., Johansen-Berg, H., Mochizuki, H., Bohning, D. E., Boorman, E. D., Groppa, S., Miniussi, C., Pascual-Leone, A., Huber, R., Taylor, P. C. J., Ilmoniemi, R. J., De Gennaro, L., Strafella, A. P., Kähkönen, S., Klöppel, S., Frisoni, G. B., … Rossini, P. M. (2009). Consensus paper: Combining transcranial stimulation with neuroimaging. *Brain Stimulation*, *2*(2), 58–80. https://doi.org/10.1016/j.brs.2008.11.002

Siebner, H. R., Conde, V., Tomasevic, L., Thielscher, A., & Bergmann, T. O. (2019). Distilling the essence of TMS-evoked EEG potentials (TEPs): A call for securing mechanistic specificity and experimental rigor. *Brain Stimulation: Basic, Translational, and Clinical Research in Neuromodulation*, *12*(4), 1051–1054.

Siebner, H. R., Funke, K., Aberra, A. S., Antal, A., Bestmann, S., Chen, R., Classen, J., Davare, M., Di Lazzaro, V., Fox, P. T., & others. (2022). Transcranial magnetic stimulation of the brain: What is stimulated?–a consensus and critical position paper. *Clinical Neurophysiology*, *140*, 59–97.

Siu, A., & Drachtman, R. (2007). Dextromethorphan: A Review of N-methyl-d-aspartate Receptor Antagonist in the Management of Pain. *CNS Drug Reviews*, *13*(1), 96–106. https://doi.org/10.1111/j.1527-3458.2007.00006.x

Song, Y., Gordon, P. C., Metsomaa, J., Rostami, M., Belardinelli, P., & Ziemann, U. (2024). Evoked EEG Responses to TMS Targeting Regions Outside the Primary Motor Cortex and Their Test–Retest Reliability. *Brain Topography*, *37*(1), 19–36. https://doi.org/10.1007/s10548-023-01018-y

Song, Y., Gordon, P. C., Roy, O., Metsomaa, J., Belardinelli, P., Rostami, M., & Ziemann, U. (2025). Involvement of muscarinic acetylcholine receptor-mediated cholinergic neurotransmission in TMS–EEG responses. *Progress in Neuro-Psychopharmacology and Biological Psychiatry*, *136*, 111167. https://doi.org/10.1016/j.pnpbp.2024.111167

Stein, E. A., Pankiewicz, J., Harsch, H. H., Cho, J.-K., Fuller, S. A., Hoffmann, R. G., Hawkins, M., Rao, S. M., Bandettini, P. A., & Bloom, A. S. (1998). Nicotine-induced limbic cortical activation in the human brain: A functional MRI study. *American Journal of Psychiatry*, *155*(8), 1009–1015.

Stokes, M. G., Chambers, C. D., Gould, I. C., Henderson, T. R., Janko, N. E., Allen, N. B., & Mattingley, J. B. (2005). Simple Metric For Scaling Motor Threshold Based on Scalp-Cortex Distance: Application to Studies Using Transcranial Magnetic Stimulation. *Journal of Neurophysiology*, *94*(6), 4520–4527. https://doi.org/10.1152/jn.00067.2005

Strafella, A. P., Vanderwerf, Y., & Sadikot, A. F. (2004). Transcranial magnetic stimulation of the human motor cortex influences the neuronal activity of subthalamic nucleus. *European Journal of Neuroscience*, *20*(8), 2245–2249.

Taylor, S. (2007). Electroconvulsive therapy: A review of history, patient selection, technique, and medication management. *Southern Medical Journal*, *100*(5), 494–499.

ter Braack, E. M., de Vos, C. C., & van Putten, M. J. A. M. (2015). Masking the Auditory Evoked Potential in TMS–EEG: A Comparison of Various Methods. *Brain Topography*, *28*(3), 520–528. https://doi.org/10.1007/s10548-013-0312-z

Tervo, A. E., Nieminen, J. O., Lioumis, P., Metsomaa, J., Souza, V. H., Sinisalo, H., Stenroos, M., Sarvas, J., & Ilmoniemi, R. J. (2022). Closed-loop optimization of transcranial magnetic stimulation with electroencephalography feedback. *Brain Stimulation*, *15*(2), 523–531. https://doi.org/10.1016/j.brs.2022.01.016

Thiele, A. (2013). Muscarinic signaling in the brain. *Annual Review of Neuroscience*, *36*, 271–294.

Thienel, R., Kellermann, T., Schall, U., Voss, B., Reske, M., Halfter, S., Sheldrick, A. J., Radenbach, K., Habel, U., Shah, N. J., & others. (2009). Muscarinic antagonist effects on executive control of attention. *International Journal of Neuropsychopharmacology*, *12*(10), 1307–1317.

Tremblay, S., Rogasch, N. C., Premoli, I., Blumberger, D. M., Casarotto, S., Chen, R., Di Lazzaro, V., Farzan, F., Ferrarelli, F., Fitzgerald, P. B., & others. (2019). Clinical utility and prospective of TMS–EEG. *Clinical Neurophysiology*, *130*(5), 802–844.

Tscherpel, C., Dern, S., Hensel, L., Ziemann, U., Fink, G. R., & Grefkes, C. (2020). Brain responsivity provides an individual readout for motor recovery after stroke. *Brain*, *143*(6), 1873–1888. https://doi.org/10.1093/brain/awaa127

Tsuboi, D., Nagai, T., Yoshimoto, J., & Kaibuchi, K. (2024). Neuromodulator regulation and emotions: Insights from the crosstalk of cell signaling. *Frontiers in Molecular Neuroscience*, *17*, 1376762.

Utter, A. A., & Basso, M. A. (2008). The basal ganglia: An overview of circuits and function. *Neuroscience & Biobehavioral Reviews*, *32*(3), 333–342.

Van Der Werf, Y. D., & Paus, T. (2006). The neural response to transcranial magnetic stimulation of the human motor cortex. I. Intracortical and cortico-cortical contributions. *Experimental Brain Research*, *175*(2), 231–245. https://doi.org/10.1007/s00221-006-0551-2

Walker, H. C., Huang, H., Gonzalez, C. L., Bryant, J. E., Killen, J., Cutter, G. R., Knowlton, R. C., Montgomery, E. B., Guthrie, B. L., & Watts, R. L. (2012). Short latency activation of cortex during clinically effective subthalamic deep brain stimulation for Parkinson's disease. *Movement Disorders*, *27*(7), 864–873.

Záborszky, L., Gombkoto, P., Varsanyi, P., Gielow, M. R., Poe, G., Role, L. W., Ananth, M., Rajebhosale, P., Talmage, D. A., Hasselmo, M. E., & others. (2018). Specific basal forebrain–cortical cholinergic circuits coordinate cognitive operations. *Journal of Neuroscience*, *38*(44), 9446–9458.

Ziemann, U., Reis, J., Schwenkreis, P., Rosanova, M., Strafella, A., Badawy, R., & Müller-Dahlhaus, F. (2015). TMS and drugs revisited 2014. *Clinical Neurophysiology*, *126*(10), 1847–1868.

Ztaou, S., & Amalric, M. (2019). Contribution of cholinergic interneurons to striatal pathophysiology in Parkinson's disease. *Neurochemistry International*, *126*, 1–10.

6 Zusammenfassung

Die Kombination aus transkranieller Magnetstimulation und Elektroenzephalographie (TMS-EEG) ist ein leistungsstarker, nicht-invasiver Ansatz zur Untersuchung der Hirnfunktion bei Gesundheit und Krankheit. Im einfachsten Fall stimuliert ein einzelner TMS-Impuls eine spezifische Hirnregion, während das EEG gleichzeitig die daraus resultierenden kortikalen Potenziale aufzeichnet. Diese Anwendung von TMS-Pulsen während der EEG-Aufzeichnung führt zu Artefakten. Besonders problematisch sind sensorische EEG-Antworten, die durch periphere Co-Stimulation verursacht werden, da sie den echten TMS-EEG-Antworten sehr ähnlich sind und zu Fehlinterpretationen führen können. Daher war das erste Ziel dieser Arbeit, ein Kontrollverfahren zum Reduzieren sensorischer Störfaktoren zu testen. Dieses Verfahren wurde auf der Basis früherer Arbeiten entwickelt.

Um TMS-EEG effektiv anzuwenden, müssen wir die zu Grunde liegenden neurophysiologischen Mechanismen besser verstehen. Dadurch, wie sich verschiedene Pharmaka auf die TMS-EEG Potenziale auswirken, können wir untersuchen, welchen Anteil über verschiedene Rezeptoren vermittelte Neurotransmission an den TMS-EEG-Antworten hat. Folglich war das zweite Ziel dieser Arbeit, den Beitrag cholinerger Neurotransmission durch den muskarinergen Acetylcholinrezeptor (mAChR) zu den TMS-EEG-Antworten zu untersuchen.

Hierzu führten wir eine randomisierte, placebokontrollierte Crossover-Studie mit 24 gesunden Teilnehmenden durch. In drei Sitzungen wurden drei Medikamente oral verabreicht: (1) der nicht-selektive mAChR-Antagonist Scopolamin, (2) der selektive mAChR-Antagonist Biperiden, (3) Placebo. Während jeder Sitzung wurden die TMS-EEG-Potenziale auf die Stimulation von drei Hirnregionen vor und nach Gabe des Medikaments gemessen. Hierbei wurde ein sensorisches Kontrollverfahren angewandt, um sensorische Artefakte zu vermeiden. Wir konnten nachweisen, dass „bereinigte“ TMS-EEG-Potenziale, bei denen sensorische Artefakte durch das Kontrollverfahren entfernt wurden, die direkte kortikale Aktivierung zuverlässig darstellen. Zudem stellten wir fest, dass Scopolamin die Amplitude einer lokalen TEP-Komponente (TMS-evoziertes EEG-Potenzial) signifikant erhöhte, die etwa 40-63 ms nach der Stimulation des supplementär-motorischen Kortex auftritt. Frühere pharmakologische TMS-EEG-

Studien legen nahe, dass diese TEP-Komponente (N45) das Gleichgewicht zwischen Erregung und Hemmung (E/I) widerspiegelt, das durch glutamaterge und GABAerge Übertragung gesteuert wird. Wir vermuten, dass die erhöhte Amplitude der N45-ähnlichen TEP-Komponente, die durch anticholinerge Medikamente verursacht wird, aus der Verschiebung des E/I-Gleichgewichts zu Gunsten der Hemmung resultieren könnte.

Unsere Ergebnisse unterstreichen die Bedeutung geeigneter Kontrollverfahren zur Reduktion von sensorischen Störfaktoren bei TMS-EEG-Studien und bieten neue Einblicke in die Neurophysiologie des Einzelimpuls-TMS-EEGs. Diese neurophysiologischen Erkenntnisse sind klinisch relevant. Sie verbessern die Interpretation von pathologisch veränderten TMS-EEG-Antworten bei cholinergen Defiziten (z.B. bei der Alzheimer-Erkrankung) und können helfen, Therapien zu unterstützen, die auf das cholinerge System abzielen.

7 Declaration of Contributions to the Dissertation

The dissertation work was carried out at the Hertie Institute for Clinical Brain Research under the supervision of Prof. Dr. Ulf Ziemann. The studies were designed in collaboration with Prof. Dr. Ulf Ziemann and Dr. Pedro Caldana Gordon. I recruited participants while Dr. Pedro Caldana Gordon performed medical screenings to check for any contraindications to TMS and study medications. I conducted the experiments under the supervision of Dr. Pedro Caldana Gordon. The TMS–EEG signal preprocessing pipeline was developed by Dr. Johanna Metsomaa, Dr. Maryam Rostami, and myself. Prof. Paolo Belardinelli, Dr. Johanna Metsomaa, and Dr. Pedro Caldana Gordon provided individual head models and code for the source reconstruction of EEG signals. I developed the statistical analysis pipeline for the EEG signals with contributions from Dr. Olivier Roy, Dr. Pedro Caldana Gordon, and Prof. Paolo Belardinelli. I programmed and processed the experimental data and conducted statistical analyses. I wrote the manuscripts and produced all the figures for the publications in which I am the first author. All authors have approved the use of the mentioned publications for this doctoral thesis.

I confirm that I wrote the thesis myself and that any additional source of information has been cited and acknowledged within the text.

During the revision, I used Grammarly and ChatGPT-4o for spelling and grammar correctness, word choice, and semantics improvement. Please find examples of ChatGPT prompts in Appendix A. The output text was carefully reviewed and edited before being incorporated into the thesis. The final text was revised based on feedback from my supervisor, Prof. Dr. Ulf Ziemann.

Signed_____

on _____ in Tübingen

8 Appendix A.

Prompt example 1 for using ChatGPT-4o to revise text.

“Hi, I am writing my PhD thesis in the field of TMS-EEG, now I want you to take the persona of a professional reviewer in academia to refine my text, including correcting the grammar and improving clarity, logic, conciseness, coherence and other points in terms of semantics. Please maintain my original intellectual inputs, and please do not eliminate detailed information unless it is super wordy and necessary. please start with this sentence: 'the sham procedure enables us to observe a late TEP component ($>$100 ms) in the central area, slightly left-lateralized (\textcolor{blue}{Figure }), indicating the activation of left SMA, which may have been obscured by the dominant complex N100-P200.”

Prompt example 2 for using ChatGPT-4o to revise text.

“I find the refined version confusing, what about now? 'ACh acts through two classes of receptors, metabotropic muscarinic receptors (mAChRs) and ionotropic nicotinic receptors (nAChRs), upon being released from cholinergic neurons in the CNS (\cite{kandel2000principles}).' ”

Prompt example 3 for using ChatGPT-4o to revise text.

“can you combine the first two sentences properly?”

“thanks, which description is more proper? vary depending on the stimulation site or vary by the stimulation site?”

9 Acknowledgments

I would like to express my gratitude to my supervisor, Prof. Dr. Ulf Ziemann, for giving me the opportunity to join his research lab and for his invaluable guidance throughout my Ph.D.

I am also thankful to the members of my Ph.D. committee, Prof. Dr. Christoph Braun and Prof. Dr. Hubert Preißl, for their time and insightful advice during progress meetings.

Special thanks go to Dr. Pedro Caldana Gordon for his significant contributions to my Ph.D. project, which have been essential to its success.

I am also grateful to all my collaborators, Dr. Olivier Roy, Prof. Paolo Belardinelli, Dr. Johanna Metsomaa, and Dr. Maryam Rostami, for their invaluable contributions that enriched my research.

To my colleagues and friends, David Vetter, Elina Song, and Maria Ermolova, thank you for the encouragement and support, especially during the challenging initial phase of my Ph.D. I am equally grateful to Dr. Dania Humaidan and Johanna Rösch for their warm and constructive advice during difficult decision-making moments. I also thank Jing Chen, Miriam Kirchhoff, and all the lab members for creating a collaborative and inspiring environment that encouraged regular scientific discussions, and helped me grow both personally and professionally.

My appreciation extends to Dr. Inka Montero and other members of the Ph.D. coordination office for their administrative assistance. I would also like to thank the Chinese Scholarship Council for offering me the opportunity to study in Germany.

To the lovely people I met during my stay in Tübingen, thank you for making these years an unforgettable and joyful experience. Lastly, I am deeply grateful to my family and friends in China for their constant support and encouragement, which gave me the strength and confidence to pursue my passions.